

AD-A099 562

TENNESSE UNIV KNOXVILLE DEPT OF ENGINEERING SCIENCE --ETC P/G 12/1  
RESEARCH ON NUMERICAL ALGORITHMS FOR THE THREE-DIMENSIONAL NAVI--ETC(U)  
FEB 81 A J BAKER AFOSR-79-0005

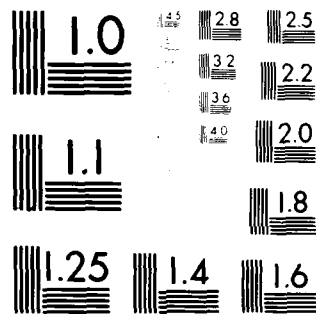
UNCLASSIFIED

AFWAL-TR-80-3157

NL

1 of 1  
AD-A  
1000000

END  
DATE  
FILMED  
6-81  
DTIC



MICROCOPY RESOLUTION TEST CHART  
NATIONAL BUREAU OF STANDARDS-1963-A

AD A099562

DNC FILE COPY

AFWAL-TR-80-3157

LEVEL

RESEARCH ON NUMERICAL ALGORITHMS FOR THE THREE-DIMENSIONAL  
NAVIER-STOKES EQUATIONS, II. DISSIPATIVE FINITE ELEMENT

A. J. BAKER

DEPARTMENT OF ENGINEERING SCIENCE & MECHANICS  
UNIVERSITY OF TENNESSEE  
KNOXVILLE, TENNESSEE 404478-1



FEBRUARY 1981

TECHNICAL REPORT AFWAL-TR-80-3157  
INTERIM REPORT FOR PERIOD OCTOBER 1979 - SEPTEMBER 1980

APPROVED FOR PUBLIC RELEASE; DISTRIBUTION UNLIMITED

FLIGHT DYNAMICS LABORATORY  
AIR FORCE WRIGHT AERONAUTICAL LABORATORIES  
AIR FORCE SYSTEMS COMMAND  
WRIGHT-PATTERSON AIR FORCE BASE, OHIO 45433

81 6 01 077



# NOTICE

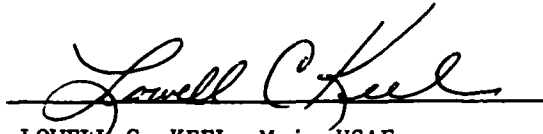
When Government drawings, specifications, or other data are used for any purpose other than in connection with a definitely related Government procurement operation, the United States Government thereby incurs no responsibility nor any obligation whatsoever; and the fact that the government may have formulated, furnished, or in any way supplied the said drawings, specifications, or other data, is not to be regarded by implication or otherwise as in any manner licensing the holder or any other person or corporation, or conveying any rights or permission to manufacture use, or sell any patented invention that may in any way be related thereto.

This report has been reviewed by the Office of Public Affairs (ASD/PA) and is releasable to the National Technical Information Service (NTIS). At NTIS, it will be available to the general public, including foreign nations.

This technical report has been reviewed and is approved for publication.



CHARLES E. JOBE  
Project Engineer



LOWELL C. KEEL, Maj, USAF  
Chief, Aerodynamics & Airframe Branch

FOR THE COMMANDER



PETER J. BUTKEWICZ, Colonel, USAF  
Chief, Aeromechanics Division

"If your address has changed, if you wish to be removed from our mailing list, or if the addressee is no longer employed by your organization please notify AFWAL/FIMM, W-PAFB, OH 45433 to help us maintain a current mailing list".

Copies of this report should not be returned unless return is required by security considerations, contractual obligations, or notice on a specific document.

SECURITY CLASSIFICATION OF THIS PAGE (When Data Entered)

REPORT DOCUMENTATION PAGE		READ INSTRUCTIONS BEFORE COMPLETING FORM	
1. REPORT NUMBER (18) AFWAL-TR-80-3157	12. GOVT ACCESSION NO. AD-A099562	3. PERFORMING ORG. REPORT NUMBER	
4. TITLE (and Subtitle) (6) RESEARCH ON NUMERICAL ALGORITHMS FOR THE THREE-DIMENSIONAL NAVIER-STOKES EQUATIONS. II. DISSIPATIVE FINITE ELEMENT.	5. TYPE OF REPORT & PERIOD COVERED (9) Interim Technical Report 1 Oct. 1979 - 30 Sept. 1980	6. PERFORMING ORG. REPORT NUMBER	
7. AUTHOR (10) A. J. Baker	8. CONTRACT OR GRANT NUMBER(s) (13) AFOSR-79-0005 x		
9. PERFORMING ORGANIZATION NAME AND ADDRESS Department of Engineering Science & Mechanics University of Tennessee, Knoxville, TN 37916	10. PROJECT ELEMENT, PROJECT, TASK AREA & WORK UNIT NUMBERS (16) 2307N428 (17) 141		
11. CONTROLLING OFFICE NAME AND ADDRESS AF Wright Aeronautical Laboratory, AFSC Flight Dynamics Laboratory (AFWAL/FIMM) Wright-Patterson AFB, Ohio 45433	12. REPORT DATE (11) February 1981	13. NUMBER OF PAGES 84 (12) 93	
14. MONITORING AGENCY NAME & ADDRESS (if different from Controlling Office)	15. SECURITY CLASS. (of this Report) Unclassified	15a. DECLASSIFICATION/DOWNGRADING SCHEDULE	
16. DISTRIBUTION STATEMENT (of this Report)  Approved for public release; distribution unlimited			
17. DISTRIBUTION STATEMENT (of the abstract entered in Block 20, if different from Report)			
18. SUPPLEMENTARY NOTES			
19. KEY WORDS (Continue on reverse side if necessary and identify by block number)  Navier-Stokes Equations Numerical Solution Algorithm Finite Element			
20. ABSTRACT (Continue on reverse side if necessary and identify by block number)  The objective of this research project is to derive and evaluate versatile, accurate and efficient numerical algorithms for solution of aerodynamic flowfields at large Reynolds number. The concept of a dissipative finite element algorithm has been refined and extended to solution of a complete equation set in aerodynamics. The resultant numerical results are highly encouraging with respect to shock resolution and overall performance, utilizing both a linear and a quadratic finite element embodiment of-			

DD FORM 1 JAN 73 1473 EDITION OF 1 NOV 65 IS OBSOLETE

SECURITY CLASSIFICATION OF THIS PAGE (When Data Entered)

404478

20. Cont'd

the theory. The theoretical formulational statement of the algorithm has been extended to a multi-dimensional description in generalized coordinates. The key efficiency feature is identification of the tensor matrix resolution of the Jacobian of the Newton algorithm for this statement. The concept of application of the continuity equation solution, as a differential constraint on the momentum equation algorithm, has been validated. The formulation is directly useful for viscous marching procedures, and with some modifications could be equally useful for a low Mach number Navier - Stokes solution algorithm.

## FOREWORD

This report describes the second year of work completed, in the Department of Engineering Science and Mechanics, University of Tennessee, on the topic of research on numerical solution algorithms for the three-dimensional Navier-Stokes equations. Sponsorship was provided by the United States Air Force under USAF Grant Number AFOSR-79-0005, Project 2307, Task N4, Work Unit 28.

The work reported herein is part of a multi-year effort and was performed during the period 1 October 1979 to 30 September 1980. The principal investigator is Dr. A. J. Baker, Professor of Engineering Science. The contract technical monitor was Dr. Charles E. Jobe, Flight Dynamics Laboratory.

The author wishes to acknowledge the valued interaction with colleagues, especially Dr. M. O. Soliman and Mr. Joseph A. Orzechowski. Mr. M. T. Chaudry was primarily responsible for completion of the Fourier stability analyses. Extensive support has been provided by the University of Tennessee Computing Center which is gratefully acknowledged.

Accession For	
NTIS GRA&I	<input checked="checked" type="checkbox"/>
DTIC TAB	<input type="checkbox"/>
Unannounced	<input type="checkbox"/>
Justification	
By _____	
Distribution/	
Availability Codes	
Dist	Avail and/or Special
A	

## TABLE OF CONTENTS

SECTION		PAGE
I.	INTRODUCTION . . . . .	1
II.	PROBLEM STATEMENTS . . . . .	3
III.	NUMERICAL SOLUTION ALGORITHM . . . . .	7
	1. Finite Element Formulation . . . . .	7
	2. Generalized Coordinates. . . . .	10
	3. Tensor Matrix Product Jacobian . . . . .	15
IV.	THEORETICAL ANALYSIS . . . . .	18
V.	DISCUSSION AND RESULTS. . . . .	28
	1. One-Dimensional Compressible Formulation . . . . .	28
	2. Numerical Results, Riemann Shock Tube. . . . .	38
	3. Numerical Results, Shocked Nozzle Flow . . . . .	44
	4. Two-Dimensional Flow Formulation . . . . .	51
	5. Numerical Results. . . . .	58
	6. Continuity-Constraint Formulation. . . . .	60
	7. Numerical Results. . . . .	62
VI.	CONCLUSIONS AND RECOMMENDATIONS. . . . .	65
	REFERENCES . . . . .	66
	APPENDIX A . . . . .	68
	Finite Element Algorithm Hypermatrices, Linear and Quadratic Basis on One-Dimensional Space	
	APPENDIX B . . . . .	77
	Finite Element Algorithm Hypermatrices, Linear Basis on Two-Dimensional Space	



# LIST OF ILLUSTRATIONS

FIGURE		PAGE
1	Biquadratic Cardinal Basis Coordinate Transformation. . . . .	12
2	Distribution of Solution to Equation 61 . . . . .	21
3	Final Station Solution For Rotating Cone Test Case, Linear Finite Element Algorithm, $v_1 = 0 = v_2$ . . . . .	22
4	Final Station Solution for Non-Linear Square Wave Test Case, Linear Finite Element Algorithm, $v_1 = .15/\sqrt{15}$ , $v_2 = 2/\sqrt{15}$ . . . . .	22
5	Final Station Solution for Linear Square Wave Test Case, Linear Finite Element Algorithm . . . . .	25
6	Linear Finite Element Algorithm Solution, Shock Tube Problem, $t = 0.14154$ , $v^1 = 0.$ , $v^2 = 1/\sqrt{15}$ . . . . .	40
7	Linear Finite Element Algorithm Solution, Shock Tube Problem, $t = 0.14154$ , $v^1_\alpha = 1/\sqrt{15}\{3/8, 0, 1/4\}$ , $v^2_\alpha = 1/\sqrt{15}\{3/4, 2, 1\}$ . . . . .	41
8	Solution for Shock Tube Problem Generated By the MUSCL Code, Reported by Van Leer (ref. 15), Courant No = 0.9, $\Delta x = 0.01$ , $t = 0.14154$ . . . . .	42
9	Finite Element and Finite Difference Algorithm Solution Comparisons, Shock Tube Problem, $t = 0.14154$ . . . . .	43
10	Quadratic Finite Element Algorithm Solution, Shock Tube Problem, $t = 0.14154$ , $v^1_\alpha = 0.$ , $v^2_\alpha = 1/\sqrt{15}$ . . . . .	45
11	Quadratic Finite Element Algorithm Solution, Shock Tube Problem, $t = 0.14154$ , $v^1_a = 0.$ , $v^2_\alpha = 1/\sqrt{15}\{1/4, 3/4, 1/2\}$ . . . . .	46
12	Finite Element and Diagonalized Finite Element Algorithm Comparisons, Shock Tube Problem, $t = 0.14154$ . . . . .	47
13	Computed Solution For Shocked Flow In A Variable Area Duct, Linear Finite Element Algorithm, — Initial Condition . . . . .	49
14	Computed Solution For Shocked Flow In A Variable Area Duct, Quadratic Finite Element Algorithm, — Initial Condition. . . . .	50
15	Confirmation Of Tensor Matrix Product Jacobian Formulation, Linear Finite Element Algorithm, Rotating Cone Test Case, One-Quarter Turn . . . . .	59
16	Computed Boundary Layer Integral Parameter Distribution For Bradshaw Relaxing Flow, Linear Finite Element Continuity Constraint Algorithm, Turbulence Kinetic Energy Closure Model . . . . .	64

# LIST OF TABLES

TABLE		PAGE
1	Rotating Cone Solution Accuracy Summary Linear Finite Element Algorithm, C=0.5. . . . .	23
2	Non-Linear Square Wave Solution Accuracy Summary Linear Finite Element Algorithm, C = 0.5. . . . .	23
3	Linear Square Wave Solution Accuracy Summary Linear Finite Element Algorithm, C = 0.5. . . . .	24
4	Convergence in $\{\delta QI\}$ for Reimann Shock Tube Simulation . . . . .	48
5	Transverse Velocity Distributions, $U_2(x_2) \times 10^3$ Laminar Incompressible Boundary Layer . . . . .	63
6	Continuity Constraint Algorithm Convergence Laminar Incompressible Boundary Layer . . . . .	63

## LIST OF SYMBOLS

a	boundary condition coefficient; sound speed
A	cross-sectional area; finite element one-dimensional hypermatrix
B	finite element two-dimensional hypermatrix
C	stress coefficient; initial-value matrix; Courant Number
d	mesh parameter
e	specific total energy
E	energy norm
f	function of known argument
F	finite element matrix; discretized equation system
g	total energy
G	finite element matrix
H	Hilbert space
i	$\sqrt{-T}$ ; index
j	index
J	Jacobian matrix
k	turbulence kinetic energy; finite element degree
$\ell$	summation index; differential operator; elemental measure
L	differential operator
m	momentum
M	number of finite elements spanning R
n	unit normal vector; dimension of space
N	finite element cardinal basis; discrete index
p	pressure; iteration index
P	intermediate solution matrix
$q_i$	heat flux vector; generalized dependent variable
$Q_i$	generalized semi-discrete dependent variable

$R$	spatial domain of differential operator
$S_e$	finite element assembly operator
$t$	time
$u_i$	velocity vector
$\overline{u_i u_j}$	Reynolds kinematic stress tensor
$v$	convection velocity
$V$	initial distribution
$x_i$	Cartesian coordinate system
$\alpha$	tensor product reference
$\beta_i$	Lagrange multiplier set
$\gamma$	ratio of specific heats; parameter
$\Gamma$	phase parameter
$\partial$	partial derivative operator
$\partial R$	boundary of solution domain $R$
$\delta$	Kronecker delta; parameter
$\delta Q$	iteration vector
$\Delta$	mesh measure; increment
$\epsilon$	specific internal energy; isotropic dissipation function; parameter
$\eta_i$	curvilinear coordinate system
$\kappa$	heat conductivity coefficient
$\lambda$	wavelength
$\mu$	dynamic viscosity; dissipation level
$\nu$	kinematic viscosity; dissipation parameter
$\rho$	density
$\sigma$	stress tensor; phase variable
$\Sigma$	summation operator
$\tau$	generalized initial-value coordinate; integration parameter

$\phi$	mass constraint variable
$\omega$	elemental measure; wave number
$\Omega$	solution domain

#### Superscripts:

h	solution approximation
o	initial condition reference
p	iteration index
T	matrix transpose
1,2	dissipation parameter reference
	ordinary derivative

#### Subscripts:

e	element reference
i,j,k,l	tensor indices
j	time step index
k	degree of polynomial
m	macro-element reference
o	reference state
$\alpha$	dependent variable dissipation index

#### Notation:

{ }	column matrix
[ ]	square matrix
$\cup$	union
$\cap$	intersection
$\in$	belongs to
$\otimes$	tensor product

## SECTION I

### INTRODUCTION

Assessment of the potential impact of finite element concepts, applied in the construction of numerical solution algorithms for computational fluid mechanics, is required and under active study. The formal elegance of the methodology has produced a sound theoretical basis for the comprehensive computational simulation capabilities now extant throughout structural mechanics (ref. 1). The verification of this impact in fluid mechanics remains to be achieved, and is the principal focus of this research project.

In its most elementary interpretation, finite element theory returns calculus and vector field theory to the construction of discrete simulation algorithms for any branch of mechanics. Of necessity, using Taylor series expansions, one must always be able to verify the equivalent (finite difference) order-of-accuracy, for any of the familiar derivative terms within the governing partial differential equation system. Specifically, linear (quadratic) finite elements yield, equivalently, second-(fourth-) order finite difference representations for linear spatial derivatives. For other than linear space derivatives, however, the finite element construction yields expressions that are not usually familiar, although upon dissection, can be related to appropriate Taylor series expansions. The important feature is that the theory produces the discrete analog expressions, completely independent of the *a posteriori* ability to construct an equivalent difference representation.

In fluid mechanics, confidence in the theoretical statement can only be attained through detailed numerical assessments for progressively more complicated (and non-linear) pertinent differential equation descriptions. This is the basic mission of the University of Tennessee project in computational fluid mechanics. Strict adherence to the convergence theory has been verified for linear, scalar parabolic partial differential equations (ref. 2), using linear, quadratic, and cubic Lagrange, and cubic Hermite finite element interpolations within the basic theoretical statement. Importantly, for a non-homogeneous gradient boundary condition, of the type omnipresent in computational fluid mechanics, this study verified

equal or higher-order convergence for the discrete analog produced by the theory. Reference 3 documents adherence to convergence theory, for solutions of the mildly non-linear (parabolic) laminar boundary layer equations, for both linear and quadratic embodiments of the finite element theory. Extraneous error mechanisms served to obliterate attainment of the theoretical performance for the cubics. Similar verifications for the linear and quadratic formulation, for the consequentially non-linear parabolic turbulent boundary layer equations is reported in reference 4. Of primary theoretical consideration, the Sobolev norm used to measure convergence was a strongly non-linear function of the dependent variable set, yet the theory accurately quantized algorithm performance.

Viscous flows at large Reynolds number, and inviscid flows are characterized by dominance of the substantial derivative. The generally dispersive character of the discrete analog is the dominant error mechanism. Reference 5 documents accuracy and convergence assessments for scalar convection problems, driven by linear and non-linear hyperbolic equations. The numerical results were highly encouraging, specifically with respect to phase accuracy and the selectivity of the derived dissipative finite element algorithm statement. The results reported herein are an extension of these theoretical and numerical considerations. The basic von Neumann stability analysis has been refined and extended. Numerical results are presented for solution of the complete Euler equations, for shocked one-dimensional flows, that firmly quantized performance and resolution of discontinuous variables. The formulation is extended to a two-dimensional description in generalized coordinates, including detailed construction of the tensor matrix product form of the algorithm Jacobian. For low speed flow prediction, a differential constraint theoretical formulation for the continuity equation is derived and evaluated.

## SECTION II

### PROBLEM STATEMENTS

The requirement is to assess the key aspects of accuracy, convergence, stability and efficiency of finite element numerical solution algorithm concepts applied to computational aerodynamics. These performance measures, as quantized by analysis and numerical experiments on simplified scalar equations modeling key aspects of the governing Navier-Stokes equations, were reported in reference 5. The current research extends the developed algorithm concepts to differential equation systems governing certain problem classes in aerodynamics. Each class is selected to permit isolation of a key theoretical and/or practical aspect. This section summarizes the various differential equation descriptions.

The partial differential equation set governing transient, three-dimensional aerodynamic flows is the familiar and very non-linear Navier-Stokes system. Each equation system studied is derived from the Navier-Stokes equations. In non-dimensional conservation form, using Cartesian tensor summation notation, the equation system governing flow of a compressible, viscous, heat-conducting fluid is

$$L(\rho) = \frac{\partial \rho}{\partial t} + \frac{\partial}{\partial x_j} [u_j \rho] = 0 \quad (1)$$

$$L(\rho u_i) = \frac{\partial (\rho u_i)}{\partial t} + \frac{\partial}{\partial x_j} \left[ u_j \rho u_i + p \delta_{ij} - \sigma_{ij} \right] = 0 \quad (2)$$

$$L(\rho e) = \frac{\partial (\rho e)}{\partial t} + \frac{\partial}{\partial x_j} [u_j \rho e + u_j p - \sigma_{ij} u_i - q_j] = 0 \quad (3)$$

In equations 1-3,  $\rho$  is density,  $\rho u_i$  is the momentum vector,  $p$  is pressure, and  $e$  is mass specific total energy. The Stokes viscous stress tensor  $\sigma_{ij}$  and heat flux vector  $q_j$ , in terms of specific internal energy  $\epsilon$ , are

$$\sigma_{ij} = \mu \left[ \frac{\partial u_i}{\partial x_j} + \frac{\partial u_j}{\partial x_i} \right] - \frac{\mu}{3} \frac{\partial u_k}{\partial x_k} \delta_{ij} \quad (4)$$



$$q_j = -\kappa \frac{\partial \epsilon}{\partial x_j} \quad (5)$$

$$\epsilon = e - \frac{1}{2} u_i u_i \quad (6)$$

Assuming a polytropic gas,  $p = (\gamma-1)\rho\epsilon$ , the convenient form for the equation of state is

$$L(p) = p - (\gamma-1)[\rho e - \frac{1}{2}\rho u_j u_j] = 0 \quad (7)$$

Finally,  $\mu$  is the absolute viscosity,  $\kappa$  is the coefficient of heat conductivity, and  $\delta_{ij}$  is the Kronecker delta.

One special form of equations 1-7 for analysis corresponds to supersonic one-dimensional shocked flow in a duct of variable cross-sectional area,  $A(x)$ . The specific form is

$$L(\rho) = \frac{\partial \rho}{\partial t} + \frac{\partial}{\partial x}(\rho u) + \rho u A' = 0 \quad (8)$$

$$L(\rho u) = \frac{\partial \rho u}{\partial t} + \frac{\partial}{\partial x}[u \rho u + p] + \rho u^2 A' = 0 \quad (9)$$

$$L(\rho e) = \frac{\partial \rho e}{\partial t} + \frac{\partial}{\partial x}[u \rho e + up] + \rho u e A' = 0 \quad (10)$$

where  $A' \equiv d(\lambda_\eta A)/dx$ . Equation 7 is unchanged by limiting  $j \equiv 1$ . A second form for analysis describes two-dimensional, subsonic laminar flow of a viscous non-heat conducting fluid. This is obtained from equations 1-7 by setting  $\kappa \equiv 0$  and constraining the index range  $1 \leq (i,j) \leq 2$ . It is further permissible to assume  $\mu$  is constant for this case.

Many confined aerodynamic flows exhibit a predominant direction of flow which permits a simplification to equations 1-7 yielding the so-called parabolic Navier-Stokes equations. Assuming the steady, constant density flow isothermal and turbulent, and employing the Reynolds velocity decomposition (ref. 6), the time-averaged parabolized form of equations 1-7 is

$$L(\rho_0) = \frac{\partial}{\partial x_j}[\bar{u}_j] = 0 \quad (11)$$

$$L(\bar{u}_i) = \frac{\partial}{\partial x_j} \left[ \bar{u}_j \bar{u}_i + \frac{\bar{p}}{\rho_0} \delta_{ij} - \bar{\sigma}_{ij} + \overline{u_i' u_j'} \right] = 0 \quad (12)$$

$$\bar{\sigma}_{ij} = \nu (1 - \delta_{j1}) \frac{\partial \bar{u}_i}{\partial x_j} \quad (13)$$

In equations 11-13, the overbar signifies the time-averaged mean variable, the underbar signifies the index is not eligible for summation, and the flow is assumed essentially aligned with the  $x_1$  coordinate direction, where  $1 \leq (i,j) \leq 3$ .

A closure model for the Reynolds stress tensor  $\overline{u_i' u_j'}$  is required. Present requirements are served using the constitutive equation (ref. 7),

$$\begin{aligned} \overline{u_i' u_j'} = & C_{ij} k \delta_{ij} - C_{ve} \frac{k^2}{\nu \epsilon} \left[ \frac{\partial \bar{u}_i}{\partial x_j} + \frac{\partial \bar{u}_j}{\partial x_i} \right] \\ & - C_{ve}^2 \frac{k^3}{\nu \epsilon^2} \left[ \frac{\partial \bar{u}_i}{\partial x_\ell} + \frac{\partial \bar{u}_\ell}{\partial x_i} \right] \left[ \frac{\partial \bar{u}_\ell}{\partial x_j} + \frac{\partial \bar{u}_j}{\partial x_\ell} \right] \end{aligned} \quad (14)$$

where  $1 \leq \ell \leq 3$ . The various correlation coefficients  $C_v^\alpha$  are defined (ref. 8). The variables  $k$  and  $\epsilon$  are the turbulence kinetic energy and isotropic dissipation function, respectively.

$$k \equiv \frac{1}{2} \overline{u_i' u_i'} \quad (15)$$

$$\epsilon \equiv \frac{2\nu}{3} \overline{\left[ \frac{\partial u_i'}{\partial x_j} \frac{\partial u_j'}{\partial x_k} \right] \delta_{jk}} \quad (16)$$

They are solutions to the corresponding parabolic form of the governing differential equations (ref. 6),

$$\begin{aligned} L(k) = & \frac{\partial}{\partial x_j} \left[ \bar{u}_j k + (1 - \delta_{j1}) \left( C_k \overline{u_i' u_j'} \frac{k}{\epsilon} - \nu \right) \frac{\partial k}{\partial x_j} \right] \\ & + \overline{u_i' u_j'} \frac{\partial \bar{u}_i}{\partial x_j} + \epsilon = 0 \end{aligned} \quad (17)$$

$$\begin{aligned}
L(\epsilon) = \frac{\partial}{\partial x_j} \left[ \bar{u}_j \epsilon + (1 - \delta_{j1}) \left( C_{\epsilon} \overline{u_i' u_j'} \frac{k}{\epsilon} \right) \frac{\partial \epsilon}{\partial x_j} \right] \\
+ C \overline{u_i' u_j'} \frac{\epsilon}{k} \frac{\partial \bar{u}_i}{\partial x_j} + C_{\epsilon}^2 \frac{\epsilon^2}{k} = 0
\end{aligned} \tag{18}$$

The correlation coefficients  $C_k$  and  $C_{\epsilon}^{\alpha}$  have been determined from analysis and experiment (ref. 8).

## SECTION III

### NUMERICAL SOLUTION ALGORITHM

#### 1. Finite Element Formulation

The Navier-Stokes equation system, and the various sub-systems for study have been expressed. Denote the dependent variable set for any given equation system as  $\{q\}$  with members  $q_i$ . Then, for the one-dimensional Euler equations 7-10,  $\{q\}^T = \{\rho, \rho u, \rho e, p\}$ , for the two-dimensional laminar flow Navier-Stokes simplification of equations 1-7,  $\{q\}^T = \{\rho, \rho u_1, \rho u_2, p\}$ , and for the three-dimensional turbulent, incompressible parabolic Navier-Stokes equations 11-18,  $\{q\}^T = \{\bar{u}_1, \bar{u}_2, \bar{u}_3, p, k, \epsilon\}$ . Upon noting that the  $x_1$  coordinate in equations 11-18 spans the domain of evolution of the solution, i.e.,  $x_1 \in [x_1^0, x]$ , the various developed problem statement differential equation systems, excepting the incompressible continuity equation 11, takes the general form.

$$L(q_i) \equiv \frac{\partial q_i}{\partial \tau} + \frac{\partial}{\partial x_j} \left[ u_j q_i + f_{ij} \right] + f_i = 0 \quad (19)$$

In equation 19,  $f_{ij}(q_j)$  and  $f_i(q_j)$  are specified non-linear functions of their arguments, as determined by the particular equation system. For example, for equation 12,  $f_{ij} \equiv (\bar{p} \delta_{ij} - \bar{\sigma}_{ij} + \overline{u_i' u_j'})$ ,  $f_i \equiv 0$ , while for equation 8,  $f_{ij} = 0$  and  $f_i = \rho u A^{-\rho_0}$ .

The  $n$ -dimensional partial differential equation system (19) is defined on the Euclidean space  $R^n$ , spanned by the  $\vec{x}$  coordinate system with scalar components  $x_i$ ,  $1 \leq i \leq n$ , and  $\tau$  is a generalized initial-value coordinate. The solution domain  $\Omega$  is defined as the product of  $R^n$  and  $\tau$ , for all elements of  $\vec{x}$  belonging to  $R^n$  and all elements of  $\tau$  belonging to the open interval measured from  $\tau_0$ , i.e.,

$$\Omega \equiv R^n \times \tau = \{(\vec{x}, \tau): \vec{x} \in R^n \text{ and } \tau \in [\tau_0, \tau]\}$$

The boundary  $\partial\Omega$  of the solution domain is the product of the boundary  $\partial R$  of  $R^n$ , spanned by  $\vec{x}$ , and  $\tau$ , i.e.,  $\partial\Omega \equiv \partial R \times \tau$ . Thereupon, a differential constraint may be applied of the form

$$\ell(q_i) = a_1 q_i + a_2 \frac{\partial}{\partial x_j} q_i \hat{n}_j + a_3 = 0 \quad (20)$$

In equation 20, the  $a_i$  are specified coefficients and  $\hat{n}_i$  is the outwards pointing unit normal vector. Finally, an initial distribution for  $q_i$  on  $\Omega_0 \equiv R^n \times \tau_0$  is required.

$$q_i(\vec{x}, \tau_0) \equiv q_i^0(\vec{x}) \quad (21)$$

The dissipative finite element solution algorithm for equations 19-21 is a modest extension on the form detailed in reference 5. The approximation  $q_i^h(x_j, \tau)$  to the (unknown) exact solution  $q_i(x_j, \tau)$  to equations 19-21, is constructed from members of a convenient finite-dimensional subspace of  $H_0^1(\Omega)$ , the Hilbert space of all functions possessing square integrable first derivatives and satisfying the boundary condition 20. While extremely flexible in theory, the usual practice is to employ the most elementary functions (polynomials truncated at degree  $k$ ) defined on disjoint interior subdomains  $\Omega_e$ , the union of which forms the discretization of  $\Omega$ . Hence,

$$q_i(\vec{x}, \tau) \approx q_i^h(\vec{x}, \tau) \equiv \sum_{e=1}^M q_i^e(\vec{x}, \tau) \quad (22)$$

and the elemental approximation definition is

$$q_i^e(x, \tau) \equiv \{N_k(\vec{x})\}^T \{QI(\tau)\}_e \quad (23)$$

In equations 22-23,  $i(I)$  is a free index denoting members of  $\{q^h\}$ , and sub- or super-script  $e$  denotes pertaining to the  $e^{th}$  finite element,  $\Omega_e \equiv R_e^n \times \tau$ . The elements of the row matrix  $\{N_k(\vec{x})\}^T$  are assumed polynomials on  $x_j$ ,  $1 \leq j \leq n$ , complete to degree  $k$  and constructed to form a cardinal basis (ref. 9).

The functional requirement of the numerical solution algorithm is to render the error in  $q_i^h$  minimum in some norm. Based upon previous experience (ref. 5), this is accomplished within the context of the finite element algorithm by requiring the error in equations 19 and 20,

i.e.,  $L(q_i^h)$  and  $\ell(q_i^h)$  be orthogonal to the space of functions employed to define  $q_i^h$ . To control non-linearly induced instabilities, it is further required that the error in  $\nabla L(q_i^h)$  also be orthogonal to  $\{N_k\}$ . For the parabolic Navier-Stokes equations (as well as the incompressible Navier-Stokes equations), it is also required that the continuity equation 11 be applied as a differential constraint on solution of equations 12-13. Identifying the (Lagrange) multiplier set  $\beta_i$ , these four independent constraints are linearly combined to form the theoretical statement of the finite element solution algorithm.

$$\int_{R^n} \{N_k\} L(q_i^h) d\vec{x} + \vec{\beta}_1 \cdot \int_{R^n} \{N_k\} \nabla L(q_i^h) d\vec{x} + \beta_2 \int_{\partial R^n} \{N_k\} \ell(q_i^h) d\vec{x} + \beta_3 \int_{R^n} \nabla \{N_k\} L(\rho_0^h) d\vec{x} \equiv \{0\} \quad (24)$$

Upon selection of  $k$  in equation 23, equation 24 represents a system of ordinary differential equations on  $\tau$ , of the form

$$[C]\{QI\}' + [U]\{QI\} + [FIJ]\{QJ\} + \{FI\} = \{0\} \quad (25)$$

A one-to-one correspondence of terms in equations 25 and 19 is inferred, with the matrices in equation 25 augmented to contain the various additional terms introduced through  $\beta_i \neq 0$  in equation 24. (Detailed expansions are presented in a latter section.) An efficient, accurate and versatile integration algorithm for equation 25 is the trapezoidal rule, see reference 2. Hence.

$$\{FI\} \equiv \{QI\}_{j+1} - \{QI\}_j - \frac{\Delta\tau}{2} [\{QI\}'_{j+1} + \{QI\}'_j] \equiv \{0\} \quad (26)$$

defines the system of non-linear algebraic equations for determination of the elements of  $\{QI(\tau)\}$ .

The Newton iterative solution algorithm for equation 26 is

$$[J(FI)]_{j+1}^p \{\delta QI\}_{j+1}^{p+1} = -\{FI\}_{j+1}^p \quad (27)$$

The dependent variable in equation 27 is the iteration vector, related to the solution in the conventional manner.

$$\{QI\}_{j+1}^{p+1} \equiv \{QI\}_{j+1}^p + \{\delta QI\}_{j+1}^{p+1} \quad (28)$$

The form of the Jacobian is,

$$[J(FI)] \equiv \frac{\partial \{FI\}}{\partial \{QJ\}} \quad (29)$$

the detailed construction of which is direct upon expansion of the equation 24 in terms of the hypermatrix formulation (ref. 3 ).

## 2. Generalized Coordinates

The classical approach to geometric flexibility using a finite element algorithm has been to utilize boundary conforming discretizations, as obtained using isoparametric triangulation in two-dimensions, for example, and retaining the global coordinate system description within equation 19. The alternative procedure, which has become universal with finite difference methods in computational aerodynamics, is to generate a boundary conforming coordinate transformation, and manipulate the solution statement 19 onto the transformed coordinate system. Only modest differences exist between this concept and the isoparametric finite element formulation. However, the transformation of the algorithm statement 24 to the transformed (regular) grid introduces a considerable flexibility and efficiency previously absent in the classical finite element formulation.

The basic requirement is to generate and utilize a regularizing coordinate transformation, that maps generally curved-sided domain boundaries  $\partial R^n$  onto coordinate surfaces of the unit square (cube). The coordinate system  $\vec{\eta}$  spanning the transformed domain is (assumed) orthogonal and regular; the coordinate transformation is simply

$$x_i = x_i(\eta_j) \quad (30)$$

The particular procedure utilized to establish equation 30 is ancillary to this development, but includes methods utilizing Poisson equation solutions (ref. 10) or any other analytical or numerical procedure (cf., ref. 11). Specifically, one candidate algebraic procedure is application

of the classical finite element isoparametric and bi-quadratic cardinal basis  $\{N_2(\vec{\eta})\}$  to interpolation of the nodal coordinate distributions defined for sub-domains  $R_m^n$  of  $R^n$ . Figure 1 illustrates the concept; referring to equation 23, the transformation statement is,

$$x_i \equiv \{N_2(\vec{\eta})\}^T \{XI\}_e \quad (31)$$

where the elements of  $\{XI\}$  are the values that  $x_i$  takes at the location of vertex and non-vertex nodes defining the (curved) boundaries of the global subdomain of  $R_m^n$ . For reference, the elements of the cardinal basis  $\{N_2(\eta_1, \eta_2)\}$  for  $R_m^2$  are

$$\{N_2(\eta_i)\} = \frac{1}{4} \begin{pmatrix} (1 - \eta_1)(1 - \eta_2)(-\eta_1 - \eta_2 - 1) \\ (1 + \eta_1)(1 - \eta_2)(\eta_1 - \eta_2 - 1) \\ (1 + \eta_1)(1 + \eta_2)(\eta_1 + \eta_2 - 1) \\ (1 - \eta_1)(1 + \eta_2)(-\eta_1 + \eta_2 - 1) \\ 2(1 - \eta_1^2)(1 - \eta_2^2) \\ 2(1 + \eta_1^2)(1 - \eta_2^2) \\ 2(1 - \eta_1^2)(1 + \eta_2^2) \\ 2(1 - \eta_1)(1 + \eta_2^2) \end{pmatrix} \quad (32)$$

The elements of  $\{N_2(\vec{\eta})\}$  for  $R_m^3$  are given in reference 1, Ch. 8.

Returning to the issue, the differential requirement is transformation of the divergence operator in equation 19, i.e.

$$\frac{\partial}{\partial x_i} = \frac{\partial \eta_j}{\partial x_i} \frac{\partial}{\partial \eta_j} \quad (33)$$

The elements of the inverse Jacobian  $J^{-1} \equiv [\partial \eta_i / \partial x_j]$  are evaluated as,

$$\left[ \frac{\partial \eta_i}{\partial x_j} \right] \equiv J^{-1} = \frac{1}{\det[J]} [\text{transformed cofactor of } J] \quad (34)$$

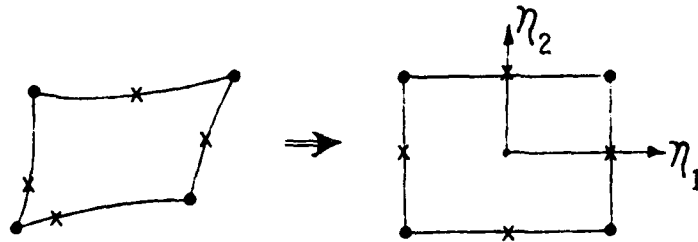
where

$$[J] \equiv \left[ \frac{\partial x_i}{\partial \eta_j} \right] \quad (35)$$

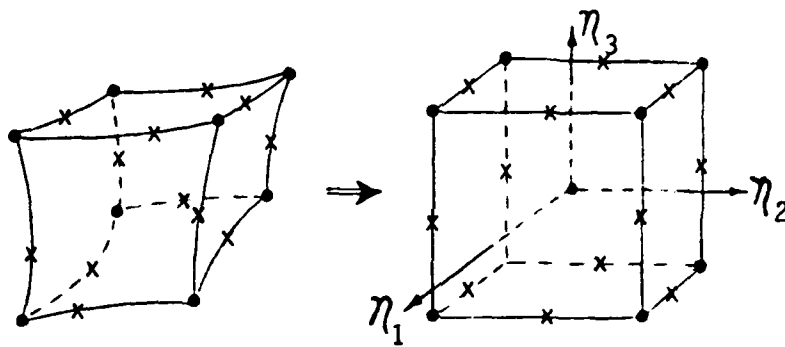


Physical Domain

Transformed Domain



a) Two-Dimensional Domain  $R^2$



b) Three-Dimensional Domain  $R^3$

Figure 1: Biquadratic Cardinal Basis Coordinate Transformation

is directly evaluable using equation 30 or 31. Furthermore, the differential element for equation 24 is

$$d\vec{x} = \det[J] d\vec{\eta} \quad (36)$$

Consider, for example, equation 19 corresponding to the momentum equation 2, and using the Green-Gauss form of the divergence theorem, the first term in equation 24 becomes

$$\begin{aligned} \int_{R^n} \{N\} L(\rho u_i^h) d\vec{x} &= \int_{R^n} \{N\} \frac{\partial \rho u_i^h}{\partial t} \det[J] d\vec{\eta} \\ &+ \oint_{\partial R^n} \{N\} \left[ u_j^h \rho u_i^h + p^h \delta_{ij} - \sigma_{ij}^h \right] \cdot \hat{n}_j \det[J] d\vec{\eta} \\ &- \int_{R^n} \frac{\partial \{N\}}{\partial \eta_k} \left[ \frac{\partial \eta_k}{\partial x_j} \right] \left[ u_j^h \rho u_i^h + p^h \delta_{ij} - \sigma_{ij}^h \right] \det[J] d\vec{\eta} \end{aligned} \quad (37)$$

Identify the contravariant components of convection velocity,

$$\bar{u}_k^h \equiv \det[J] \left[ \frac{\partial \eta_k}{\partial x_j} \right] u_j^h \quad (38)$$

with scalar components parallel to the  $\eta_k$  coordinate system. Note that in using an algebraic transformation, equation 31,  $\det[J]$  cancels in equation 34 yielding

$$\bar{u}_k^h = [\text{Cof.}J] u_j^h \quad (39)$$

where  $[\text{Cof.}J]$  is the transformed co-factor matrix of  $[J]$ . Otherwise, only the elements  $\partial \eta_k / \partial x_j$  are known at node coordinates, and equation 38 is evaluated directly.

Using equations 22-23, 38-39, and neglecting the surface integral for the moment, equation 37 becomes

$$\begin{aligned}
\int_{R^n} \{N\} L(\rho u_i^h) dx \Rightarrow S_e \left[ \int_{R_e^n} \{DET\}_e^T \{N\} \{N\}^T \{RHOUI\}_e dn \right. \\
- \int_{R_e^n} \{UBARK\}_e^T \{N\} \frac{\partial}{\partial \eta_k} \{N\} \{N\}^T \{RHOUI\}_e dn \\
- \int_{R_e^n} \{ETAKI\}_e^T \{N\} \frac{\partial}{\partial \eta_k} \{N\} \{N\}^T \{P\}_e dn \\
\left. + \int_{R_e^n} \{ETAKJ\}_e^T \{N\} \frac{\partial}{\partial \eta_k} \{N\} \{N\}^T \{SIGIJ\}_e dn \right] \quad (40)
\end{aligned}$$

For equation 40, since the  $\{N_k\}$  for  $q_i^h$  are locally defined on  $R_e^n$ , the limits for the integrals correspond, and  $S_e$  is the operator projecting element contributions to the corresponding global matrices, equation 25. Furthermore, the determinant of  $J$  is assumed interpolated on the element domain  $R_e^n$  using  $\{N_k\}$  and the nodal values. Similarly,  $(\partial \eta_k / \partial x_i)$  is recast as its interpolate  $\{ETAKI\}_e^T \{N_k\}$  (and also  $\det J(\partial \eta_k / \partial x_j)$ ). The e-subscripted terms in equation 40 are independent of  $\eta_k$  and can be extracted from the integrand, leaving only products of the polynomials and derivatives in  $\{N_k\}$ . These are directly evaluable, independent of the particular choice for equation 30, using numerical quadrature. Hence, the standardized solution form, for the first term in equation 24, as formed from equation 2, is

$$\begin{aligned}
\int_{R^n} \{N\} L(\rho u_i^h) dx \Rightarrow S_e \left[ \{DET\}_e^T [M3000] \{RHOUI\}_e \right. \\
- \{UBARK\}_e^T [M30K0] \{RHOUI\}_e \\
- \{ETAKI\}_e^T [M30K0] \{P\}_e \\
\left. + \{ETAKL\}_e^T [M30K0] \{SIGIL\}_e \right] \quad (41)
\end{aligned}$$

In equation 41, the indices K and L obey the tensor summation rule, I is the free index (for  $\rho u_i^h$ ),  $S_e$  is the assembly operator, and [M30K0] is the hypermatrix equivalent of  $\partial/\partial \eta_j$  (transformed) contracted with corresponding element distributions. From the standpoint of the coordinate transformation,  $\{DET\}_e$  is the nodal distribution of  $\det [J]$  on  $R_e^n$ , while  $\{ETAKI\}_e$  and  $\{ETAKL\}_e$  are corresponding nodal distributions of components of  $J^{-1}$  on  $R_e^n$ .

Within this generalized coordinate framework for the finite element algorithm, the grid and metric data required for a numerical simulation are the nodal distributions of  $J^{-1} = [\partial \eta_k / \partial x_j]$ ,  $\det [J] = \det [\partial x_i / \partial \eta_k]$ , and the elemental partition measures  $\Delta_e$ . These parameters need only be sufficiently smooth such that interpolation on the elemental domain  $R_e^n$  makes sense. Using a Poisson equation-generated coordinate transformation, for example, these parameters are globally smooth since they are determined on the global domain  $R^n$ . Alternatively, the transformation parameters constructed on the union of macro-domains  $R_m^e$  is further discretized into the union of finite element domains  $R_m^n$ , and J is smooth on  $R_m^n$ .

### 3. Tensor Matrix Product Jacobian

From the standpoint of efficiency, it is desirable to construct a tensor matrix product form of the Jacobian defined in equations 27 and 29. Such a construction is readily accomplished, provided the tensor product cardinal basis function set  $\{N_k(\vec{\eta})\}$  is utilized, spanning quadrilateral and hexahedron domains on  $R^2$  and  $R^3$  respectively. In this instance, the Jacobian matrix  $[J(FI)]$ , equation 27, is replaced by the tensor (outer) product construction

$$[J(FI)] \Rightarrow [J_1] \otimes [J_2] \otimes [J_3] \quad (42)$$

Each component  $[J_\alpha]$  is constructed from its definition, equation 29, assuming interpolation and differentiation are one-dimensional. The corresponding formalism in finite difference methodology is called approximate factorization cf., ref. 12. Using equation 42, the solution statement 27 becomes

$$[J_1] \otimes [J_2] \otimes [J_3] \{QI\}_{j+1}^{p+1} = - \{FI\}_{j+1}^p \quad (43)$$

Define

$$\begin{aligned}
 [J_2] \otimes [J_3] \{\delta QI\}_{j+1}^{p+1} &\equiv -\{P1\}_{j+1}^{p+1} \\
 [J_3] \{\delta QI\}_{j+1}^{p+1} &\equiv -\{P2\}_{j+1}^{p+1}
 \end{aligned} \tag{44}$$

Then, the operational sequence for equation 43 is

$$\begin{aligned}
 [J_1] \{P1\}_{j+1}^{p+1} &= -\{FI\}_{j+1}^p \\
 [J_2] \{P2\}_{j+1}^{p+1} &= -\{P1\}_{j+1}^{p+1} \\
 [J_3] \{\delta QI\}_{j+1}^{p+1} &= -\{P2\}_{j+1}^{p+1}
 \end{aligned} \tag{45}$$

Obviously, other permutations of the index structure for  $[J_\alpha]$  could be utilized for equations 44-45. The key aspect of the tensor matrix product Jacobian is the replacement of the very large (albeit sparse) matrix  $[J]$ , with  $\alpha$  block-diagonal structured matrices  $[J_\alpha]$ . The primary attribute is up to several orders of magnitude reduction in computer core storage requirements for the Jacobian, as well as significantly reduced CPU to construct the LU decomposition and perform the back substitution. It must be emphasized that this procedure in no way affects the formation of  $\{FI\}$ , equation 27, wherein lies the accuracy features intrinsic to the finite element algorithm statement, equation 24. Compromises in the construction of  $\{FI\}$  will invariably produce inferior results for equation 19 non-homogeneous and a vector.

As an example of construction of  $[J_\alpha]$ , consider only the initial-value term equation 37. The corresponding term in the Jacobian, equation 29, using equations 25, 26 and 41, is

$$\frac{\partial \{FI\}}{\partial \{QJ\}} = S_e \left[ \Delta_e \{DET\}_e^T [M3000] \delta_{IJ} \right] \tag{46}$$

where  $\delta_{IJ}$  is the (discrete index) Kronecker delta. Then, referring to equation 40,

$$[J]_e = \Delta_e \{DET\}_e^T [M3000] \equiv \int_{R_e^n} \{DET\}_e^T \{N_k(\vec{\eta})\} \{N_k(\vec{\eta})\} \{N_k(\vec{\eta})\}^T d\vec{\eta} \quad (47)$$

Assume for simplicity the most elementary case, i.e.,  $k = 1$ ,  $n = 2$  and  $\vec{x} \equiv \vec{\eta}$ , i.e., identity coordinate transformation. Equation 47 becomes, assuming  $M \equiv B$  for  $n = 2$

$$\Delta_e \{ONE\}_e^T [B3000] = \Delta_e [B200] \equiv \int_{R_e^2} \{N_1(\vec{x})\} \{N_1(\vec{x})\}^T d\vec{x} \quad (48)$$

Assuming the rectangular element domain  $R_e^2$  described by measures  $\ell$  and  $\omega$ , the evaluation of equation 48 yields

$$[J]_e = \Delta_e [B200] = \ell\omega [B200] = \frac{\ell\omega}{36} \begin{bmatrix} 4 & 2 & 1 & 2 \\ & 4 & 2 & 1 \\ & & 4 & 2 \\ (sym) & & & 4 \end{bmatrix} \quad (49)$$

The tensor product construction for this matrix involves the evaluation of equation 48 constrained to one-dimension. Hence, denoting  $M \equiv A$  for  $n = 1$ ,

$$[J_\alpha]_e \equiv \Delta_e^\alpha [A200] = \int_{R_e^\alpha} \{N_1(x_\alpha)\} \{N_1(x_\alpha)\}^T dx_\alpha \quad (50)$$

and

$$[J_1]_e = \frac{\ell}{6} \begin{bmatrix} 2 & 1 \\ 1 & 2 \end{bmatrix} \quad (51)$$

assuming  $\Delta_e^1 = \ell$  and  $\Delta_e^2 = \omega$ . By keeping track of entry locations in  $[J]$ , it is easy to show that

$$[J_1]_e \otimes [J_2]_e = [J]_e \quad (52)$$

The extension to more complicated terms in the Jacobian, and to  $k > 1$ ,  $n > 2$ , builds upon the elementary concept.

## SECTION IV

### THEORETICAL ANALYSIS

In reference 5, an elementary truncation error analysis was documented for the one-dimensional linear form of equation 24, assuming  $\beta_3 \equiv 0$ . The results of numerical experiments reported therein indicated that superior accuracy accrued to definition of a family of coefficients  $\vec{\beta}_1^i$ , with distinct values utilized in each term in equation 24, as produced for the study equation

$$L(u) = \frac{\partial q}{\partial t} + U_0 \frac{\partial q}{\partial x} = 0 \quad (53)$$

A comprehensive von Neumann stability analysis has been completed for equation 53, assuming that  $\vec{\beta}_1^i \equiv \{v_1 \Delta_e, v_2 \Delta_e\} \hat{i}$ , where  $v_1$  and  $v_2$  are employed for the first and second terms in equation 53, respectively. The Fourier solution for equation 53 is

$$q(x,t) = V \exp [i\omega(x-U_0 t)] \quad (54)$$

The semi-discrete Fourier solution is

$$q^h(j\Delta x, t) = V \exp [i\omega(j\Delta x - \Gamma t)] \quad (55)$$

Here,  $\Gamma \equiv \sigma + i\delta$ , where  $\sigma$  and  $\delta$  are real numbers,  $i = \sqrt{-1}$ ,  $\omega = 2\pi/\lambda$  is the wave number for wavelength  $\lambda$ , and  $V$  is the initial distribution. Using the linear finite element basis,  $k=1$  in equation 23, the algorithmic statement (equations 24-25) for equation 53 can be written in the finite difference recursion form (ref. 5),

$$S_e \left[ [C_\alpha]_e \{Q\}_e \right] \Rightarrow \frac{\Delta \alpha}{6} \left[ (1+3v_1)Q_{j-1} + 4Q_j + (1-3v_1)Q_{j+1} \right] \quad (56)$$

$$S_e \left[ [U_\alpha]_e \{Q\}_e \right] \Rightarrow \frac{U_0}{2} \left[ -(1+2v_2)Q_{j-1} + 4v_2 Q_j + (1-2v_2)Q_{j+1} \right]$$

$$= \frac{U_0}{2} [-Q_{j-1} + Q_{j+1}] + U_0 v_2 [-Q_{j-1} + 2Q_j - Q_{j+1}] \quad (57)$$

assuming a uniform discretization of  $R^\alpha$  of measure  $\Delta^\alpha$ . The second form in equation 57 emphasizes the role of  $U_0 v_2$  as a "viscosity." Substituting equation 55 in 56-57, and proceeding through the lengthy algebra yields

$$\begin{aligned} \sigma &= \frac{U_0 \left[ 1 - \frac{2d^2}{3!} + \frac{6d^4}{5!} + 0(d^6) + v_1 v_2 \left[ d^2 - \frac{d^4}{4} + 0(d^6) \right] \right]}{\left[ 1 - \frac{d^2}{3!} + \frac{d^4}{18} + 0(d^6) \right] + v_1^2 \left[ d^2 - \frac{d^4}{4} + 0(d^6) \right]} \\ \delta &= \frac{U_0 \left[ v_2 \left( -d + \frac{d^3}{4} + 0(d^5) \right) + v_1 \left( d - \frac{d^3}{3} + 0(d^5) \right) \right]}{\left[ 1 - \frac{d^2}{3} + \frac{d^4}{18} + 0(d^6) \right] + v_1^2 \left[ d^2 - \frac{d^4}{3} + 0(d^6) \right]} \end{aligned} \quad (58)$$

where  $d = \omega \Delta x$  and 0 indicates order. Expanding the denominator and retaining all terms to order  $d^6$  yields

$$\sigma \approx U_0 \left[ 1 - v_1(v_1 - v_2)d^2 + \left\{ \frac{-1}{180} + \frac{v_1 v_2}{12} + v_1^3(v_1 - v_2) \right\} d^4 + 0(d^6) \right] \quad (59a)$$

$$\delta \approx U_0 \left[ (v_1 - v_2)d - \left\{ \frac{v_2}{12} - v_1^2(v_1 - v_2) \right\} d^3 + 0(d^5) \right] \quad (59b)$$

Setting  $v_1 \equiv v_2 \equiv v = 1/\sqrt{15}$  yields the results of reference 5.

$$\begin{aligned} \sigma &\approx U_0 [1 + 0(d^6)] \\ \delta &\approx U_0 \left[ \frac{-d^3}{12} + 0(d^5) \right] \end{aligned} \quad (60)$$



as obtained by requiring the third coefficient in equation 59a to vanish. The corresponding level of artificial diffusion ( $\delta$ ) is documented as excessive for the linear and nonlinear example problems computed in reference 5. By not requiring  $v_1$  and  $v_2$  be equal, enforcing sixth order accuracy in equation 59a yields

$$v_2 = \frac{v_1^2 + \frac{d^2}{180} - v_1^4 d^2}{v_1(1 + \frac{d^2}{12} - v_1^2 d^2)} \quad (61)$$

Noting that  $d \equiv \omega \Delta x = 2\pi/n$ , since the approximate solution resolves discrete wave lengths  $\lambda_n = n\Delta^\alpha$ , equation 61 can be solved for a range of  $v_1 > 0$  and  $n \geq 2$ . Figure 2 is a plot of this solution. Only for large  $n$  is the relationship linear, for  $v_1$  sufficiently large, and all solutions converge at  $v_1 = 1/\sqrt{15} = v_2$ .

The linear and nonlinear two-dimensional pure convection test cases, originally reported in reference 5, were computationally reexamined. Figure 3 illustrates a typical final solution for the linear rotating cone test case, with its attendant loss in peak level and trailing dispersion wake. Table 1 summarizes solution inaccuracy on these basis, as well as loss of symmetry, for a range of  $v_1$  and  $v_2$ . The best accuracy accrues to use of  $v_1 \approx 0.01$  and  $v_2/v_1 \approx 0.75$ . Both levels are well below the optimal order-of-accuracy determination, see Figure 2, or the elementary analysis results  $v_2 = v_1 = v = 1/\sqrt{15}$ . This determination changes only modestly over the Courant number range  $0.1 \leq C \leq 0.7$ , and is unchanged using the conservative form for equation 53.

Figure 4 illustrates a typical final solution for the nonlinear traveling square wave test case, wherein  $U_0$  in equation 53 is replaced by the dependent variable  $q$ . Table 2 summarizes solution accuracy in the wave center region, in terms of plateau level, depth of the precursor wake and the spread of the wave front (in units of mesh measure  $\Delta$ ). For the nonconservative form of equation 53, the "optimal"  $v_2 = 1/\sqrt{15}$  and setting  $v_1$  zero yields an acceptably accurate solution, except for the spread to  $4\Delta$  of the original  $1\Delta$  interpolation of the wave. Decreasing  $v_2$  by  $\sqrt{2}$  sharpens the front and induces a modest peak at the plateau interface. For the conservative equation statement,

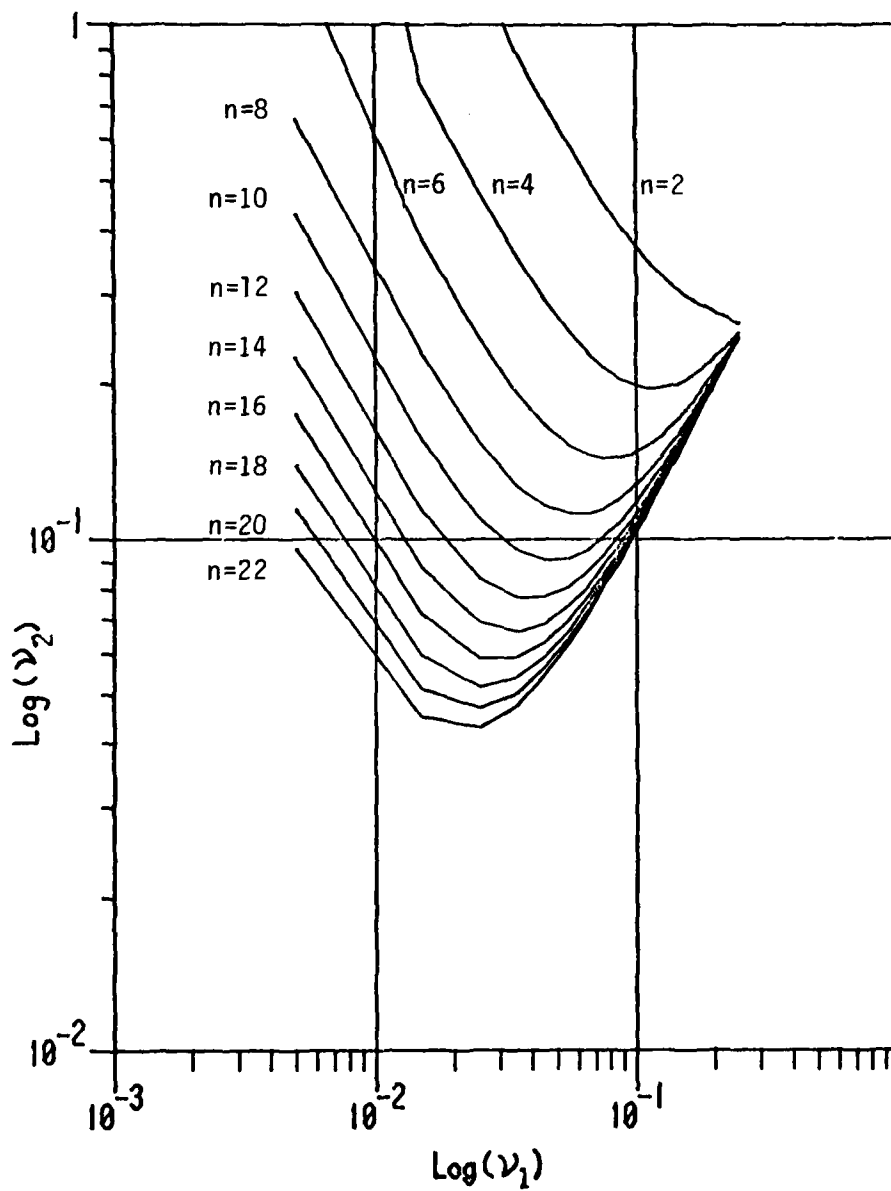


Figure 2. Distribution of Solution to Equation 61

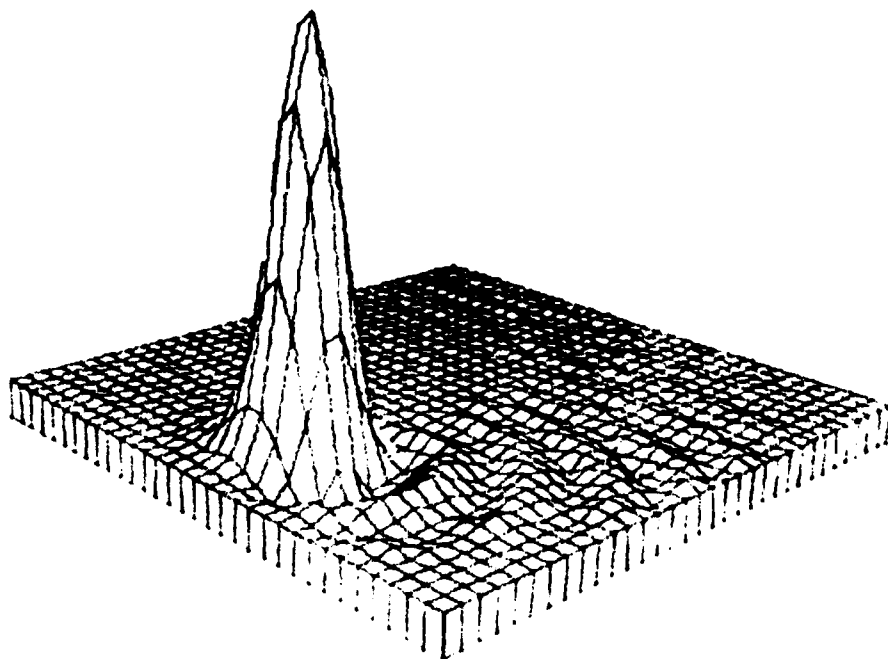


Figure 3. Final Station Solution for Rotating Cone Test Case,  
Linear Finite Element Algorithm,  $v_1 = 0 = v_2$ .

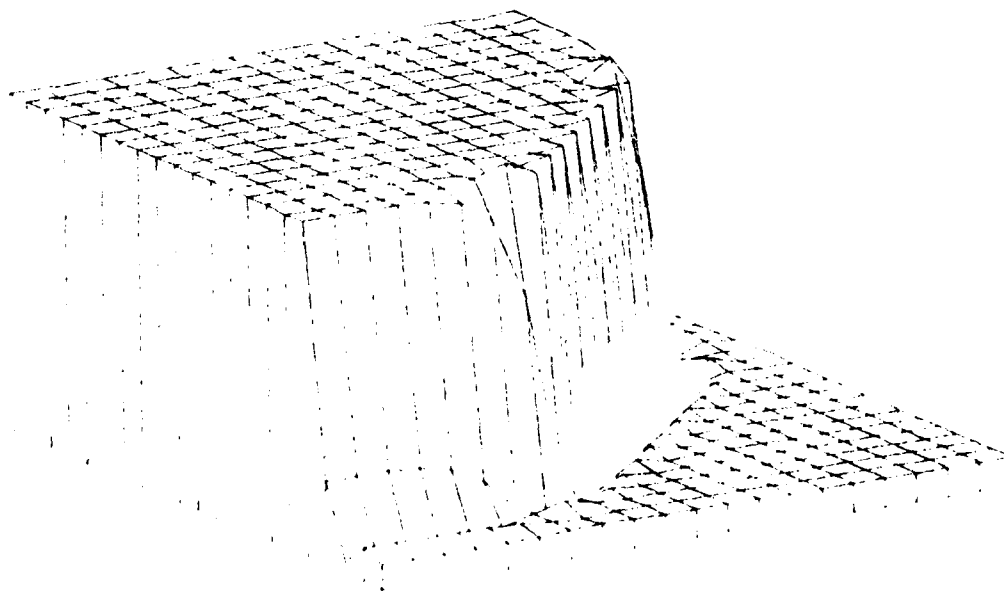


Figure 4. Final Station Solution for Non-Linear Square Wave  
Test Case, Linear Finite Element Algorithm,  
 $v_1 = .15/\sqrt{T5}$ ,  $v_2 = 2/\sqrt{T5}$ .

Table 1  
Rotating Cone Solution Accuracy Summary  
Linear Finite Element Algorithm, C=0.5

Dissipation Levels		Solution Error (Percent)		
$v_1$	$v_2$	Peak	Symmetry	Wake
.0	.0	-7.0	-1.0	-17.0
.0	.0076	-22.0	-5.0	-9.0
.012	.0076	+2.0	-2.0	-21.0
.012	.0092	-2.0	$\pm 0.0$	-19.0
.012	.0114	-7.0	$\pm 0.0$	-16.0
.015	.0076	+10.0	-6.0	-26.0
.030	.0076	+17.0	-50.0	-74.0
.258	.258	-22.0	-	0.

Table 2  
Non-Linear Square Wave Solution Accuracy Summary  
Linear Finite Element Algorithm, C = 0.5

Dissipation Levels x (1/ $\sqrt{15}$ )		Solution Error			Algorithm Form
$v_1$	$v_2$	Wave Peak	Precursor Wake	Wave Spread ( $\Delta$ )	
.0	1/ $\sqrt{2}$	+.07	-.05	2	Non-Conservative
.0	1.0	-.04	-.05	4	"
.0	$\sqrt{2}$	-.13	-.06	4	"
.0	1.0	+.21	-.10	2	"
.0	$\sqrt{2}$	+.09	-.05	2	Conservative
.0	2.0	-.04	-.05	4	"
.10	"	-.01	-.05	2	"
.15	"	.00	-.05	2	"
.20	"	+.01	-.06	2	"
.10	1.0	+.11	-.11	2	"
.1/ $\sqrt{2}$	$\sqrt{2}$	+.15	-.09	2	"

$$L(q) = \frac{\partial q}{\partial t} + \frac{1}{2} \frac{\partial}{\partial x} (q^2) = 0$$

the "optimal" level of  $\nu_2$  is multiplied by 2 for compensation. The wave front sharpness is refined without inducing a plateau peak by setting  $\nu_1/\nu_2 \approx 0.1$ . These determinations remain generally valid over the range of useful Courant numbers.

The square wave test was repeated for the linear advection equation 53. Even though the problem specification is linear, the resultant coarse grid introduces unacceptable dispersion error to the non-dissipative solution, see Figure 5a. Figure 5b illustrates the error control achieved using  $\nu_2 = 1/\sqrt{15}$  and  $\nu_1/\nu_2 = 2/3$ , and Table 3 summarizes solution fidelity on the same basis as the non-linear square wave. These results further confirm the utility of distinct levels for  $\nu_1$  and  $\nu_2$ .

Table 3  
Linear Square Wave Solution Accuracy Summary  
Linear Finite Element Algorithm,  $C = 0.5$

Dissipation Levels x (1/ $\sqrt{15}$ )		Solution Error		
		Wave Peak	Precursor Wake (%)	Wave Spread ( $\Delta$ )
$\nu_1$	$\nu_2$			
.0	.0	+.40	-3	2
.5	1.0	.00	-1	3
.67	1.0	.00	-1	3
1.0	1.0	.26	-5	2

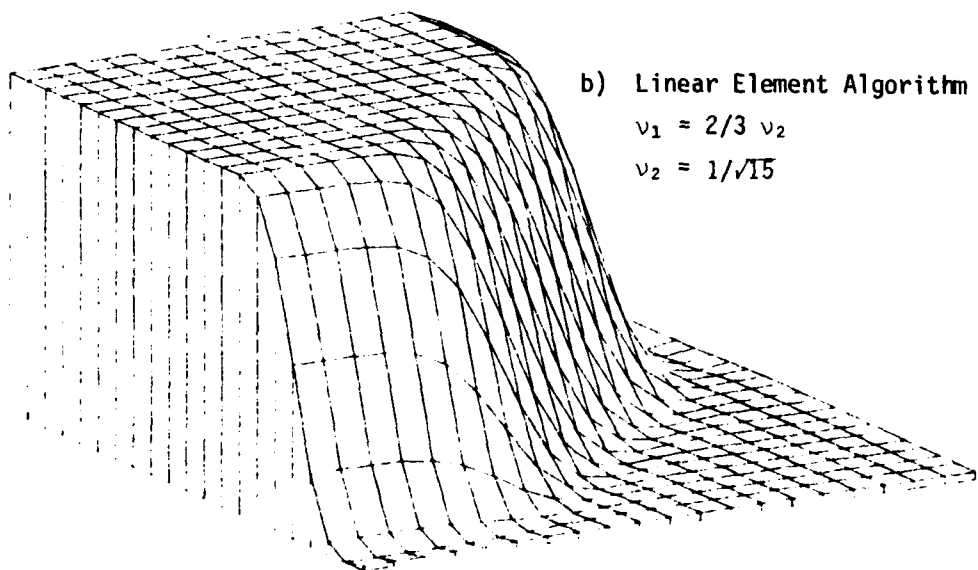
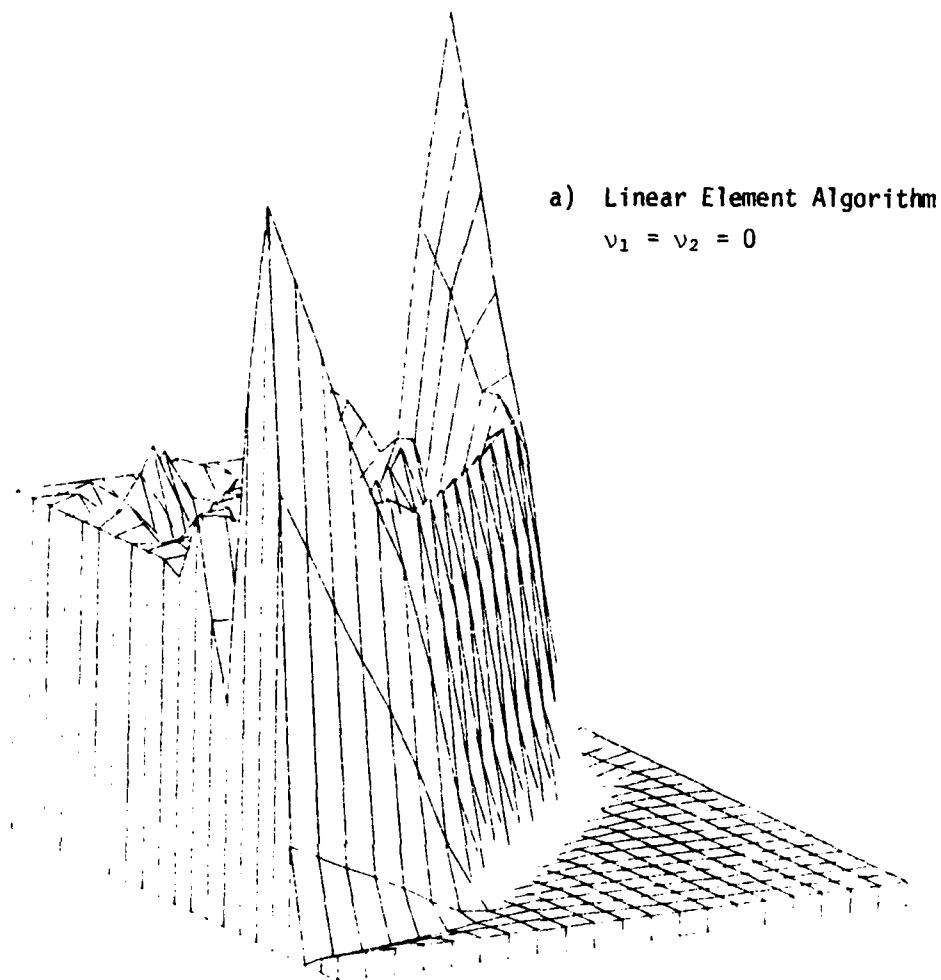


Figure 5. Final Station Solution for Linear Square Wave Test Case, Linear Finite Element Algorithm.

Viewing these results, it is apparent that modest levels of  $v_1$  can exert a profound impact on solution fidelity in both linear and nonlinear applications. The correction mechanism appears as inducement of a leading phase error that compensates for the lagging error intrinsic to the basic algorithm. Selecting optimal order-of-accuracy as the criterion for determination of  $v_2$  does not appear inappropriate for the linear problem, for which the Fourier analysis is exact. In concert, this analysis does estimate the near-optimal level of  $v_2$  for the nonlinear problem. Viewing Figure 2, the coordinate  $v_2 = 2/\sqrt{15}$ ,  $v_1/v_2 = 0.1$ , lies near the centroid of the distribution on  $n$ , indicating existence of the computational compromise.

The von Neumann stability analysis has been extended to the quadratic element algorithm statement,  $k = 2$  in equation 23. For a uniform discretization, with  $\Delta_e = 2\Delta x$ , the finite difference recursion relation forms for the two terms in equation 53, at the vertex nodes of the discretization, are

$$S_e \left[ [C]_e \{Q\}_e \right] \Rightarrow \frac{\Delta^2}{30} \left[ -(1+5v_1)Q_{j-2} + 2(1+10v_1)Q_{j+1} + 8Q_j \right. \\ \left. + 2(1-10v_1)Q_{j+1} - (1-5v_1)Q_{j+2} \right] \quad (63)$$

$$S_e \left[ [U_\alpha]_e \{Q\}_e \right] \Rightarrow \frac{U_0}{6} \left[ (1+2v_2)Q_{j-2} - 4(1+4v_2)Q_{j-1} + 28v_2Q_j \right. \\ \left. + 4(1-4v_2)Q_{j+1} - (1-2v_2)Q_{j+2} \right] \\ = \frac{U_0}{6} \left[ Q_{j-2} - 4Q_{j-1} + 4Q_{j+1} - Q_{j+2} \right] \\ + \frac{v_2 U_0}{3} \left[ Q_{j-2} - 8Q_{j-1} + 14Q_j - 8Q_{j+1} + Q_{j+2} \right] \quad (64)$$

The second form for equation 64 again emphasizes the role of  $v_2 U_0$  as a "viscosity." Inserting equation 55 in 63-64, and proceeding through the lengthy algebra yields a simultaneous equation system for  $\sigma$  and  $\delta$ . Expanding the determinant and retaining all terms to  $O(d^6)$  yields

$$\begin{aligned} \sigma \approx U_0 \left[ 1 - 4v_1 v_2 + \frac{d^2}{15} (-14 + 184v_1 v_2 - 60v_1^2 + 240 v_1^3 v_2) \right. \\ \left. + d^4 \left( \frac{2}{5} - \frac{542}{150} v_1 v_2 + \frac{8}{3} v_1^2 - \frac{672}{15} v_1^3 v_2 + 16 v_1^4 - 64 v_1^5 v_2 \right) \right. \\ \left. + O(d^6) \right] \quad (65) \end{aligned}$$

Equation 65 indicates the quadratic element algorithm only second order accurate for  $v_1 = 0$  and/or  $v_2 = 0$ . Numerical experience, to be discussed, indicates  $v_1 = 0$  and  $v_2 \approx O(1/\sqrt{15})$  is preferable for accuracy. The recursion relations for the non-vertex nodes of the quadratic algorithm are provided by equations 56-57, by making the identities  $j \Rightarrow j+1$  and  $j \Rightarrow j-1$ . Hence, the interaction of these two relations, in concert with  $v_1 = 0$ , must reinforce to provide the excellent phase accuracy associated with use of the quadratic element formulation.

As will become documented, this linearized theoretical analysis does accurately estimate approximate levels for  $v_1$  and  $v_2$ . Importantly, the theoretical statement of the finite element algorithm, equation 24, is confirmed to induce a phase-selective dissipation capable of controlling non-linearly induced instabilities as well as distributed phase celerity. The progression to more complete equation systems is required for further quantization.



## V. DISCUSSION AND RESULTS

### 1. One-Dimensional Compressible Flow

Equations 7-10 express the conservative formulation for one-dimensional, inviscid compressible flow in a duct of variable cross-section. The nonconservative form is

$$L(\rho) = \frac{\partial \rho}{\partial t} + u \frac{\partial \rho}{\partial x} + \rho \frac{\partial u}{\partial x} + \rho u A' = 0 \quad (66)$$

$$L(u) = \rho \frac{\partial u}{\partial t} + \rho u \frac{\partial u}{\partial x} + \frac{\partial p}{\partial x} + \rho u^2 A' = 0 \quad (67)$$

$$L(e) = \rho \frac{\partial e}{\partial t} + \rho u \frac{\partial e}{\partial x} + u \frac{\partial p}{\partial x} + p \frac{\partial u}{\partial x} + \rho u e A' = 0 \quad (68)$$

$$L(p) = p - (\gamma - 1) \rho (e - \frac{1}{2} u^2) = 0 \quad (69)$$

For the dissipative, finite element algorithm statement, equation 24,  $\beta_3 \equiv 0$  is appropriate for either equation system. Denoting the elements of  $\{QI\}$  and  $\{FI\}$ ,  $1 < I < 4$ , as  $\{R, U, E, P\}$  and  $\{FR, FU, FE, FP\}$  for clarity, the algorithm statement equation (26) then becomes, for the nonconservative continuity equation 66, for example

$$\begin{aligned} \{FR\} &= ([A200] + v_1^1 [A210]) \{R\}_{j+1,j} + \frac{\Delta t}{2} \left[ \{U\}^T ([A3001] + [A3100]) \{R\} \right. \\ &\quad \left. + v_1^2 \{U\}^T ([A3011] + A3110) \{R\} + \{U\}^T ([A40001] \{A\}) \{R\} \right]_{j+1,j} \\ &= \{0\} \end{aligned} \quad (70)$$

The A-prefix on the matrices in equation 70 denote a one-dimensional evaluation of the corresponding integrals in equation 24. By defining a common denominator, the elements of each matrix are integers with values dependent strictly on the degree  $k$  of the approximation polynomial, equation 23. These matrices, for  $1 < k < 2$ , are given in

Appendix A. The Boolean index 1 indicates the location of the spatial derivative within each term, the 0 indicates simple interpolation, and  $v_1^\alpha$  are the dissipation parameters for the dependent variable  $\rho$ . The index pair  $j+1, j$  denotes evaluation of each term in brackets, using  $\{QI\}_{j+1}^p$  and  $\{QI\}_j$ , and summing, while  $\{ \}^{\sim}_{j+1, j}$  denotes  $\{QI\}_{j+1}^p - \{QI\}_j$ , see equation 26.

The form of equation 70 is particularly attractive for programming, as well as generation of a Jacobian, and a modest expansion for  $k = 1$  elements illustrates the notational structure. In particular, see Appendix A, for  $k = 1$ ,

$$\begin{aligned} [A200]_e &\equiv \frac{\Delta_e}{6} \begin{bmatrix} 2 & 1 \\ 1 & 2 \end{bmatrix} \\ [A210]_e &= \frac{\Delta_e}{2} \begin{bmatrix} -1 & 1 \\ -1 & 1 \end{bmatrix} \end{aligned} \quad (71)$$

The time-derivative term in equation 66, when inserted into equation 24, yields two terms

$$\begin{aligned} \int_{R^1} \{N_k\} \frac{\partial \rho}{\partial t} dx - \beta_1 \int_{R^1} \frac{\partial}{\partial x} \{N_1\} \frac{\partial \rho}{\partial t} dx \\ = S_e \left[ \int_{R_e^1} \{N_1\} \{N_1\}^T dx \{R\}^{\sim} \right. \\ \left. - v_1^1 \Delta_e \int_{R_e^1} \frac{\partial}{\partial x} \{N_1\} \{N_1\}^T dx \{R\}^{\sim} \right] \\ = S_e \left[ \Delta_e [A200]_e \{R\}_e^{\sim} - v_1^1 [A210] \{R\}_e^{\sim} \right] \quad (72) \end{aligned}$$

Inserting equation 71 into 72, assuming  $\Delta_e$  uniform, and assembling ( $S_e$ ) the element contribution at a common node "j" yields identically equation 56. If  $\Delta_e$  was not uniform, then the finite difference recursion relation 72 would have to reflect this, as is already embedded within the hypermatrix form in equation 70. By the same token, for  $\Delta_e$  and  $u_e$  uniform, equation 57 is the finite difference recursion relation

equivalent of the first convection term in equation 66,

$$\begin{aligned}
 & \int_{R^1} \{N_k\} u \frac{\partial \rho}{\partial x} dx - \beta_1 \int_{R^1} \frac{\partial}{\partial x} \{N_k\} u \frac{\partial \rho}{\partial x} dx \\
 &= S_e \left[ \Delta_e \{U\}_e^T [A3001]_e \{R\}_e + v_1^2 \{U\}_e^T [A3011]_e \{R\}_e \right] \\
 &\equiv \left\{ \{U\}^T [A3001] + v_1^2 \{U\}_e^T [A3011] \right\} \{R\} \quad (73)
 \end{aligned}$$

The remaining two terms in equation 70 stem from  $\rho \frac{\partial u}{\partial x}$  and  $\rho u A'$ ; hence

$$\begin{aligned}
 & \int_{R^1} \{N_k\} \left\{ \rho \frac{\partial u}{\partial x} + \rho u A' \right\} dx - \beta_1 \int_{R^1} \frac{\partial}{\partial x} \{N_k\} \rho \frac{\partial u}{\partial x} dx \\
 &= S_e \left[ \Delta_e \{R\}_e^T [A3001] \{U\}_e + v_1^2 \{R\}_e^T [A3011] \{U\}_e \right. \\
 &\quad \left. + \Delta_e \{U\}_e^T [A40001] \{A\}_e \right] \{R\}_e \\
 &\equiv \{U\}^T [A3100] \{R\} + v_1^2 \{U\}_e^T [A3110] \{R\} \\
 &\quad + \{U\}_e^T [A40001] \{A\}_e \{R\} \quad (74)
 \end{aligned}$$

The two right side forms for equation 74 illustrate transposition of pre- and post-contraction vectors. The elements of  $\{A\}_e$  are element nodal values of  $\ln A(x)$ , and  $[A40001]$  is of global rank two and hyper-rank two, see Appendix A.

The finite element algorithm statements for the remaining equations 67-69 are

$$\begin{aligned}
 \{FU\} &= \{R\}^T \left( [A3000] + v_2^2 [A3010] \right) \{U\}_{j+1,j} \\
 &\quad + \frac{\Delta t}{2} \left\{ \{R\}^T [A40010] \{U\} \right\} \{U\} + [A201] \{P\}
 \end{aligned}$$

$$\begin{aligned}
& + v_2^2 \{R\}^T ([A40110] \{U\}) \{U\} \\
& + \{R\}^T (\{U\}^T [A500001] \{A\}) \{U\} \Big]_{j+1,j} = \{0\} \quad (75)
\end{aligned}$$

$$\begin{aligned}
\{FE\} &= \{R\}^T ([A3000] + v_3^1 [A3010]) \{E\}_{j+1,j} \\
&+ \frac{\Delta t}{2} \left[ \{R\}^T ([A40010] \{U\}) \{E\} + \{U\}^T ([A3001] + [A3100]) \{P\} \right. \\
&\quad + v_2^2 \{R\}^T ([A40110] \{U\}) \{E\} \\
&\quad \left. + \{R\}^T (\{U\}^T [A500001] \{A\}) \{E\} \right]_{j+1,j} \\
&= \{0\} \quad (76)
\end{aligned}$$

$$\begin{aligned}
\{FP\} &= [A200] \{P\} - (\gamma-1) \{R\}^T [A3000] \{E\} \\
&+ \frac{\gamma-1}{2} \{R\}^T ([A40000] \{U\}) \{U\} = \{0\} \quad (77)
\end{aligned}$$

In equations 75-76, the matrix [A500001] is of hyperrank three, i.e., the elements are square matrices with column matrices as elements. Equation 77 is simply the interpolation equivalent of an algebraic equation.

The next requirement is to construct the Jacobian of the iteration algorithm, equation 27. From its definition, equation 29, and equations 70, 75-77

$$\begin{aligned}
\frac{\partial \{FR\}}{\partial \{R\}} &\equiv [JRR] = [A200] + v_1^1 [A210] \\
&+ \frac{\Delta t}{2} \{U\}^T \left[ [A3001] + [A3100] + v_1^2 [A3011] \right.
\end{aligned}$$

$$\begin{aligned}
& + v_1^2[A3110] + [A40001]\{A\} \Big]_{j+1}^P \\
\frac{\partial\{FR\}}{\partial\{U\}} \equiv [JRU] &= \frac{\Delta t}{2}\{R\}^T \Big[ [A3100] + [A3001] + v_1^2[A3110] \\
& + v_1^2[A3011] + [A40001]\{A\} \Big]_{j+1}^P \\
[JRE] &= [0] \\
[JRP] &= [0] \tag{78}
\end{aligned}$$

$$\begin{aligned}
\frac{\partial\{FU\}}{\partial\{R\}} \equiv [JUR] &= \frac{1}{2}\{U_{j+1}^P - U_j\}^T ([A3000] + v_1^2[A3010]) \\
& + \frac{\Delta t}{2}\{U\}^T \Big[ [A40001]\{U\} + v_2^2[A41100]\{U\} \\
& + \{U\}^T [A500001]\{A\} \Big]_{j+1}^P \\
[JUU] &= \{R\}^T (A3000) + v_2^1[A3010]) \\
& + \frac{\Delta t}{2}\{R\}^T \Big[ ([A40010] + [A40001] + v_2^2[A40110] \\
& + v_2^2[A40101])\{U\} \\
& + 2(\{U\}^T [A500001]\{A\}) \Big]_{j+1}^P
\end{aligned}$$

$$\begin{aligned}
[JUE] &= [0] \\
[JUP] &= \frac{\Delta t}{2} [A201] \tag{79}
\end{aligned}$$

$$\begin{aligned}
\frac{\partial \{FE\}}{\partial \{R\}} &\equiv [JER] = \frac{1}{2} \{E_{j+1}^P - E_j\}^T ([A3000] + v_3^1 [A3010]) \\
&\quad + \frac{\Delta t}{2} \{E\}^T [A40001] \{U\} + v_3^2 [A41100] \{U\} \\
&\quad + \{U\}^T [A500001] \{A\} \Big]_{j+1}^P \\
[JEU] &= \frac{\Delta t}{2} \left[ \{E\}^T [A41000] \{R\} + v_3^2 [A41100] \{R\} \right. \\
&\quad + \{R\}^T [A500001] \{A\} \Big] \\
&\quad + \{P\}^T ([A3100] + [A3001]) \Big]_{j+1}^P \\
[JEE] &= \{R\}^T ([A3000] + v_3^1 [A3010]) \\
&\quad + \frac{\Delta t}{2} \{R\}^T [A40010] \{U\} + v_3^2 [A40110] \{U\} \\
&\quad + \{U\}^T [A500001] \{A\} \Big]_{j+1}^P \\
[JEP] &= \frac{\Delta t}{2} \{U\}^T [A3001] + [A3100] \Big]_{j+1}^P \tag{80}
\end{aligned}$$

$$\begin{aligned}
\frac{\partial \{FP\}}{\partial \{R\}} &\equiv [JPR] = \left[ -(\gamma-1) \{E\}^T [A3000] + \frac{\gamma-1}{2} \{U\}^T [A40000] \{U\} \right]_{j+1}^P \\
[JPU] &= \left[ (\gamma-1) \{R\}^T [A40000] \{U\} \right]_{j+1}^P \\
[JPE] &= \left[ -(\gamma-1) \{R\}^T [A3000] \right]_{j+1}^P \\
[JPP] &= [A200] \tag{81}
\end{aligned}$$

Note in the formation of equations 79-81, that the Boolean indices in the various A-matrices are permuted to facilitate differentiation of each expression by the last right contraction matrix. Note also the considerable commonality pervading the Jacobian construction. The elements of each Jacobian are formed on the finite element domain  $R_e^1$ , using the element matrices listed in Appendix A, and then assembled into the global form using the operator  $S_e$ . In actual practice, the column matrix  $\{\delta QI\}$  is ordered on degrees of freedom at a node, e.g.,  $\{\dots, \delta R_j, \delta U_j, \delta E_j, \delta P_j, \delta R_{j+1}, \dots\}^T$ . Hence, the global Jacobian  $[J]$ , equation 27, is block tri-diagonal, using the linear ( $k = 1$ ) finite element formulation, and block penta-diagonal for quadratic ( $k = 2$ ) elements.

For the conservative form of the governing differential equation system 7-10, identify the volume-specific dependent variables  $m \equiv \rho u$  and  $g \equiv \rho e$ , yielding

$$L(\rho) = \frac{\partial \rho}{\partial t} + \frac{\partial}{\partial x} [m + mA] = 0 \quad (82)$$

$$L(m) = \frac{\partial m}{\partial t} + \frac{\partial}{\partial x} [m^2/\rho + p] + m^2/\rho \partial A/\partial x = 0 \quad (83)$$

$$L(g) = \frac{\partial g}{\partial t} + \frac{\partial}{\partial x} [(mg/\rho + mp/\rho)] + m/\rho (g+p) \partial A/\partial x = 0 \quad (84)$$

$$L(p) = p - (\gamma-1) [g - m^2/2\rho] = 0 \quad (85)$$

For equations 82-85, A is defined as  $\ln A(x)$ . The omnipresence of inverse density can be eliminated by introducing the (contravariant) convection velocity  $(\bar{u})$   $v \equiv m/\rho$ ; hence,

$$L(\rho) = \frac{\partial \rho}{\partial t} + \frac{\partial}{\partial x} [m + \rho v A] = 0 \quad (82A)$$

$$L(m) = \frac{\partial m}{\partial t} + \frac{\partial}{\partial x} [vm + p] + mv \partial A/\partial x \quad (83A)$$

$$L(g) = \frac{\partial g}{\partial t} + \frac{\partial}{\partial x} [vg + vp] + v(g+p)\partial A/\partial x = 0 \quad (84A)$$

$$L(p) = p - (\gamma-1) \left[ g - \frac{1}{2} vm \right] = 0 \quad (85A)$$

The finite element solution algorithm statement, equations 24-26, applied to equations 82A-85A, yields

$$\begin{aligned} \{FR\} = & ([A200] + v_1^1[A210])\{R\}_{j+1} \\ & + \frac{\Delta t}{2} \left[ [A210]\{M\} + v_1^2\{V\}^T[A3011]\{R\} \right. \\ & \left. + \{A\}^T([A41000]\{V\})\{R\} \right]_{j+1,j} = \{0\} \end{aligned} \quad (86)$$

$$\begin{aligned} \{FM\} = & ([A200] + v_2^1[A210])\{M\}_{j+1} \\ & + \frac{\Delta t}{2} \left[ -\{V\}^T[A3010]\{M\} - [A210]\{P\} \right. \\ & \left. + v_2^2\{V\}^T[A3011]\{M\} + \{A\}^T([A41000]\{V\})\{M\} \right]_{j+1,j} \\ & = \{0\} \end{aligned} \quad (87)$$

$$\begin{aligned} \{FG\} = & ([A200] + v_3^1[A210])\{G\}_{j+1} \\ & + \frac{\Delta t}{2} \left[ \{V\}^T[A3010]\{G\} + \{V\}^T[A3010]\{P\} \right. \\ & \left. + v_3^2\{V\}^T[A3011]\{G\} + \{A\}^T([A41000]\{V\})\{GP\} \right]_{j+1,j} \\ & = \{0\} \end{aligned} \quad (88)$$



$$\{FP\} = [A200]\{P\} - (\gamma-1) \left[ [A200]\{G\} - \frac{1}{2} \{V\}^T [A3000]\{M\} \right] = \{0\} \quad (89)$$

Note that equations 86-89 are rather less complicated in appearance than equations 70, 75-77, and in conformation with the multi-dimensional generalized coordinates formulation, see equation 41. The definition of convection velocity has been utilized for the dissipation ( $v_2^1$ ) term in equation 86 to enhance overall uniformity, and  $\{GP\} \equiv \{G + P\}$ .

The construction of the Jacobian contributions for the Newton iteration algorithm, equations 27-29, proceeds directly. Recalling that  $v = m/\rho$ , and using the chain rule as required,

$$\frac{\partial \{FR\}}{\partial \{R\}} \equiv [JRR] = [A200] + v_1^1 [A210]$$

$$[JRM] = \frac{\Delta t}{2} \left[ [A210] + v_1^2 [A211] + \{A\}^T [A3100] \right]_{j+1}^P$$

$$[JRG] = 0$$

$$[JRP] = 0 \quad (90)$$

$$\begin{aligned} \frac{\partial \{FM\}}{\partial \{R\}} \equiv [JMR] = & - \frac{\Delta t}{2} \left( \frac{\bar{m}}{\bar{\rho}^2} \right) \{M\}^T \left[ - [A3010] + v_2^2 [A3110] \right. \\ & \left. + [A40001]\{A\} \right]_{j+1}^P \end{aligned}$$

$$[JMM] = [A200] + v_2^1 [A210]$$

$$\begin{aligned} & + \frac{\Delta t}{2} \{V\}^T \left[ [A3010] + v_2^2 [A3011] + [A40001]\{A\} \right]_{j+1}^P \\ & + \frac{\Delta t}{2} \left( \frac{1}{\bar{\rho}} \right) \{M\}^T \left[ [A3010] + v_2^2 [A3110] + [A40001]\{A\} \right]_{j+1}^P \end{aligned}$$

$$[JMG] = [0]$$

$$[JMP] = \frac{\Delta t}{2} [A210] \quad (91)$$

$$\begin{aligned}
\frac{\partial \{FG\}}{\partial \{R\}} &\equiv [JGR] = -\frac{\Delta t}{2} \left( \frac{\bar{m}}{\bar{\rho}^2} \right) \left[ \{G\}^T ([A3010] + v_3^2 [A3110] + [A40001] \{A\}) \right. \\
&\quad \left. + \{P\}^T [A3010] \right]_{j+1}^P \\
[JGM] &= \frac{\Delta t}{2} \left( \frac{1}{\bar{\rho}} \right) \left[ \{G\}^T ([A3010] + v_3^2 [A3110] + [A40001] \{A\}) \right. \\
&\quad \left. + \{P\}^T [A3010] \right]_{j+1}^P \\
[JGG] &= [A200] + v_3^1 [A210] \\
&\quad + \frac{\Delta t}{2} \{V\}^T \left[ [A3010] + v_3^2 [A3011] + [A40001] \{A\} \right]_{j+1}^P \\
[JGP] &= \frac{\Delta t}{2} \{V\}^T \left[ [A3010] + [A40001] \{A\} \right]_{j+1}^P \quad (92) \\
\frac{\partial \{FP\}}{\partial \{R\}} &\equiv [JPR] = -\left( \frac{\gamma-1}{2} \right) \left( \frac{\bar{m}}{\bar{\rho}^2} \right) \{M\}^T [A3000] \Big|_{j+1}^P \\
[JPM] &= \frac{\gamma-1}{2} \left[ \{V\}^T [A3000] + \left( \frac{1}{\bar{\rho}} \right) \{M\}^T [A3000] \right]_{j+1}^P \\
[JPG] &= -(\gamma-1) [A200] \\
[JPP] &= [A200] \quad (93)
\end{aligned}$$

In equations 91-93, the superscript bar on  $m$  and  $\rho$  indicate the assembly of elemental averages of the variable, i.e.,  $\bar{m}_e \equiv \{A10\}^T \{M\}_e$ ,  $\bar{\rho}_e \equiv \{A10\}^T \{R\}_e$ . The various defined matrices are listed in Appendix A, for  $k = 1$  and  $2$  in equation 23.

## 2. Numerical Results, Riemann Shock Tube

The primary requirement for the computational tests is to evaluate the various dissipation constants within the finite element algorithm for compressible flowfields possessing sharp gradients and shocks. An equally important requirement is to assess construction of the Jacobian; specifically, is the favorable quadratic convergence rate for the Newton iteration algorithm retained in the present formulation? Two test cases meeting these requirements are the Riemann problem and off-design (shocked) flow in a nozzle. Following some numerical experimentation, the nonconservative formulation, equations 70, 75-77, was relegated to history in favor of the conservative algorithm form.

The Riemann problem corresponds to the one-dimensional, exploding diaphragm shock tube experiment (see Shapiro, ref. 13., page 1007), with uniform sound speed in both the high and low pressure chambers. Upon (computational) removal of the diaphragm, a shock wave propagates into the initially low-pressure region, and a rarefaction wave propagates in the opposite direction. The more interesting case, corresponding to different initial sound speeds in the two chambers, has been recently examined in considerable detail by several researchers in computational methodology. Particular reference has been made to establishment of the "ultimate" flux-corrected conservative difference scheme, cf., Sod (ref. 14), Van Leer (ref. 15), Zalesak (ref. 16). These methods generally employ a Lagrangian, or mixed Lagrangian-Eulerian formulation, in distinction to the implicit, strictly Eulerian finite element algorithm, which is not at all "hard-wired" for the problem.

The selected Riemann problem specification corresponds to that of Sod (ref. 14), wherein a unit duct length is uniformly subdivided by 100 nodes. The diaphragm is located at node 50, with the initially high pressure region occupying the left half. For the finite element simulation, the linear ( $k = 1$ ) algorithm employed 99 uniform elements, while for the quadratic ( $k = 2$ ), the last node was deleted and the discretization contained 49 elements. The initial conditions are  $u(x) = 0$ ,  $p = \rho = 1$  for  $x \leq 0.5$ ,  $p = 0.1$ , and  $\rho = 0.125$  for  $x > 0.5$ ,

and  $\gamma = 1.4$ . Figure 6 shows the base case  $k = 1$  algorithm solution, at  $t = 0.14154s$ , for  $v_{\alpha}^2 = 1/\sqrt{15}$  and  $v_{\alpha}^1 = 0$ , where  $\alpha$  denotes dependent variable (number) and the dissipation parameter indices (1,2) are now superscripts. The shock is located at node 75, and the rarefaction wave is centered on node 62. The symbols correspond to nodal values of  $\{QI\}$ , while the various solid lines bound the inviscid solution (ref. 15) for the shock, rarefaction wave and the interspersed plateaus. Considering the simplicity of the  $k = 1$  algorithm, these results are quite accurate, except for the modestly sloped plateaus in density and momentum, and the overshoot for all  $\{QI\}$  on the high pressure side of the shock.

Following some experimentation, the improved results shown in Fig. 7 were obtained for  $v_{\alpha}^1 = 1/\sqrt{15} \{3/8, 0, 1/4\}$  and  $v_{\alpha}^2 = 1/\sqrt{15} \{3/4, 2, 1\}$ , for  $1 \leq \alpha \leq 3$ . The plateau in momentum and density behind the shock is nearly planar, no overshoot occurs in any  $\{QI\}$ , and the shock is interpolated across approximately two elements. The second density plateau is also modestly improved, but the "trashiness" in  $\{QI\}$  on  $x < 0.4$  has been somewhat aggravated. Since the velocity is zero in this region, the algorithm is operating without any dissipation, and  $v^1 > 0$  in the absence of dissipation is well known to induce this type of leading phase error.

For comparison, Figure 8 is a reproduction of the results of Van Leer (ref. 15, Figure 6), for this problem specification, as obtained using the MUSCL algorithm. The upstream density plateau of this algorithm is better, but the results in the shock vicinity are nominally comparable. The solution parameters of velocity and internal energy are rather better descriptions for algorithm performance, see the two right side plots in Figure 8. Figure 9a shows these data computed from the  $k = 1$  solution of Figure 7. Comparing to Figure 8, the shock sharpness is comparable, as is the high temperature plateau behind the shock. The low temperature plateau behind the rarefaction wave is modestly less planar. For comparison, Figure 9b shows these identical data as obtained using the Crank-Nicolson implicit finite difference equivalent of the  $k = 1$  algorithm, with  $v^2 = 1/\sqrt{15}$  and  $v^1 = 0$  (by definition). This ad hoc modification is again verified to degrade solution accuracy. Upstream overshoot is excessive, the shock is interpolated across six

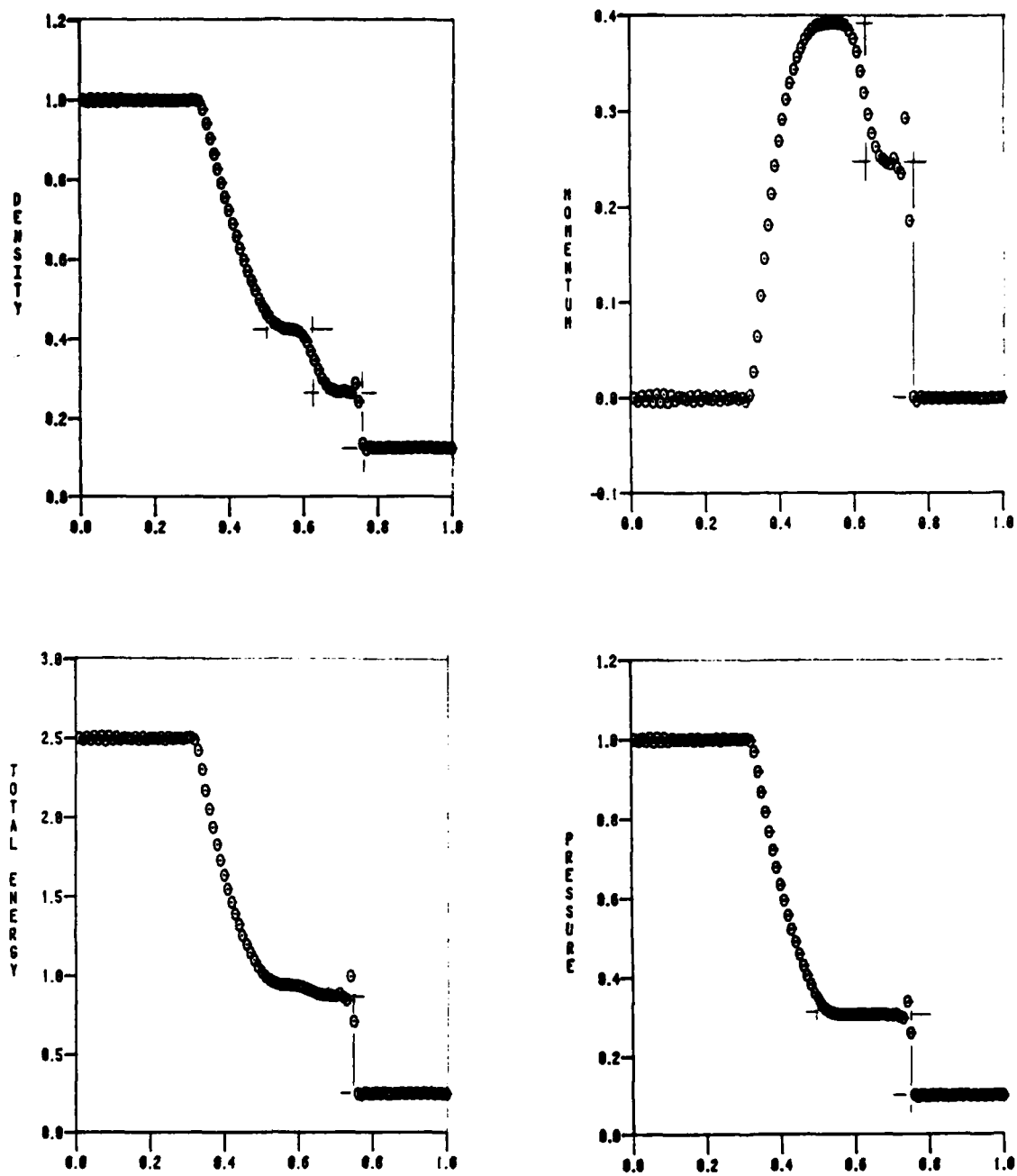


Figure 6. Linear Finite Element Algorithm Solution, Shock Tube Problem,  
 $t = 0.14154$ ,  $v^1 = 0.$ ,  $v^2 = 1/\sqrt{15}$ .

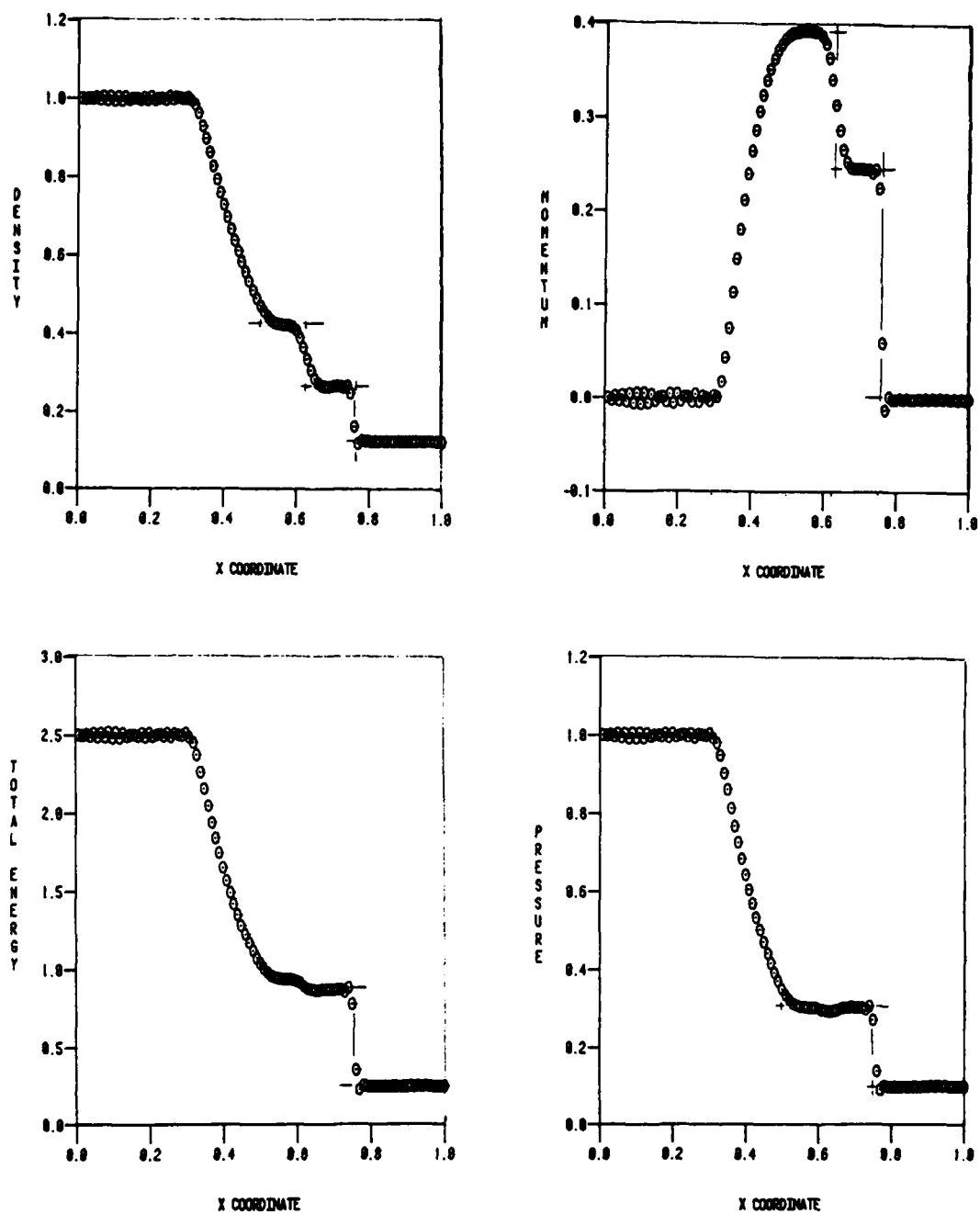


Figure 7. Linear Finite Element Algorithm Solution, Shock Tube Problem,  
 $t = 0.14154$ ,  $v_{\alpha}^1 = 1/\sqrt{5}\{3/8, 0, 1/4\}$ ,  $v_{\alpha}^2 = 1/\sqrt{5}\{3/4, 2, 1\}$ .

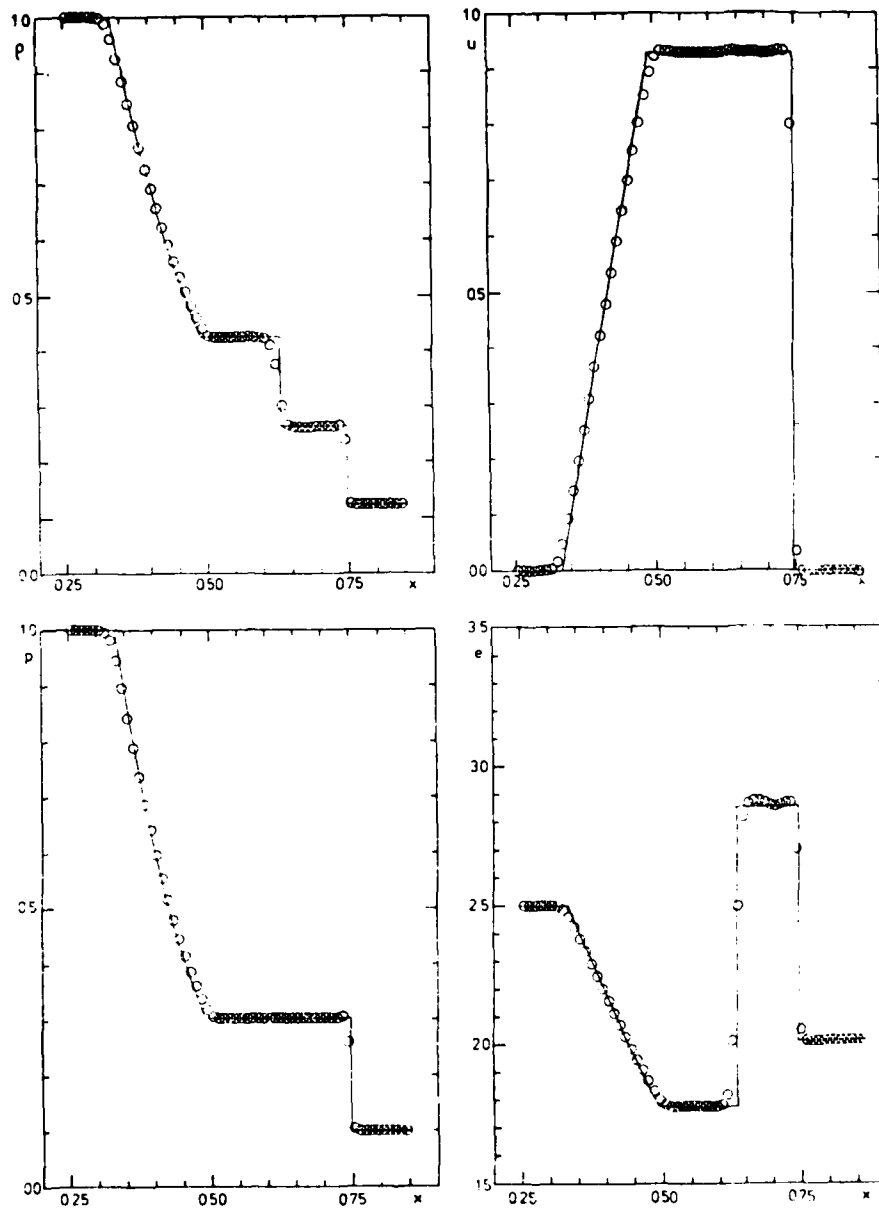
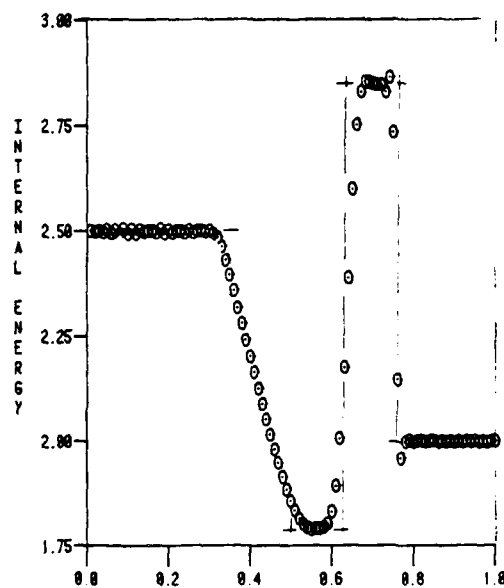
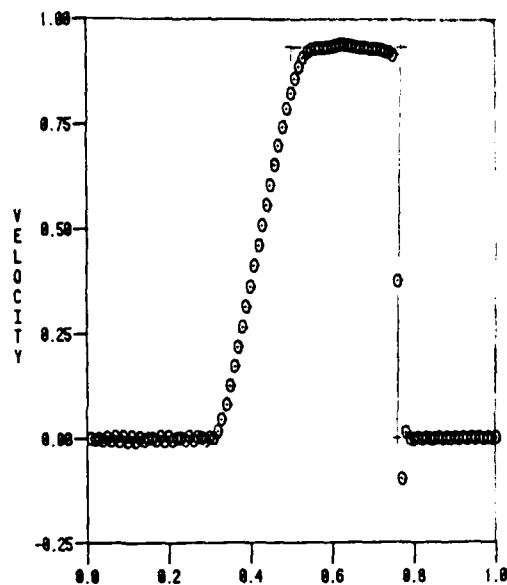
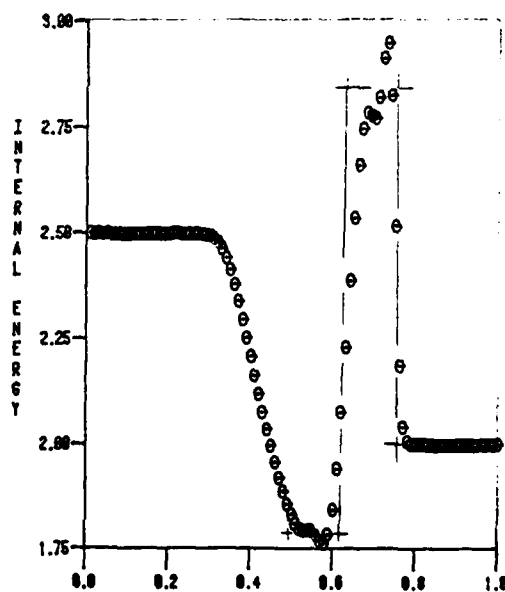
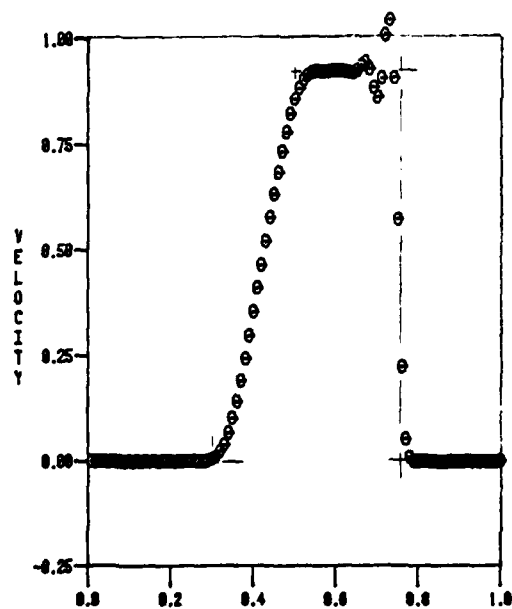


Figure 8. Solution for Shock Tube Problem Generated By the MUSCL Code, Reported by Van Leer (ref. 15), Courant No. = 0.9,  $\Delta x = 0.01$ ,  $t = 0.14154$ .



a) Linear Finite Element, Solution of Figure 7.



b) Finite Difference,  $v_\alpha^2 = 1/\sqrt{5}$ .

Figure 9. Finite Element and Finite Difference Algorithm Solution Comparisons, Shock Tube Problem,  $t = 0.14154$



difference cells, and the high temperature plateau is barely recognizable and underpredicted.

The performance of the quadratic ( $k = 2$ ) algorithm formulation is an improvement, in accord with previous numerical experience. Figure 10 shows the  $k = 2$  solution field  $\{QI\}$  at  $t = 0.14154$  s, using the linear analysis dissipation levels  $v_{\alpha}^2 = 1/\sqrt{15}$ ,  $v_{\alpha}^1 = 0$ . The solution is devoid of the plateaus, and the shock is smeared over several elements, indicative of excess diffusion. Figure 11 illustrates the improvements accrued to use of  $v_{\alpha}^2 = 1/\sqrt{15} \{1/4, 3/4, 1/2\}$  and  $v_{\alpha}^1 = 0$ . The shock exists across only one element and the density and momentum plateaus are clearly evident. A modest level of solution "trashiness" is evidenced in both extreme solution regions wherein the dissipation level is zero (due to zero convection velocity). Figure 12a shows the velocity and internal energy fields computed from this quadratic solution, and the fidelity is generally excellent. In this instance (the quadratic element algorithm), the reduction of the initial-value matrix to the Crank-Nicolson finite difference equivalent does not adversely affect solution accuracy, Figure 12b, except in the high temperature plateau behind the shock.

The construction of equation system Jacobian, as presented for both  $k = 1$  and  $k = 2$ , retains the favorable nominally quadratic rate of convergence. Table 4 presents the extremum elements of  $\{\delta QI\}$ , for a typical integration step involving three iterations, and the nodal location of these extrema. Convergence is at least quadratic, including the algebraic pressure equation. The sharply defined solutions, as obtained using minimal levels for  $v_{\alpha}^2$ , typically required 250 iterations to reach  $t = 0.14154$  s. This corresponds to an extremum Courant number ( $C = |u+a|\Delta t/\Delta x$ ) of approximately 0.35. No attempt was made to extremize Courant number during this study.

### 3. Numerical Results, Shocked Nozzle Flow

The results for prediction of an off-design nozzle problem confirm these data for dissipation parameter levels. The test case initial condition corresponds to a subsonic-supersonic expansion on  $0.75 \leq M \leq 1.35$ , followed by a normal shock and subsonic expansion on  $0.75 \leq M \leq 0.7$ . The values of  $\rho$ ,  $u$  and  $p$  were specified at the inlet, and  $p$  was computed from

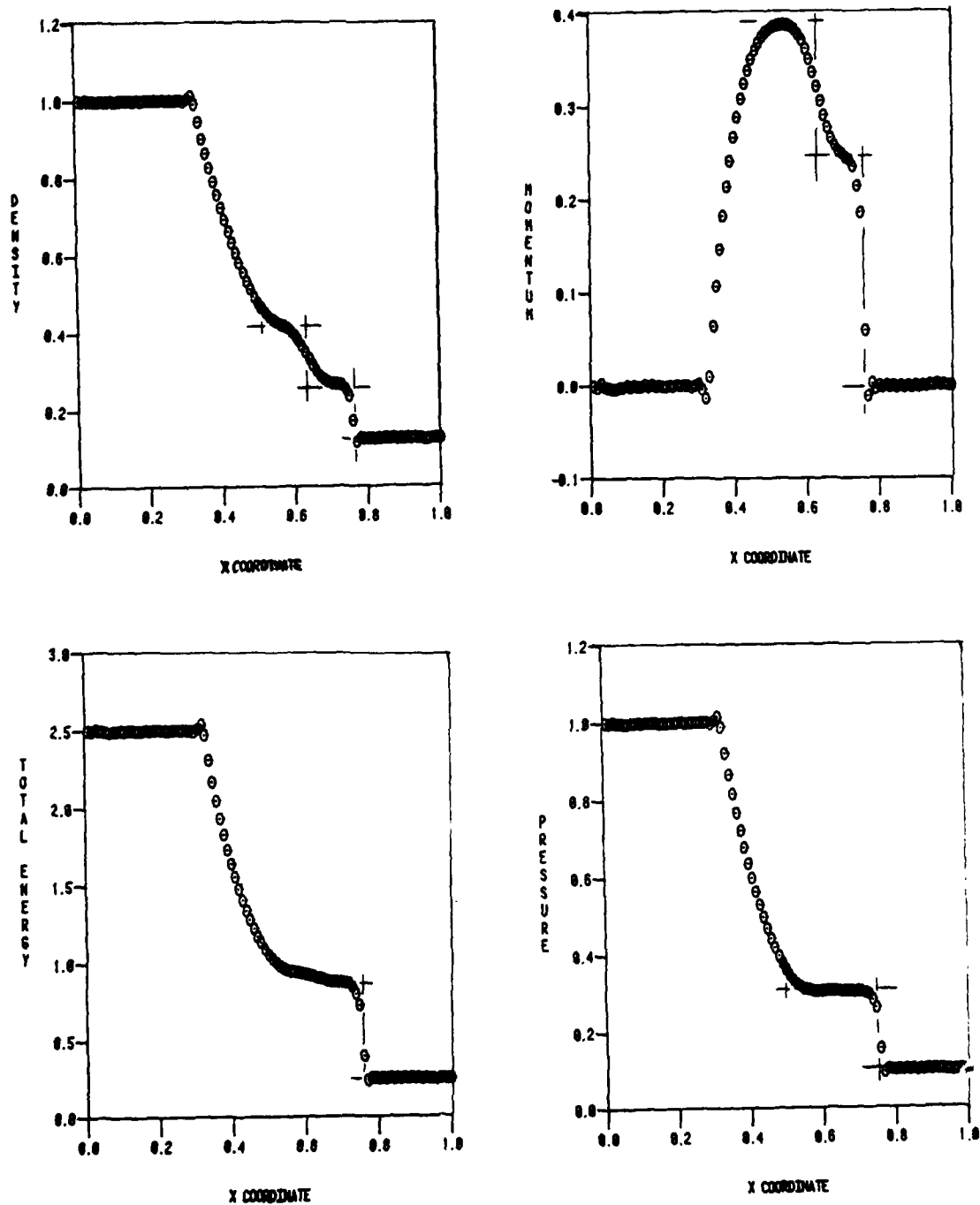


Figure 10. Quadratic Finite Element Algorithm Solution, Shock Tube Problem,  $t = 0.14154$ ,  $v_{\alpha}^1 = 0.$ ,  $v_{\alpha}^2 = 1/\sqrt{15}$ .

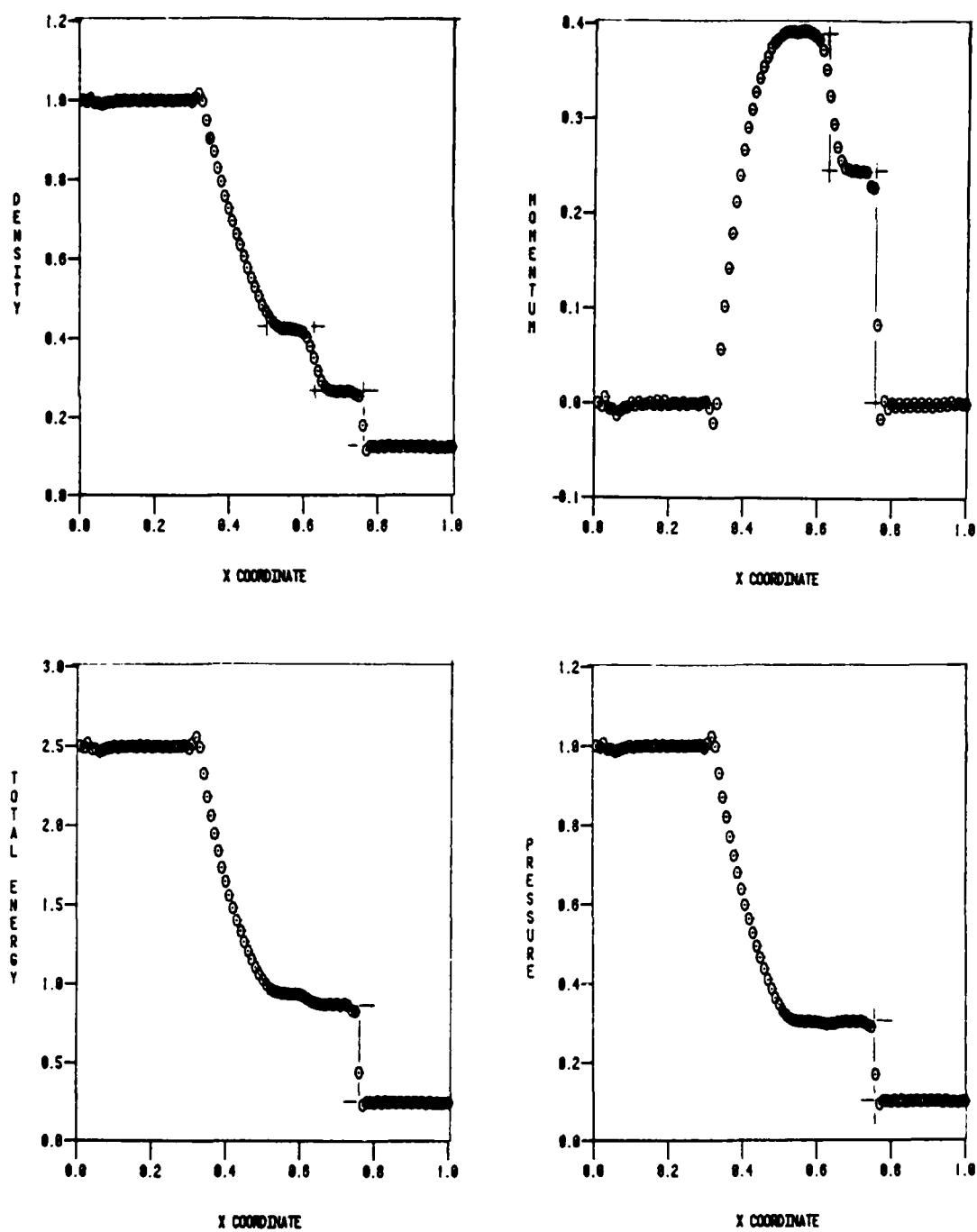
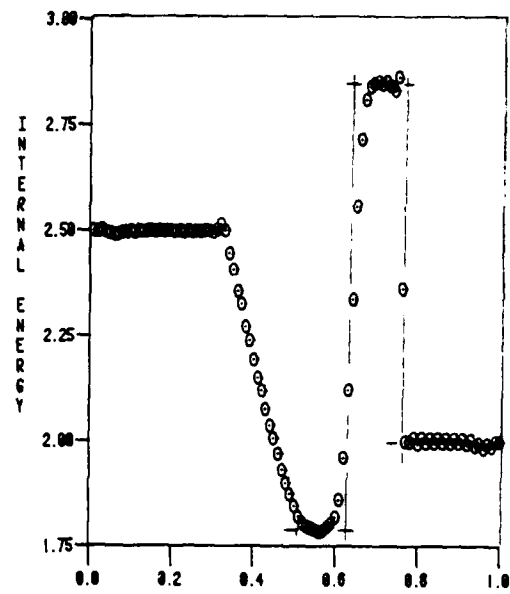
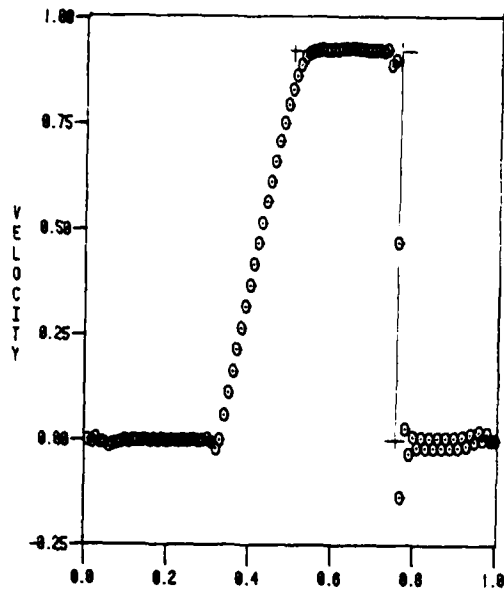
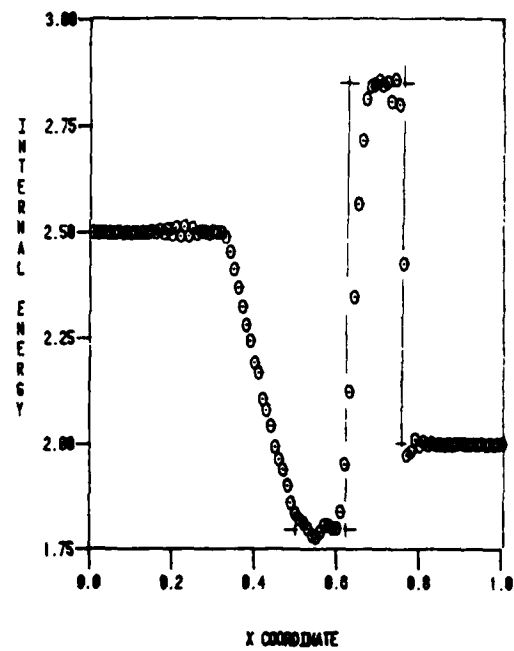
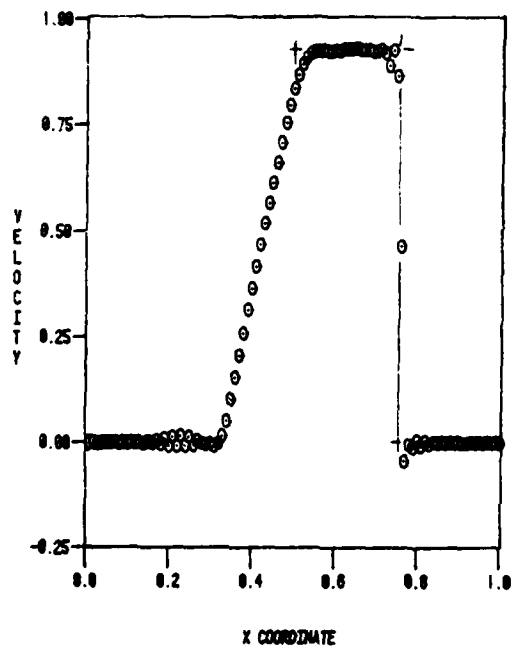


Figure 11. Quadratic Finite Element Algorithm Solution, Shock Tube Problem,  $t = 0.14154$ ,  $v_{\alpha}^1 = 0.$ ,  $v_{\alpha}^2 = 1/\sqrt{5}\{1/4, 3/4, 1/2\}$ .



a) Quadratic Finite Element,  $v_{\alpha}^1 = 0.$ ,  $v_{\alpha}^2 = 1/\sqrt{5}\{1/4, 3/4, 1/2\}$



b) Diagonalized Quadratic,  $v_{\alpha}^1 = 0.$ ,  $v_{\alpha}^2 = 1/\sqrt{5}\{1/4, 3/4, 1/2\}$

Figure 12. Finite Element and Diagonalized Finite Element Algorithm Comparisons, Shock Tube Problem,  $t = 0.14154$ .

TABLE 4

CONVERGENCE IN  $\{\delta QI\}$  FOR RIEMANN  
SHOCK TUBE SIMULATION

<u>Iteration</u>	<u><math>\{\delta R\}_{\max}</math></u>	<u>Node</u>	<u><math>\{\delta M\}_{\max}</math></u>	<u>Node</u>
1	-0.87325E-02	70	-0.20780E-01	70
2	0.13072E-02	69	0.31246E-02	69
3	0.21915E-03	69	0.69326E-03	69

	<u><math>\{\delta G\}_{\max}</math></u>	<u>Node</u>	<u><math>\{\delta P\}_{\max}</math></u>	<u>Node</u>
1	-0.23351E-01	70	-0.75154E-01	70
2	0.34658E-02	70	-0.51826E-02	71
3	0.46731E-03	70	-0.50114E-03	68

the equation of state. The subsonic outlet conditions, applied at the end of a uniform cross-section extension of the nozzle, were specified pressure and vanishing normal derivative for  $\rho$ ,  $p_u$  and  $p_e$ . For the test, the exit pressure was raised by 15%, such that the shock must move upstream into a previously supersonic region of flow. At all points, upstream of the translating shock location, the supersonic flow must remain undisturbed from the initial conditions. Figure 13 shows the  $k = 1$  algorithm solution for  $\{QI\}$  and Mach number distribution at  $t = 2.4s$ , compared to the initial conditions shown as a solid line. The variables upstream of the new shock location are unaltered, and the downstream distributions are smooth. The specified levels of dissipation parameters, set at one-half those of the Riemann problem, were adequate to suppress overshoot and to produce a sharply defined shock. Figure 14 presents the similar comparison for the quadratic algorithm solution, as obtained using one half the dissipation parameter levels of the Riemann specification. The results are essentially indistinguishable from those of Figure 13.

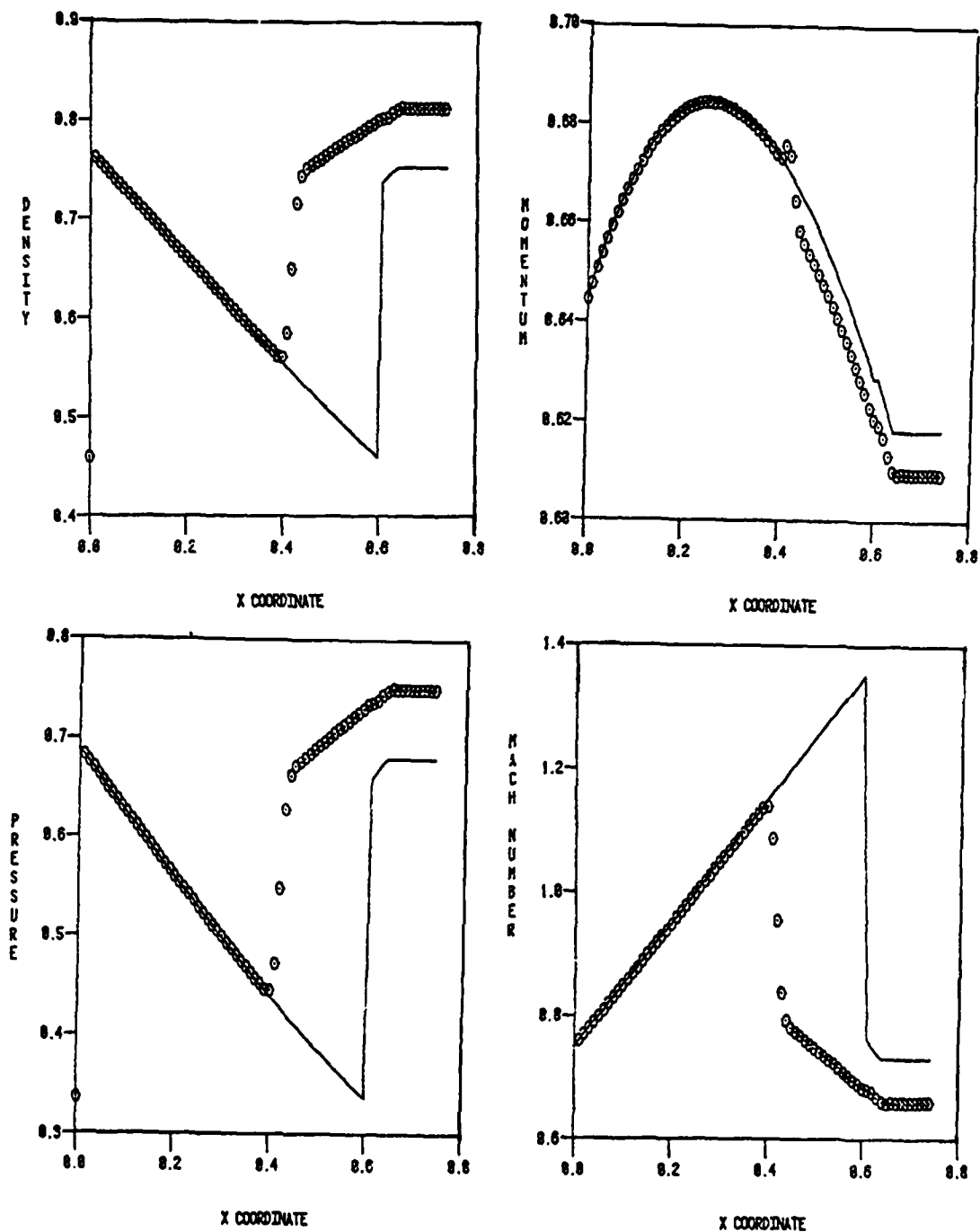


Figure 13. Computed Solution for Shocked Flow in a Variable Area Duct, Linear Finite Element Algorithm,—Initial Condition.

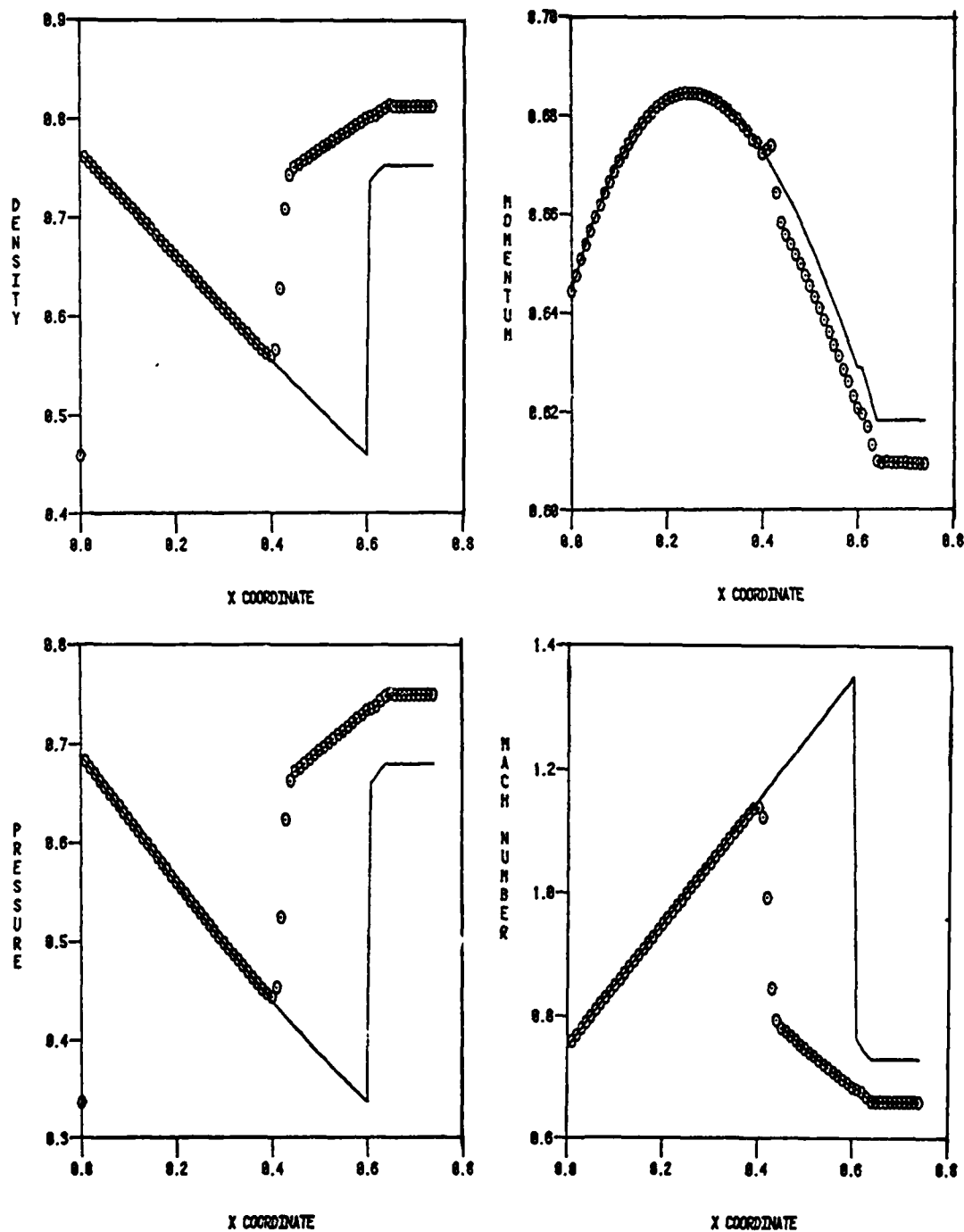


Figure 14. Computed Solution for Shocked Flow in a Variable Area Duct, Quadratic Finite Element Algorithm,—Initial Condition.

#### 4. Two-Dimensional Flow Formulation

The extension of the formulation of the dissipative finite element algorithm to a two-dimensional flow description in generalized coordinates is direct. Identify the volume-specific dependent variable set  $\rho$ ,  $m_i = \rho u_i$ ,  $1 \leq i \leq 2$ , and  $g = \rho e$ , and the parameters  $\sigma_{ij}$  and  $q_j$ . Recall the definition of the convection velocity, as expressed in contravariant scalar components  $\bar{u}_k$  equation 38. For a multi-dimensional problem, the dissipation parameter  $\bar{\beta}_1$  is a vector, with contravariant scalar components  $v_i^\alpha \Delta_e$ , see equation 24, where  $\alpha$  denotes initial-or boundary-value definition. Finally, as before for compressible flow,  $\beta_3 \equiv 0$ .

Equation 26 expresses the non-linear algebraic equation system resulting from substitution of equations 1-7 into equation 24. Denote the discrete dependent variable set  $\{Q\}^T = \{R, M(I), G, P, S(I,J), Q(I)\}$ . The respective algorithmic statements  $\{FI\}$  in the generalized coordinate description  $\eta_i$  become, see equations 37-41,

$$\begin{aligned} \{FR\} = & (\{DET\}^T [B3000] + v_{IJ}^1 \{ETAKJ\}^T ([B40K00] \{DET\})) \{R\}_{j+1} \\ & + \frac{\Delta t}{2} \left[ -\{ETAKI\}^T [B30K0] \{MI\} + v_{IJ}^2 \{ETAKJ\}^T [B30KL] \{MBARL\} \right]_{j+1, j} \end{aligned} \quad (94)$$

$$\begin{aligned} \{FMI\} = & (\{DET\}^T [B3000] + v_{IJ}^1 \{ETAKJ\}^T ([B40K00] \{DET\})) \{MI\}_{j+1} \\ & + \frac{\Delta t}{2} \left[ -\{UBARK\}^T [B30K0] \{MI\} - \{ETAKI\}^T [B30K0] \{P\} \right. \\ & + \{ETAKJ\}^T [B30K0] \{SIGIJ\} \\ & + v_{IJ}^2 \{ETAKJ\}^T ([B40KLO] \{MI\}) \{UBARL\} \\ & \left. + v_{IJ}^2 \{ETAKJ\}^T ([B40KLO] \{UBARL\}) \{MI\} \right]_{j+1, j} \end{aligned} \quad (95)$$



$$\begin{aligned}
\{FG\} = & (\{DET\}^T[B3000] + v_{4J}^1\{ETAKJ\}^T[B40K00]\{DET\}))\{G\}_{j+1} \\
& + \frac{\Delta t}{2}[-\{UBARK\}^T[B30K0]\{G\} + \{P\} + \{ETAKL\}^T[B30K0]\{QBARK\} \\
& + \{ETAKJ\}^T([B40K00]\{UL\})\{SIGLJ\} \\
& + v_{4J}^2\{ETAKJ\}^T([B40KLO]\{G\})\{UBARK\} \\
& + v_{4J}^2\{ETAKJ\}^T([B40KLO]\{UBARK\})\{G\}]_{j+1,j} \quad (96)
\end{aligned}$$

$$\begin{aligned}
\{FP\} = & \{DET\}^T[B3000]\{P\} - (\gamma-1)(\{DET\}^T[B3000]\{G\} \\
& - \frac{1}{2}\{DET\}^T([B40000]\{UJ\})\{MJ\})_{j+1} \quad (97)
\end{aligned}$$

A few comments on notation in equations 94-97 are appropriate. The matrix B-prefix denotes the expressions obtained by integrals over a two-dimensional elemental domain, i.e.,  $R_e^2$ . The defined element matrices are listed in Appendix B for  $k=1$ , equation 23. The concept of the Boolean indices (0,1) is generalized to replace 1 by K, indicative of the corresponding scalar component of  $\vec{v}$  in the  $\eta_k$  coordinate system, hence,  $1 \leq K \leq 2$ . In all terms, the discrete indices J, K, L occurring in both matrix and variable (FORTRAN) names, are tensor summation indices with range  $1 \leq (J, K, L) \leq 2$ . The index I is a free index denoting Cartesian scalar components of  $m_i$ , i.e., {MI}. As noted, the expansion coefficient  $\bar{p}_1^>$ , equation 24, is expressed in Cartesian scalar components  $v_j$ , with distinct values for each dependent variable and each term. The arrays {DET} and {ETAKJ} contain nodal values of, respectively, the determinant J of the forward transformation  $x_i = x_i(\eta_j)$  and elements  $\partial \eta_k / \partial x_j$  of the inverse transformation, see equations 33-34. The nodal values of the contravariant scalar components of the solution vectors  $\bar{u}_k$ , and  $\bar{m}_k$  and  $\bar{q}_k$  are denoted {UBARK}, {MBARK} and {QBARK}. The elements of {SIGIJ} are nodal values of the stress tensor. The corresponding algorithm statement, using the homogeneous form of equation 4, is

$$\begin{aligned}
\{FSIJ\} &= \{DET\}^T [B3000] \{SIGIJ\} \\
&- \mu \left[ \{ETAKJ\}^T ([B400K0] \{DET\}) \{UI\} \right. \\
&+ \{ETAKI\}^T ([B400K0] \{DET\}) \{UJ\} \\
&\left. - \frac{1}{3} \delta_{IJ} \{ETAKL\}^T ([B400K0] \{DET\}) \{UL\} \right]_{j+1}
\end{aligned} \tag{98}$$

where  $\delta_{IJ}$  is the Kronecker delta. The corresponding expression for the definition of energy flux  $q_j$ , equations 5-6, is,

$$\begin{aligned}
\{FQI\} &= \{DET\}^T [B3000] \{QI\} \\
&- \kappa \{ETAKI\}^T ([B40K00] \{DET\}) (\{GSR\} - \{UIUI\})_{j+1}
\end{aligned} \tag{99}$$

In equation 99, the elements of  $\{GSR\}$  are nodal values of  $e \equiv g/\rho$ , while those of  $\{UIUI\}$  are nodal values of specific kinetic energy  $\frac{1}{2}u_i u_i$ . In all equations, the notation  $\{\cdot\}'_{j+1}$  denotes  $\{\cdot\}^P_{j+1} - \{\cdot\}_j$ , and  $]_{j+1,j}$  denotes evaluation of the argument at  $t_{j+1}$  and  $t_j$  followed by addition.

As can be observed, the finite element two-dimensional Navier-Stokes algorithm statement in generalized coordinates, equations 94-99, is considerably more involved than the predecessor one-dimensional algorithm. By the same token, equations 94-99 also completely express the three-dimensional algorithm by the exchange of B-prefix matrices with C and extension of the discrete tensor index range to  $1 \leq (J,K,L) \leq 3$ .

The remaining step in the algorithm formulation is construction of the tensor matrix product form of the Jacobian,

$$[J(\{FI\})] \equiv \frac{\partial \{FI\}}{\partial \{QJ\}} \tag{100}$$

equation 29. The construction and subsequent solution procedure was outlined in Section II.3. The lead term in each of the equations is

$$[DET]^T[B3000]\{QJ\}_{j+1}$$

Hence, the corresponding component of  $[J]$  is

$$[J]_1 = \frac{\partial \{FI\}_1}{\partial \{QJ\}} = \{DET\}^T[B3000]\delta_{1J} \quad (101)$$

For illustration, assume an affine rectangular Cartesian coordinate transformation,  $\det[J] = 1$ , hence  $\{DET\}^T = \{ONE\}^T$ , the array of unit values. By direct substitution,

$$\{ONE\}^T[B3000] = [B200] \quad (102)$$

and the matrix whose tensor product yields  $[B200]$  is simply  $[A200]$ , see equations 49-51. Recalling that global expressions are obtained by the assembly operation  $S_e$  over element-level operations, equation 101 is formulated as

$$\begin{aligned} \{DET\}^T[B3000] &\equiv S_e \left[ \Delta_e \{DET\}_e^T[B3000]_e \right] \\ &= S_e \left[ \Delta_e^1 \{DET\}_e^T[A3000]_e \otimes \Delta_e^2 \{DET\}_e^T[A3000]_e \right] \end{aligned} \quad (103)$$

Recall the superscripts on  $\Delta_e^\alpha$  denote the appropriate one-dimensional element measure, e.g., length and width of a rectangular element.

The second term in the Jacobian for  $\rho$  and  $g$  is

$$[J]_2 = v_{IJ}^1 \{ETAKJ\}^T[B30K0]$$

where  $I$  equals 1 or 4 for two-dimensional flow, and summation is implied for repeated indices. By the direct extension of operations yielding

equation 103,

$$\begin{aligned}
 v_{IJ}^1 \{ETAKJ\}^T [B30K0] &\equiv S_e \left[ \Delta_e v_{IJ}^1 \{ETAKJ\}^T [B30K0]_e \right] \\
 &= S_e \left[ \Delta_e v_{IJ}^1 \{ETA1J\}^T [A3010]_e \right. \\
 &\quad \left. \otimes \Delta_e^2 v_{IJ} \{ETA2J\}^T [A3010]_e \right] \quad (104)
 \end{aligned}$$

As before, the superscripts on  $\Delta_e^\alpha$  denote coordinate direction, with the corresponding indication in the elemental arrays  $\{ETAKJ\}$ . The element derivative matrix  $[A3010]$  is independent of  $\alpha$  and identical with the one-dimensional form given in Appendix A.

The construction of certain remaining terms in the Jacobian involves differentiation with respect to the parameter  $\bar{u}_k = \bar{m}_k / \rho$ . Using the chain rule and equation 38-39, then

$$\begin{aligned}
 \frac{\partial}{\partial \{MI\}} &= \frac{\partial}{\partial \{MI\}} + \frac{\partial}{\partial \{\bar{MK}\}} \frac{\partial \{\bar{MK}\}}{\partial \{MI\}} + \frac{\partial}{\partial \{\bar{UK}\}} \frac{\partial \{\bar{UK}\}}{\partial \{MI\}} \\
 &= \frac{\partial}{\partial \{MI\}} + \det J \frac{\partial n_k}{\partial x_i} \left[ \frac{\partial}{\partial \{\bar{MK}\}} + \frac{1}{\bar{\rho}} \frac{\partial}{\partial \{\bar{UK}\}} \right] \\
 \frac{\partial}{\partial \{R\}} &= \frac{\partial}{\partial \{R\}} - \left( \frac{\bar{m}_k}{\rho^2} \right) \frac{\partial}{\partial \{\bar{UK}\}} \quad (105)
 \end{aligned}$$

which is the generalization of the one-dimensional construction. Recalling again that all operations are performed on the elemental level, denoting  $\bar{D}_{KI}$  as the element average of  $\left[ \det J \frac{\partial n_k}{\partial x_i} \right]_e$ , and letting  $K$  signify the discrete free index corresponding to  $\partial / \partial n_k$ , the non-empty tensor product Jacobians for equations 94-99 are:

$$[JRR] = \{DET\}^T [A3000] + v_{IJ}^1 \{ETAKJ\}^T [A3010]$$

$$\begin{aligned}
[J R M I] &= \frac{\Delta t}{2} \left[ -\{E T A K I\}^T [A 3 0 1 0] \right. \\
&\quad \left. + v_{IJ}^2 \bar{D}_{KI} \{E T A K J\}^T [A 3 0 1 1] \right]
\end{aligned} \tag{106}$$

$$\begin{aligned}
[J M I R] &= \frac{\Delta t}{2} \left( \frac{\bar{m}_k}{\bar{\rho}^2} \right) \left[ \{M I\}^T [A 3 0 1 0] \right. \\
&\quad \left. + v_{IJ}^2 \{E T A K J\}^T ([A 4 0 1 1 0] + [A 4 0 1 0 1]) \{M I\} \right]
\end{aligned}$$

$$\begin{aligned}
[J M I M I] &= \{D E T\}^T [A 3 0 0 0] + v_{IJ}^1 \{E T A K J\}^T [A 4 0 1 0 0] \{D E T\} \\
&\quad + \frac{\Delta t}{2} \left[ -\{U B A R K\}^T [A 3 0 1 0] - \bar{D}_{KI} \{M I\}^T [A 3 0 1 0] \left( \frac{1}{\bar{\rho}} \right) \right. \\
&\quad \left. + v_{IJ}^2 \{E T A K J\}^T \left\{ \left( [A 4 0 1 0 1] + [A 4 0 1 1 0] \right) \left( \{U B A R K\} \right. \right. \right. \\
&\quad \left. \left. \left. + \left( \frac{1}{\bar{\rho}} \right) \{M I\} \right) \right\} \right]
\end{aligned}$$

$$\begin{aligned}
[J M I M J] &= \frac{\Delta t}{2} \left( \frac{\bar{D}_{KJ}}{\bar{\rho}} \right) \left( \frac{1}{\bar{\rho}} \right) \left[ -\{M J\}^T [A 3 0 1 0] \right. \\
&\quad \left. + v_{JL}^2 \{E T A K L\}^T ([A 4 0 1 0 1] + [A 4 0 1 1 0]) \{M J\} \right]
\end{aligned}$$

$$[J M I P] = -\frac{\Delta t}{2} \{E T A K I\}^T [A 3 0 1 0]$$

$$[J M I S I J] = \frac{\Delta t}{2} \left[ \{E T A K J\}^T ([A 4 0 1 0 0] \{D E T\}) \right] \tag{107}$$

$$\begin{aligned}
[J G R] &= \frac{\Delta t}{2} \left( \frac{\bar{m}_k}{\bar{\rho}^2} \right) \left[ \{G+P\} [A 3 0 1 0] \right. \\
&\quad \left. + v_{4J}^2 \{E T A K J\}^T ([A 4 0 1 1 0] + [A 4 0 1 0 1]) \{G\} \right]
\end{aligned}$$

$$\begin{aligned}
[JGMI] &= \frac{\Delta t}{2} \left( \bar{D}_{KI} \right) \left( \frac{1}{\bar{\rho}} \right) \left[ -\{G+P\}^T [A3010] \right. \\
&\quad \left. + v_{4L}^2 \{ETAKL\}^T (\{[A40101] + [A40110]\} \{MI\}) \right] \\
[JGG] &= \{DET\}^T [A3000] + v_{4J}^2 \{ETAKJ\}^T [A3010] \\
&\quad + \frac{\Delta t}{2} \left[ -\{UBARK\}^T [A3010] \right. \\
&\quad \left. + v_{4J}^2 \{ETAKJ\}^T ([A40110] + [A40101]) \{UBARK\} \right] \\
[JGP] &= -\frac{\Delta t}{2} \{UBARK\}^T [A3010] \\
[JGSIJ] &= \frac{\Delta t}{2} \left[ \{ETAKJ\}^T (\{ \{UI\}^T [A500100] \} \{DET\}) \right] \\
[JGQI] &= \frac{\Delta t}{2} \left( \bar{D}_{LI} \right) \{ETAKL\}^T [A3010] \tag{108} \\
[JPR] &= -\left( \frac{\gamma-1}{2} \right) \left( \frac{\bar{m}_k}{\bar{\rho}^2} \right) \{DET\}^T ([A40000] \{MK\}) \\
[JPMK] &= \left( \frac{\gamma-1}{2} \right) \left[ \{DET\}^T ([A40000] \{UK\}) + \left( \frac{1}{\bar{\rho}} \right) \{DET\}^T ([A40000] \{MK\}) \right] \\
[JPG] &= -(\gamma-1) \{DET\}^T [A3000] \\
[JPP] &= \{DET\}^T [A3000] \tag{109}
\end{aligned}$$

The Jacobians for  $\{FSIJ\}$  and  $\{FQI\}$  are constructed in the manner identical to equation 109.

Observing equations 94-109, the multi-dimensional, generalized coordinate formulation is considerably more detailed than the one-dimensional form. However, the calculus and algebra procedures build directly upon the elementary concepts.

## 5. Numerical Results

The numerical evaluation of the two-dimensional algorithm is in its beginning stage, and only cursory results are completed. A critically important confirmation of the tensor product Jacobian formulation is completed for the scalar dependent variable and the rotating cone test case. Figure 15 summarizes the significant portion of the  $k = 1$  algorithm solutions fields at the quarter turn. The results in Figure 15a) were produced using the time split formulation (ref. 5), which may be considered as exact. Figure 15b) shows the tensor product Jacobian algorithm results, generated by the algorithm specification in equations 42-45 for a two-dimensional problem. Agreement is within the  $\pm 1$  band allowed by truncation of floating point to the integer data used for output. For comparison, Figure 15c) is the solution produced by the tensor product algorithm, applied to equations 26-27 rewritten to account specifically for linearity,

$$[J_u]\{Q1\}_{j+1} = \{RHS\}_j \quad (110)$$

where  $\{RHS\}_j$  is the time level  $j$  evaluation of the difference in the initial value and convection contributions, see reference 5, equation 36. The tensor product Jacobian form of equation 110 is,

$$[J_1]\{P1\}_{j+1} = \{RHS\}_j$$

$$[J_2]\{Q1\}_{j+1} = \{P1\}_{j+1} \quad (111)$$

where  $\{P1\}$  is an intermediate solution. Comparing Figures 15a) - 15c) confirms this procedure introduces significant error into the solution, in distinction to the accurate representation provided by the (Newton) iterative formulation.

The construction of the generalized coordinates formulation has been validated using for comparison the potential solution to incompressible flow about a cylinder. For this case, the contravariant components of convection velocity correspond (to within  $\det[J] = r$ ) to the radial and azimuthal velocity components. The construction of  $\{FR\}$  and  $\{FMI\}$ , and the corresponding Jacobian tensor product matrices were also verified.

0	0	1	0	0	0	0	0	0	0	0
1	2	0	-2	-2	0	1	1	0	0	0
2	0	-4	-3	3	12	15	11	5	1	0
1	-4	-4	5	25	43	47	34	17	5	1
0	-4	-1	16	48	79	84	62	32	11	2
0	-5	-1	18	56	93	101	76	40	14	3
0	-4	-3	13	44	77	85	64	33	12	2
1	-2	-3	4	23	42	48	35	18	5	1
2	0	-3	-3	2	11	14	10	4	1	0
1	1	0	-2	-2	0	0	0	0	0	0
0	1	2	1	0	0	0	0	0	0	0

a) Time-Split Algorithm Solution

0	0	0	0	0	0	0	0	0	0	0
0	1	0	0	0	0	0	0	0	0	0
2	0	-3	-1	5	12	13	8	3	0	0
0	-4	-4	6	27	44	45	32	16	5	1
0	-5	-2	17	50	80	83	60	32	12	3
-1	-6	-2	18	58	94	100	74	40	16	4
0	-5	-3	13	47	79	84	62	33	13	3
0	-4	-4	4	25	44	47	34	17	6	1
2	-1	-4	-3	4	12	14	9	4	1	0
2	1	0	-2	-2	0	0	0	0	0	0
0	1	2	1	0	0	0	0	0	0	0

b) Tensor Product Solution, Non-Linear Formulation

-1	0	0	0	0	0	0	0	0	0	0
1	0	0	0	2	4	4	3	1	0	0
0	-1	-3	0	10	19	19	12	5	1	0
1	-3	-3	7	29	48	48	32	15	4	1
0	-6	-3	14	49	80	81	56	26	9	1
0	-6	-3	16	57	96	100	70	33	11	2
0	-6	-6	10	46	83	88	61	29	9	1
2	-4	-6	1	24	48	52	35	15	4	0
3	0	-5	-4	3	14	17	11	4	0	0
2	2	0	-3	-2	0	0	0	0	0	0
0	1	2	1	0	0	0	0	0	0	0

c) Tensor Product Solution, Linear Formulation

Figure 15. Confirmation of Tensor Matrix Product Jacobian Formulation, Linear Finite Element Algorithm, Rotating Cone Test Case, One-Quarter Turn.



## 6. Continuity Constraint Formulation

An important aerodynamics problem corresponds to low subsonic ( $M < 0.3$ ) flows, wherein the fluid is essentially constant density. As a consequence, the time derivative term is lost in the continuity equation 1. Correspondingly, in many of these aerodynamic applications, the steady flow is dominantly unidirectional, amenable to prediction using a viscous marching procedure, typically termed parabolic Navier - Stokes. Equations 11-18 provide the appropriate differential equation system. The basic requirement is to develop and evaluate a numerical algorithm for enforcement of the continuity equation upon solution of the parabolic partial differential equation system. Specifically, under the order of magnitude analysis applied for generation of parabolic Navier - Stokes, the non-parabolic continuity equation governs first-order effects, while the parabolic transverse momentum equations describe second and higher-order effects.

The theoretical concept, borrowed from the variational calculus, is enforcement of the continuity equation (solution) as a differential constraint on solution of the transverse momentum equations. This measure for continuity must be global, i.e., span  $R^n$ , and the deviation will vanish as continuity becomes satisfied. An appropriate global measure of the deviation from the solution of equation 11 is the harmonic function  $\phi$ , satisfying

$$L(\phi) \equiv \frac{\partial^2 \phi}{\partial x_j^2} - \frac{\partial}{\partial x_j}(\bar{u}_j) = 0 \quad (112)$$

subject to the boundary conditions on  $\partial R$ ,

$$\ell(\phi) = \frac{\partial \phi}{\partial x_j} \hat{n}_j = 0 \quad (113)$$

and setting  $\phi = 0$  at least at one location on  $\partial R$ . As equation 11 becomes satisfied as a differential constraint, equations 112-113 become homogeneous and the solution vanishes. Hence,  $L(\rho_0^h)$  in equation 24 is replaced by  $L(\phi^h)$ , the discretized statement of equations 112-113.

Assessment of algorithm performance focuses on determination of the expansion coefficient  $\beta_3$ , as well as implementation of the algorithm se-

quencing. Following consequential numerical experimentation,  $\beta_3 \equiv \Delta\tau$ , the downstream marching step, was determined suitable, coupled with a procedure for summing sequential contributions to the constructed derivative matrix. Specifically, considering for exposition boundary layer flow, the most elementary form of parabolic Navier - Stokes, the algorithm statement (equation 26) for the  $u_2$  momentum equation is

$$\begin{aligned} \{FU2\} \equiv \{U1\}^T [A3000] (\{U2\}_{j+1}^p - \{U2\}_j) \\ + \Delta\tau (\{GU2\}_{j+1}^p + \{GU2\}_j) = \{0\} \end{aligned} \quad (114)$$

where  $\{GU2\}$  contains the contributions due to spatial distributions of transverse convection, pressure and viscosity, as well as the continuity constraint. At the  $p^{th}$  iteration for step  $j+1$ , following solution of  $L(\phi^h)$  for  $\{\phi\}_{j+1}^p$ , the contribution to the continuity constraint is evaluated as,

$$\{GU2\phi\}_{j+1}^p \equiv [A210] \{\phi\}_{j+1}^p \quad (115)$$

This contribution is accumulated into the previous evaluations, yielding

$$\{GU2\}_{j+1}^p \equiv \sum_{n=1}^{p-1} \{GU2\phi\}_{j+1}^n \quad (116)$$

as the action of the continuity constraint in equation 114. Hence, each successive determination of  $\{\phi\}$  corrects the action of all previous iterations, such that  $\{\phi\}_{j+1}^p \rightarrow \{\epsilon\}$ , where  $|\epsilon| > 0$  is an acceptable discrete level of computed zero, in the limit as  $p$  increases without bound. This procedure thus admits the correct (continuity preserving) solution for equations 112-113, i.e.,  $\phi \approx 0$  everywhere. Using the finite element algorithm statement, equation 24, with  $\vec{\beta}_1 \equiv \vec{0}$ , the solution statement for equations 112-113 is.

$$\{FPHI\} = [A211] \{\phi\}_{j+1}^p + ([A200] \{U1\}_{j+1}^p + [A201] \{U2\}_{j+1}^p) \quad (117)$$

A backwards difference formula is used to evaluate the elements of  $\{U\}_{j+1}^*$ . The various A prefix matrices are familiar, see Appendix A.

## 7. Numerical Results

A definitive test case for the continuity constraint algorithm is provided by the two-dimensional boundary layer equations for laminar flow in zero pressure gradient. The freestream level of  $u_1(x_1)$  remains invariant, yet the corresponding plateau in  $u_2(x_2 > \delta)$  must decay uniformly as  $x^{-1/2}$ . The Poisson formulation, equations 112-113, admits the required global coupling. The level of  $u_2(x_2)$  ranges over five digits on  $0 \leq x_2 \leq \delta$ , and the computational solution must induce a vanishing normal derivative for  $u_2(x_2 = 0)$ , see equation 11, since  $\partial u_1 / \partial x_1 = 0$  at  $x_2 = 0$ .

Using a  $M = 32$  non-uniform discretization of  $R^1$ , the results generated using the conventional finite element boundary layer algorithm (ref. 3), and the continuity-constrained parabolic Navier-Stokes algorithm plot as essentially identical. Table 5 summarizes these comparison solutions, in terms of coordinates  $x_2/\delta$  for which  $u_2/u_\infty$  changes by an order of magnitude. The agreement is excellent over the entire range, as is the approximation to  $\partial u_2 / \partial x_2 = 0$  at  $x_2/\delta = 0$ . The constraint algorithm converges to  $\{\|\delta QI\|\} \leq 10^{-5}$  in typically 4 to 5 iterations per step. An intrinsic error measure for equation 112 is the energy norm.

$$E(\phi, \phi) \equiv \int_{R^1} \frac{\partial \phi}{\partial x_2} \frac{\partial \phi}{\partial x_2} dx_2 \quad (118)$$

In  $E(\phi, \phi)$ , the error in satisfaction of continuity typically decreases by a factor or two for each iteration, as illustrated in Table 6 for a typical integration step. For laminar flow, the algorithm maintains  $E(\phi, \phi) \leq 10^{-8}$  for iteration convergence to  $\epsilon \approx 10^{-5}$ .

The corresponding levels for turbulent boundary layer prediction are  $E(\phi, \phi) < 10^{-5}$  for  $\epsilon \approx 10^{-4}$ . Figure 16 compares the continuity constraint algorithm results to data (ref. 17) for the Bradshaw turbulent relaxing flow experiment. This solution is indistinguishable from the direct boundary layer solution, and was obtained using the turbulence kinetic energy-dissipation function closure model and the complete equation system

12-18. The continuity constraint algorithm is equally applicable to ducted and/or semi-bounded flows, and should find considerable use in computational aerodynamics.

Table 5  
Transverse Velocity Distributions,  $U_2(x_2) \times 10^3$   
Laminar Incompressible Boundary Layer

<u>Coordinate</u> <u><math>(x_2/\delta)</math></u>	<u>Boundary</u> <u>Layer Solution</u>	<u>Continuity</u> <u>Constraint Solution</u>
0.0	.0	.0
0.0009	.0000011	.0000001
0.0021	.0000054	.0000030
0.0035	.0000149	.0000114
⋮	⋮	⋮
0.0095	.00011	.00011
⋮	⋮	⋮
0.031	.00118	.00118
⋮	⋮	⋮
0.10	.0128	.0127
⋮	⋮	⋮
0.67	.139	.138
⋮	⋮	⋮
1.0	.218	.218

Table 6  
Continuity Constraint Algorithm Convergence  
Laminar Incompressible Boundary Layer

<u>Iteration</u>	<u>Energy Norm, <math>E(\phi, \phi)</math></u>
1	0.69432 E(-9)
2	0.30670 E(-9)
3	0.15692 E(-9)
4	0.08028 E(-9)

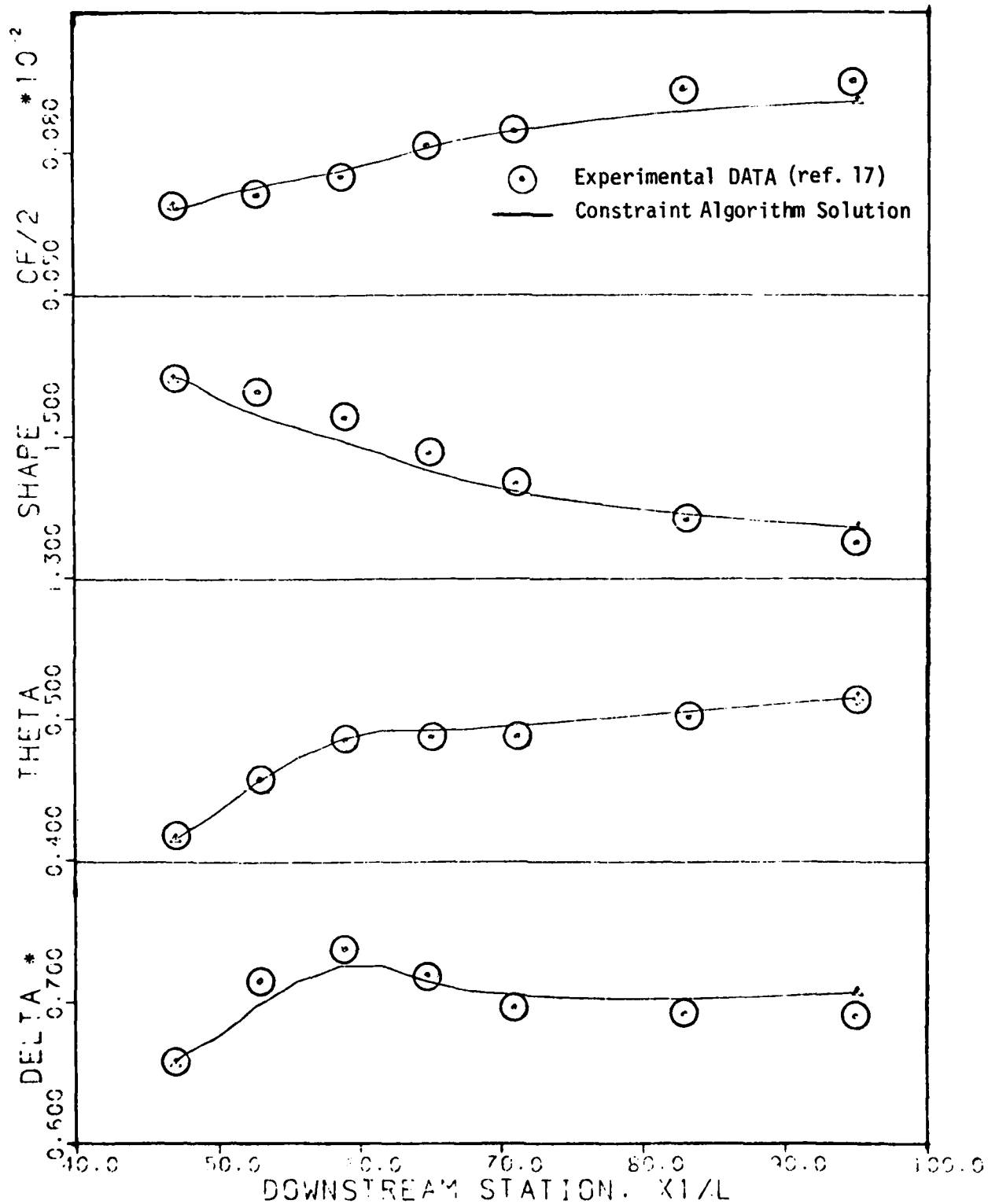


Figure 16. Computed Boundary Layer Integral Parameter Distributions For Bradshaw Relaxing Flow, Linear Finite Element Continuity Constraint Algorithm, Turbulence Kinetic Energy Closure Model.

## SECTION VI

### CONCLUSIONS AND RECOMMENDATIONS

The objective of this research project is to derive and evaluate versatile, accurate and efficient numerical algorithms for solution of aerodynamic flowfields at large Reynolds number. Building upon work reported in reference 5, the concept of a dissipative finite element algorithm has been refined and extended to solution of a complete equation set in aerodynamics. The test case numerical results are highly encouraging with respect to shock resolution and overall performance, utilizing both a linear and a quadratic finite element embodiment of the theory. The theoretical formulational statement of the algorithm has been extended to a multi-dimensional description in generalized coordinates. The key efficiency feature is identification of the tensor matrix resolution of the Jacobian of the Newton algorithm for this statement. Finally, the concept of application of the continuity equation solution, as a differential constraint on the momentum equation algorithm, has been validated. The formulation is directly useful for viscous marching procedures, and with some modifications could be equally useful for a low Mach number Navier - Stokes solution algorithm.

These results on application of finite element solution concepts in computational aerodynamics are highly encouraging. It is recommended that the multi-dimensional computer program development be pursued with vigor, to facilitate performance quantization for the next level of problem complexity.

## REFERENCES

1. Zienkiewicz, O. C., The Finite Element Method, McGraw-Hill, London, 1977.
2. Baker, A. J., and Soliman, M. O., "Utility of a Finite Element Solution Algorithm for Initial-Value Problems," J. Comp. Phys., V. 32, No. 3, pp. 289-324, 1979.
3. Soliman, M. O., and Baker, A. J., "Accuracy And Convergence of A Finite Element Algorithm For Laminar Boundary Layer Flow," J. Computers & Fluids, V. 9, pp. 43 - 62, 1981.
4. Soliman, M. O. and Baker, A. J., " Accuracy And Convergence of a Finite Element Algorithm For Turbulent Boundary Layer Flow," J. Computer Mtd. in Appl. Mech. & Engr., to appear 1981.
5. Baker, A. J., "Research On Numerical Algorithms For The Three-Dimensional Navier - Stokes Equations, I. Accuracy, Convergence and Efficiency," USAF Report AFFDL - TR - 79 - 3141, 1980.
6. Cebeci, T., and Smith, A. M. O., Analysis of Turbulent Boundary Layers, Academic Press, New York, 1974.
7. Baker, A. J., Yu, J. C., Orzechowski, J. A., and Gatski, T. B., "Prediction and Measurement of Turbulent Aerodynamic Trailing Edge Flows," AIAA Paper No. 80-1395, 1980.
8. Hanjalic, K. and Launder, B. E., "A Reynolds Stress Model of Turbulence and Its Application to Thin Shear Flows," J. Fluid Mech., V. 52, Pt. 4, pp. 609-638, 1972.
9. Prenter, P. M., Splines and Variational Methods, John Wiley, New York, 1975.
10. Thames, F. C., Thompson, J. F., Mastin, C. W., and Walker, R. L., "Numerical Solutions for Viscous and Potential Flow about Arbitrary Two-Dimensional Bodies Using Body-Fitted Coordinate Systems," J. Comp. Phys., Vol. 24, No. 3, pp. 245-273, 1977.
11. NASA Workshop On Numerical Grid Generation Techniques for Partial Differential Equations, held at NASA Langley Research Center, October 6-7, 1980.
12. Beam, R. M. and Warming, R. F., "An Implicit Factored Scheme for the Compressible Navier-Stokes Equations," AIAA J., V. 16, pp. 393-402, 1978.
13. Shapiro, A. H., The Dynamics And Thermodynamics of Compressible Fluid Flow, Vol. II, Ronald Press, NY, 1953.
14. Sod, G. A., "A Survey of Several Finite Difference Methods for Systems of Non-Linear Hyperbolic Conservation Laws," J. Comp. Phys., V. 27, pp. 1-31, 1978.

15. Van Leer, B., "Towards the Ultimate Conservative Difference Scheme. V. A Second-Order Sequel to Godunov's Method," J. Comp. Phys., V. 32, pp. 101-136, 1979.
16. Zalesak, S. T., "High Order ZIP Differencing of Convective Terms," NRL Report No. 4218, May, 1980.
17. Coles, D. A. & Hirst, E. A., Editors, Proceedings AFOSR-IFP-Stanford Conference on Computation of Turbulent Boundary Layers, Volume II, Mech. Engr. Dept., Stanford Univ., CA, 1968.



APPENDIX A

FINITE ELEMENT ALGORITHM HYPERMATRICES

LINEAR AND QUADRATIC BASIS ON ONE DIMENSIONAL SPACE

1. Linear Finite Element Formulation

$$\{A10\} = \frac{1}{2} \begin{Bmatrix} 1 \\ 1 \end{Bmatrix}$$

$$[A200] = \frac{1}{6} \begin{bmatrix} 2 & 1 \\ 1 & 2 \end{bmatrix}$$

$$[A201] = \frac{1}{2\Delta_e} \begin{bmatrix} -1 & 1 \\ -1 & 1 \end{bmatrix}$$

$$[A210] = \frac{1}{2\Delta_e} \begin{bmatrix} -1 & -1 \\ 1 & 1 \end{bmatrix}$$

$$[A3000] = \frac{1}{12} \begin{bmatrix} \begin{Bmatrix} 3 \\ 1 \end{Bmatrix} \begin{Bmatrix} 1 \\ 1 \end{Bmatrix} \\ \begin{Bmatrix} 1 \\ 1 \end{Bmatrix} \begin{Bmatrix} 1 \\ 3 \end{Bmatrix} \end{bmatrix}$$

$$[A3001] = \frac{1}{6\Delta_e} \begin{bmatrix} \begin{Bmatrix} -2 \\ -1 \end{Bmatrix} \begin{Bmatrix} 2 \\ 1 \end{Bmatrix} \\ \begin{Bmatrix} -1 \\ -2 \end{Bmatrix} \begin{Bmatrix} 1 \\ 2 \end{Bmatrix} \end{bmatrix}$$

$$[A3010] = \frac{1}{6\Delta_e} \begin{bmatrix} \begin{Bmatrix} -2 \\ -1 \end{Bmatrix} & \begin{Bmatrix} -1 \\ -2 \end{Bmatrix} \\ \begin{Bmatrix} 2 \\ 1 \end{Bmatrix} & \begin{Bmatrix} 1 \\ 2 \end{Bmatrix} \end{bmatrix}$$

$$[A3100] = \frac{1}{6\Delta_e} \begin{bmatrix} \begin{Bmatrix} -2 \\ 2 \end{Bmatrix} & \begin{Bmatrix} -1 \\ 1 \end{Bmatrix} \\ \begin{Bmatrix} -1 \\ 1 \end{Bmatrix} & \begin{Bmatrix} -2 \\ 2 \end{Bmatrix} \end{bmatrix}$$

$$[A3011] = \frac{1}{2\Delta_e^2} \begin{bmatrix} \begin{Bmatrix} 1 \\ 1 \end{Bmatrix} & \begin{Bmatrix} -1 \\ -1 \end{Bmatrix} \\ \begin{Bmatrix} -1 \\ -1 \end{Bmatrix} & \begin{Bmatrix} 1 \\ 1 \end{Bmatrix} \end{bmatrix}$$

$$[A3110] = \frac{1}{2\Delta_e^2} \begin{bmatrix} \begin{Bmatrix} 1 \\ -1 \end{Bmatrix} & \begin{Bmatrix} 1 \\ -1 \end{Bmatrix} \\ \begin{Bmatrix} -1 \\ 1 \end{Bmatrix} & \begin{Bmatrix} -1 \\ 1 \end{Bmatrix} \end{bmatrix}$$

$$[A40000] = \frac{1}{60} \begin{bmatrix} \begin{bmatrix} 12 & 3 \\ 3 & 2 \end{bmatrix} & \begin{bmatrix} 3 & 2 \\ 2 & 3 \end{bmatrix} \\ \begin{bmatrix} 3 & 2 \\ 2 & 3 \end{bmatrix} & \begin{bmatrix} 2 & 3 \\ 3 & 12 \end{bmatrix} \end{bmatrix}$$

$$[A40001] = \frac{1}{12\Delta_e} \begin{bmatrix} \begin{bmatrix} -3 & 3 \\ -1 & 1 \end{bmatrix} & \begin{bmatrix} -1 & 1 \\ -1 & 1 \end{bmatrix} \\ \begin{bmatrix} -1 & 1 \\ -1 & 1 \end{bmatrix} & \begin{bmatrix} -1 & 1 \\ -3 & 3 \end{bmatrix} \end{bmatrix}$$

$$[A40010] = \frac{1}{12\Delta_e} \begin{bmatrix} \begin{bmatrix} -3 & -1 \\ -1 & -1 \end{bmatrix} & \begin{bmatrix} 3 & 1 \\ 1 & 1 \end{bmatrix} \\ \begin{bmatrix} -1 & -1 \\ -1 & -3 \end{bmatrix} & \begin{bmatrix} 1 & 1 \\ 1 & 3 \end{bmatrix} \end{bmatrix}$$

$$[A41000] = \frac{1}{12\Delta_e} \begin{bmatrix} \begin{bmatrix} -3 & -1 \\ 3 & 1 \end{bmatrix} & \begin{bmatrix} -1 & -1 \\ 1 & 1 \end{bmatrix} \\ \begin{bmatrix} -1 & -1 \\ 1 & 1 \end{bmatrix} & \begin{bmatrix} -1 & -3 \\ 1 & 3 \end{bmatrix} \end{bmatrix}$$

$$[A40011] = \frac{1}{6\Delta_e} \begin{bmatrix} \begin{bmatrix} 2 & -2 \\ 1 & -1 \end{bmatrix} & \begin{bmatrix} -2 & 2 \\ -1 & 1 \end{bmatrix} \\ \begin{bmatrix} 1 & -1 \\ 2 & -2 \end{bmatrix} & \begin{bmatrix} -1 & 1 \\ -2 & 2 \end{bmatrix} \end{bmatrix}$$

$$[A40110] = \frac{1}{6\Delta_e^2} \begin{bmatrix} \begin{bmatrix} 2 & 1 \\ 1 & 2 \end{bmatrix} & \begin{bmatrix} -2 & -1 \\ -1 & -2 \end{bmatrix} \\ \begin{bmatrix} -2 & -1 \\ -1 & -2 \end{bmatrix} & \begin{bmatrix} 2 & 1 \\ 1 & 2 \end{bmatrix} \end{bmatrix}$$

$$[A41100] = \frac{1}{6\Delta_e^2} \begin{bmatrix} \begin{bmatrix} 2 & 1 \\ -2 & -1 \end{bmatrix} & \begin{bmatrix} 1 & 2 \\ -1 & -2 \end{bmatrix} \\ \begin{bmatrix} -2 & -1 \\ 2 & 1 \end{bmatrix} & \begin{bmatrix} -1 & -2 \\ 1 & 2 \end{bmatrix} \end{bmatrix}$$

$$[A40101] = \frac{1}{6\Delta_e^2} \begin{bmatrix} \begin{bmatrix} 2 & -2 \\ -2 & 2 \end{bmatrix} & \begin{bmatrix} 1 & -1 \\ -1 & 1 \end{bmatrix} \\ \begin{bmatrix} 1 & -1 \\ -1 & 1 \end{bmatrix} & \begin{bmatrix} 2 & -2 \\ -2 & 2 \end{bmatrix} \end{bmatrix}$$

## 2. Quadratic Finite Element Formulation

$$\{A10\} = \frac{1}{6} \begin{Bmatrix} 1 \\ 4 \\ 1 \end{Bmatrix}$$

$$[A200] = \frac{1}{30} \begin{bmatrix} 4 & 2 & -1 \\ 2 & 16 & 2 \\ -1 & 2 & 4 \end{bmatrix}$$

$$[A201] = \frac{1}{6\Delta_e} \begin{bmatrix} -3 & 4 & -1 \\ -4 & 0 & 4 \\ 1 & -4 & 3 \end{bmatrix}$$

$$[A210] = \frac{1}{6\Delta_e} \begin{bmatrix} -3 & -4 & 1 \\ 4 & 0 & 4 \\ -1 & 4 & 3 \end{bmatrix}$$

$$[A3000] = \frac{1}{420} \begin{bmatrix} \begin{Bmatrix} 39 \\ 20 \\ -3 \end{Bmatrix} & \begin{Bmatrix} 20 \\ 16 \\ -8 \end{Bmatrix} & \begin{Bmatrix} -3 \\ -8 \\ -8 \end{Bmatrix} \\ \begin{Bmatrix} 20 \\ 16 \\ -8 \end{Bmatrix} & \begin{Bmatrix} 16 \\ 192 \\ 16 \end{Bmatrix} & \begin{Bmatrix} -8 \\ 16 \\ 20 \end{Bmatrix} \\ \begin{Bmatrix} -3 \\ -8 \\ -3 \end{Bmatrix} & \begin{Bmatrix} -8 \\ 16 \\ 20 \end{Bmatrix} & \begin{Bmatrix} -3 \\ 20 \\ 39 \end{Bmatrix} \end{bmatrix}$$

$$[A3001] = \frac{1}{90\Lambda_e} \begin{bmatrix} \begin{Bmatrix} -30 \\ -18 \\ 3 \end{Bmatrix} & \begin{Bmatrix} 36 \\ 24 \\ 0 \end{Bmatrix} & \begin{Bmatrix} -6 \\ -6 \\ -3 \end{Bmatrix} \\ \begin{Bmatrix} -18 \\ -48 \\ 6 \end{Bmatrix} & \begin{Bmatrix} 24 \\ 0 \\ -24 \end{Bmatrix} & \begin{Bmatrix} -6 \\ 48 \\ 18 \end{Bmatrix} \\ \begin{Bmatrix} 3 \\ 6 \\ 6 \end{Bmatrix} & \begin{Bmatrix} 0 \\ -24 \\ -36 \end{Bmatrix} & \begin{Bmatrix} -3 \\ 18 \\ 30 \end{Bmatrix} \end{bmatrix}$$

$$[A3010] = \frac{1}{30\Delta_e} \begin{bmatrix} \begin{pmatrix} -10 \\ -6 \\ 1 \end{pmatrix} & \begin{pmatrix} -6 \\ -16 \\ 2 \end{pmatrix} & \begin{pmatrix} 1 \\ 2 \\ 2 \end{pmatrix} \\ \begin{pmatrix} 12 \\ 8 \\ 0 \end{pmatrix} & \begin{pmatrix} 8 \\ 0 \\ -8 \end{pmatrix} & \begin{pmatrix} 0 \\ -8 \\ -12 \end{pmatrix} \\ \begin{pmatrix} -2 \\ -2 \\ -1 \end{pmatrix} & \begin{pmatrix} -2 \\ 16 \\ 6 \end{pmatrix} & \begin{pmatrix} -1 \\ 6 \\ 10 \end{pmatrix} \end{bmatrix}$$

$$[A3100] = \frac{1}{30\Delta_e} \begin{bmatrix} \begin{pmatrix} -10 \\ 12 \\ -2 \end{pmatrix} & \begin{pmatrix} -6 \\ 8 \\ -2 \end{pmatrix} & \begin{pmatrix} 1 \\ 0 \\ -1 \end{pmatrix} \\ \begin{pmatrix} -6 \\ 8 \\ -2 \end{pmatrix} & \begin{pmatrix} -16 \\ 0 \\ 16 \end{pmatrix} & \begin{pmatrix} 2 \\ -8 \\ 6 \end{pmatrix} \\ \begin{pmatrix} 1 \\ 0 \\ -1 \end{pmatrix} & \begin{pmatrix} 2 \\ -8 \\ 6 \end{pmatrix} & \begin{pmatrix} 2 \\ -12 \\ 10 \end{pmatrix} \end{bmatrix}$$

$$[A3011] = \frac{1}{30\Delta_e^2} \begin{bmatrix} \begin{pmatrix} 37 \\ 36 \\ -3 \end{pmatrix} & \begin{pmatrix} -44 \\ -32 \\ -4 \end{pmatrix} & \begin{pmatrix} 7 \\ -4 \\ 7 \end{pmatrix} \\ \begin{pmatrix} -44 \\ -32 \\ -4 \end{pmatrix} & \begin{pmatrix} 48 \\ 64 \\ 48 \end{pmatrix} & \begin{pmatrix} -4 \\ -32 \\ -44 \end{pmatrix} \\ \begin{pmatrix} 7 \\ -4 \\ 7 \end{pmatrix} & \begin{pmatrix} -4 \\ -32 \\ -44 \end{pmatrix} & \begin{pmatrix} -3 \\ 36 \\ 37 \end{pmatrix} \end{bmatrix}$$

$$[A3110] = \frac{1}{30\Delta_e^2} \begin{bmatrix} \begin{Bmatrix} 37 \\ -44 \\ 7 \end{Bmatrix} & \begin{Bmatrix} 36 \\ -32 \\ -4 \end{Bmatrix} & \begin{Bmatrix} -3 \\ -4 \\ 7 \end{Bmatrix} \\ \begin{Bmatrix} -44 \\ 48 \\ -4 \end{Bmatrix} & \begin{Bmatrix} -32 \\ 64 \\ -32 \end{Bmatrix} & \begin{Bmatrix} -4 \\ 48 \\ 44 \end{Bmatrix} \\ \begin{Bmatrix} 7 \\ 4 \\ -3 \end{Bmatrix} & \begin{Bmatrix} -4 \\ -32 \\ 36 \end{Bmatrix} & \begin{Bmatrix} 7 \\ -44 \\ 37 \end{Bmatrix} \end{bmatrix}$$

$$[A40000] = \frac{1}{630} \begin{bmatrix} \begin{bmatrix} 46 & 16 & -3 \\ 16 & 16 & -2 \\ -3 & -2 & -1 \end{bmatrix} & \begin{bmatrix} 16 & 16 & -2 \\ 16 & 16 & -8 \\ -2 & -8 & -2 \end{bmatrix} & \begin{bmatrix} -3 & -2 & 1 \\ -2 & -8 & -2 \\ 1 & -2 & -3 \end{bmatrix} \\ \begin{bmatrix} 16 & 16 & -2 \\ 16 & 16 & -8 \\ -2 & -8 & -2 \end{bmatrix} & \begin{bmatrix} 16 & 16 & -8 \\ 16 & 256 & 16 \\ -8 & 16 & 16 \end{bmatrix} & \begin{bmatrix} -2 & -8 & -2 \\ -8 & 16 & 16 \\ -2 & 16 & 16 \end{bmatrix} \\ \begin{bmatrix} -3 & -2 & 1 \\ -2 & -8 & -2 \\ 1 & -2 & -3 \end{bmatrix} & \begin{bmatrix} -2 & -8 & -2 \\ -8 & 16 & 16 \\ -2 & 16 & 16 \end{bmatrix} & \begin{bmatrix} 1 & -2 & -3 \\ -2 & 16 & 16 \\ -3 & 16 & 46 \end{bmatrix} \end{bmatrix}$$

$$[A40001] = \frac{1}{420\Delta_e} \begin{bmatrix} \begin{bmatrix} -105 & 132 & -27 \\ -44 & 48 & -4 \\ 9 & -12 & 3 \end{bmatrix} & \begin{bmatrix} -44 & 48 & -4 \\ -48 & 64 & -16 \\ 8 & 0 & -8 \end{bmatrix} & \begin{bmatrix} 9 & -12 & 3 \\ 8 & 0 & -8 \\ -3 & 12 & -9 \end{bmatrix} \\ \begin{bmatrix} -44 & 48 & -4 \\ -48 & 64 & -16 \\ 8 & 0 & -8 \end{bmatrix} & \begin{bmatrix} -48 & 64 & -16 \\ -192 & 0 & 192 \\ 16 & -64 & 48 \end{bmatrix} & \begin{bmatrix} 8 & 0 & -8 \\ 16 & -64 & 48 \\ 4 & -48 & 44 \end{bmatrix} \\ \begin{bmatrix} 9 & -12 & 3 \\ 8 & 0 & -8 \\ -3 & 12 & -9 \end{bmatrix} & \begin{bmatrix} 8 & 0 & -8 \\ 16 & -64 & 48 \\ 4 & -48 & 44 \end{bmatrix} & \begin{bmatrix} -3 & 12 & -9 \\ 4 & -48 & 44 \\ 27 & -132 & 105 \end{bmatrix} \end{bmatrix}$$

$$[A40010] = \frac{1}{420\Delta_e} \begin{bmatrix} \begin{bmatrix} -105 & -44 & 9 \\ -44 & -48 & 8 \\ 9 & 8 & -3 \end{bmatrix} & \begin{bmatrix} 132 & 48 & -12 \\ 48 & 64 & 0 \\ -12 & 0 & 12 \end{bmatrix} & \begin{bmatrix} -27 & -4 & 3 \\ -4 & -16 & -8 \\ 3 & -8 & -9 \end{bmatrix} \\ \begin{bmatrix} -44 & -48 & 8 \\ -48 & -192 & 16 \\ 8 & 16 & 4 \end{bmatrix} & \begin{bmatrix} 48 & 64 & 0 \\ 64 & 0 & -64 \\ 0 & -64 & -48 \end{bmatrix} & \begin{bmatrix} -4 & -16 & -8 \\ -16 & 192 & 48 \\ -8 & 48 & 44 \end{bmatrix} \\ \begin{bmatrix} 9 & 8 & -3 \\ 8 & 16 & 4 \\ -3 & 4 & 27 \end{bmatrix} & \begin{bmatrix} -12 & 0 & 12 \\ 0 & -64 & -48 \\ 12 & -48 & -132 \end{bmatrix} & \begin{bmatrix} 3 & -8 & -9 \\ -8 & 48 & 44 \\ -8 & 44 & 105 \end{bmatrix} \end{bmatrix}$$

$$[A41000] = \frac{1}{420\Delta_e} \begin{bmatrix} \begin{bmatrix} -105 & -44 & 9 \\ -44 & -48 & 8 \\ 9 & 8 & -3 \end{bmatrix} & \begin{bmatrix} -44 & -48 & 8 \\ -48 & -192 & 16 \\ 8 & 16 & 4 \end{bmatrix} & \begin{bmatrix} 9 & 8 & -3 \\ 8 & 16 & 4 \\ -3 & 4 & 27 \end{bmatrix} \\ \begin{bmatrix} 132 & 48 & -12 \\ 48 & 64 & 0 \\ -12 & 0 & 12 \end{bmatrix} & \begin{bmatrix} 48 & 64 & 0 \\ 64 & 0 & -64 \\ 0 & 64 & -48 \end{bmatrix} & \begin{bmatrix} -12 & 0 & 12 \\ 0 & -64 & -48 \\ 12 & -48 & -132 \end{bmatrix} \\ \begin{bmatrix} -27 & -4 & 3 \\ -4 & -16 & -8 \\ 3 & -8 & -9 \end{bmatrix} & \begin{bmatrix} -4 & -16 & -8 \\ -16 & 192 & 48 \\ -8 & 48 & 44 \end{bmatrix} & \begin{bmatrix} 3 & -8 & -9 \\ -8 & 48 & 44 \\ -9 & 44 & 105 \end{bmatrix} \end{bmatrix}$$

$$[A40011] = \frac{1}{210\Delta_e^2} \begin{bmatrix} \begin{bmatrix} 184 & -228 & 44 \\ 94 & -104 & 10 \\ -19 & 24 & -5 \end{bmatrix} & \begin{bmatrix} -228 & 288 & -60 \\ -104 & 96 & 8 \\ 24 & -48 & 24 \end{bmatrix} & \begin{bmatrix} 44 & -60 & 16 \\ 10 & 8 & -18 \\ -5 & 24 & -19 \end{bmatrix} \\ \begin{bmatrix} 94 & -104 & 10 \\ 176 & -128 & -48 \\ -18 & 8 & 10 \end{bmatrix} & \begin{bmatrix} -104 & 96 & 8 \\ -128 & 256 & -128 \\ 8 & 96 & -104 \end{bmatrix} & \begin{bmatrix} 10 & 8 & -18 \\ -48 & -128 & 176 \\ 10 & -104 & 94 \end{bmatrix} \\ \begin{bmatrix} -19 & 24 & -5 \\ -18 & 8 & 10 \\ 16 & -60 & 44 \end{bmatrix} & \begin{bmatrix} 24 & -48 & 24 \\ 8 & 96 & -104 \\ -60 & 288 & -228 \end{bmatrix} & \begin{bmatrix} -5 & 24 & -19 \\ 10 & -104 & 94 \\ 44 & -228 & 184 \end{bmatrix} \end{bmatrix}$$



$$[A40110] = \frac{1}{210\Delta^2 e} \begin{bmatrix} \begin{bmatrix} 184 & 94 & -19 \\ -228 & -104 & 24 \\ 44 & 10 & -5 \end{bmatrix} & \begin{bmatrix} -228 & -104 & 24 \\ 288 & 96 & -48 \\ -60 & 8 & 24 \end{bmatrix} & \begin{bmatrix} 44 & 10 & -5 \\ -60 & 8 & 24 \\ 16 & -18 & -19 \end{bmatrix} \\ \begin{bmatrix} 94 & 176 & -18 \\ -104 & -128 & 8 \\ 10 & -48 & 10 \end{bmatrix} & \begin{bmatrix} -104 & -128 & 8 \\ 96 & 256 & 96 \\ 8 & -128 & -104 \end{bmatrix} & \begin{bmatrix} 10 & -48 & 10 \\ 8 & -128 & -104 \\ -18 & 176 & 94 \end{bmatrix} \\ \begin{bmatrix} -19 & -18 & 16 \\ 24 & 8 & -60 \\ -5 & 10 & 44 \end{bmatrix} & \begin{bmatrix} 24 & 8 & -60 \\ -48 & 96 & 288 \\ 24 & -104 & -228 \end{bmatrix} & \begin{bmatrix} -5 & 10 & 44 \\ 24 & -104 & -228 \\ -19 & 94 & 184 \end{bmatrix} \end{bmatrix}$$

$$[A41100] = \frac{1}{210\Delta^2 e} \begin{bmatrix} \begin{bmatrix} 184 & 94 & -19 \\ -228 & -104 & 24 \\ 44 & 10 & -5 \end{bmatrix} & \begin{bmatrix} 94 & 176 & -18 \\ -104 & -128 & 8 \\ 10 & -48 & 10 \end{bmatrix} & \begin{bmatrix} -19 & -18 & 16 \\ 24 & 8 & -60 \\ -5 & 10 & 44 \end{bmatrix} \\ \begin{bmatrix} -228 & -104 & 24 \\ 288 & 96 & -48 \\ -60 & 8 & 24 \end{bmatrix} & \begin{bmatrix} -104 & -128 & 8 \\ 96 & 256 & 96 \\ 8 & -128 & -104 \end{bmatrix} & \begin{bmatrix} 24 & 8 & -60 \\ -48 & 96 & 288 \\ 24 & -104 & -228 \end{bmatrix} \\ \begin{bmatrix} 44 & 10 & -5 \\ -60 & 8 & 24 \\ 16 & -18 & -19 \end{bmatrix} & \begin{bmatrix} 10 & -48 & 10 \\ 8 & -128 & -104 \\ -18 & 176 & 94 \end{bmatrix} & \begin{bmatrix} -5 & 10 & 44 \\ 24 & -104 & -228 \\ -19 & 94 & 184 \end{bmatrix} \end{bmatrix}$$

$$[A40101] = \frac{1}{210\Delta^2 e} \begin{bmatrix} \begin{bmatrix} 184 & -228 & 44 \\ -228 & 288 & -60 \\ 44 & -60 & 16 \end{bmatrix} & \begin{bmatrix} 94 & -104 & 10 \\ -104 & 96 & 8 \\ 10 & 8 & -18 \end{bmatrix} & \begin{bmatrix} -19 & 24 & -5 \\ 24 & -48 & 24 \\ -5 & 24 & -19 \end{bmatrix} \\ \begin{bmatrix} 94 & -104 & 10 \\ -104 & 96 & 8 \\ 10 & 8 & -18 \end{bmatrix} & \begin{bmatrix} 176 & -128 & -48 \\ -128 & 256 & -128 \\ -48 & -128 & 176 \end{bmatrix} & \begin{bmatrix} -18 & 8 & 10 \\ 8 & 96 & -104 \\ 10 & -104 & 94 \end{bmatrix} \\ \begin{bmatrix} -19 & 24 & -5 \\ 24 & -48 & 24 \\ -5 & 24 & -19 \end{bmatrix} & \begin{bmatrix} -18 & 8 & 10 \\ 8 & 96 & -104 \\ 10 & -104 & 94 \end{bmatrix} & \begin{bmatrix} 16 & -60 & 44 \\ -60 & 288 & -228 \\ 44 & -228 & 184 \end{bmatrix} \end{bmatrix}$$

APPENDIX B  
FINITE ELEMENT ALGORITHM HYPERMATRICES  
LINEAR BASIS ON TWO-DIMENSIONAL SPACE

1. Linear Tensor Product Basis ( $\Delta_e = \det J$ ):

$$\{B_{10}\} = \begin{Bmatrix} 1 \\ 1 \\ 1 \\ 1 \end{Bmatrix}$$

$$[B_{200}] = \frac{1}{9} \begin{bmatrix} 4 & 2 & 1 & 2 \\ & 4 & 2 & 1 \\ & & 4 & 2 \\ \text{(sym)} & & & 4 \end{bmatrix}$$

$$[B_{3000}] = \frac{1}{36} \begin{bmatrix} 9 & 3 & 1 & 3 \\ 3 & 3 & 1 & 1 \\ & 1 & 1 & 1 \\ 3 & 1 & 1 & 3 \\ 3 & 3 & 1 & 1 \\ 3 & 9 & 3 & 1 \\ 1 & 3 & 3 & 1 \\ 1 & 1 & 1 & 1 \\ 1 & 1 & 1 & 1 \\ 1 & 3 & 3 & 1 \\ 1 & 3 & 1 & 3 \\ 1 & 1 & 3 & 3 \\ 3 & 1 & 1 & 3 \\ 1 & 1 & 1 & 1 \\ 1 & 1 & 3 & 3 \\ 3 & 1 & 3 & 9 \end{bmatrix}$$

$$[B3001] = \frac{1}{36} \begin{bmatrix} -6 & 6 & 2 & -2 \\ -3 & 3 & 1 & -1 \\ -1 & 1 & 1 & -1 \\ -2 & 2 & 2 & -2 \\ -3 & 3 & 1 & -1 \\ -6 & 6 & 2 & -2 \\ -2 & 2 & 2 & -2 \\ -1 & 1 & 1 & -1 \\ -1 & 1 & 1 & -1 \\ -2 & 2 & 2 & -2 \\ -2 & 2 & 6 & -6 \\ -1 & 1 & 3 & -3 \\ -2 & 2 & 2 & -2 \\ -1 & 1 & 1 & -1 \\ -1 & 1 & 3 & -3 \\ -2 & 2 & 6 & -6 \end{bmatrix}$$

$$[B3010] = \frac{1}{36} \begin{bmatrix} -6 & -3 & -1 & -2 \\ -3 & -6 & -2 & -1 \\ -1 & -2 & -2 & -1 \\ -2 & -1 & -1 & -2 \\ 6 & 3 & 1 & 2 \\ 3 & 6 & 2 & 1 \\ 1 & 2 & 2 & 1 \\ 2 & 1 & 1 & 2 \\ 2 & 1 & 1 & 2 \\ 1 & 2 & 2 & 1 \\ 1 & 2 & 6 & 3 \\ 2 & 1 & 3 & 6 \\ -2 & -1 & -1 & -2 \\ -1 & -2 & -2 & -1 \\ 1 & -2 & -6 & -3 \\ 2 & -1 & -3 & -6 \end{bmatrix}$$

$$[B3002] = \frac{1}{36} \begin{bmatrix} -6 & -2 & 2 & 6 \\ -2 & -2 & 2 & 2 \\ -1 & -1 & 1 & 1 \\ -3 & -1 & 1 & 3 \\ 2 & -2 & 2 & 2 \\ 2 & -6 & 6 & 2 \\ 1 & -3 & 3 & 1 \\ -1 & -1 & 1 & 1 \\ -1 & -1 & 1 & 1 \\ -1 & -3 & 3 & 1 \\ 2 & -6 & 6 & 2 \\ -2 & -2 & 2 & 2 \\ -3 & -1 & 1 & 3 \\ -1 & -1 & 1 & 1 \\ 2 & -2 & 2 & 2 \\ -6 & -2 & 2 & 6 \end{bmatrix}$$

$$[B3020] = \frac{1}{36} \begin{bmatrix} -6 & -2 & -1 & -3 \\ 2 & -2 & -1 & -1 \\ 1 & -1 & -2 & -2 \\ -3 & -1 & -2 & -6 \\ -2 & -2 & -1 & -1 \\ -2 & -6 & -3 & -1 \\ -1 & -3 & -6 & -2 \\ -1 & -1 & -2 & -2 \\ 2 & 2 & 1 & 1 \\ 2 & 6 & 3 & 1 \\ 1 & 3 & 6 & 2 \\ 1 & 1 & 2 & 2 \\ 6 & 2 & 1 & 3 \\ 2 & 2 & 1 & 1 \\ 1 & 1 & 2 & 2 \\ 3 & 1 & 2 & 6 \end{bmatrix}$$

$$[B3011] = \frac{1}{36} \begin{bmatrix} 4 & -4 & -1 & 1 \\ 4 & -4 & -1 & 1 \\ 1 & -1 & -1 & 1 \\ 1 & -1 & -1 & 1 \\ -4 & 4 & 1 & -1 \\ -4 & 4 & 1 & -1 \\ -1 & 1 & 1 & -1 \\ -1 & 1 & 1 & -1 \\ -1 & 1 & 1 & -1 \\ -1 & 1 & 1 & -1 \\ 1 & -1 & -1 & 1 \\ 1 & -1 & -1 & 1 \\ 1 & -1 & -1 & 1 \\ 1 & -1 & -1 & 1 \end{bmatrix}$$

$$[B3012] = \frac{1}{36} \begin{bmatrix} 4 & 2 & -2 & -4 \\ 4 & 4 & -4 & -2 \\ 2 & 2 & -2 & -1 \\ 2 & 1 & -1 & -2 \\ -4 & -2 & 2 & 4 \\ -2 & -4 & 4 & 2 \\ -1 & -2 & 2 & 1 \\ 2 & -1 & 1 & 1 \\ 2 & -1 & 1 & 1 \\ -1 & -2 & 2 & 1 \\ -2 & -4 & 4 & 2 \\ -4 & -2 & 2 & 4 \\ 2 & 1 & -1 & -2 \\ 1 & 2 & -2 & -1 \\ 2 & 4 & -4 & -2 \\ 4 & 2 & -2 & -4 \end{bmatrix}$$

$$[B3022] = \frac{1}{36} \begin{bmatrix} 4 & 1 & 1 & -4 \\ 1 & 1 & 1 & 1 \\ 1 & 1 & -1 & 1 \\ 1 & 1 & 1 & 4 \\ 1 & 1 & 1 & 1 \\ 1 & 1 & 4 & 1 \\ 1 & 1 & 1 & 1 \\ 1 & 1 & 1 & 1 \\ 1 & 1 & 1 & 1 \\ 1 & 1 & 1 & 1 \\ 1 & 1 & 1 & 1 \\ 1 & 1 & 1 & 1 \\ 1 & 1 & 1 & 1 \\ 4 & 1 & 1 & 4 \end{bmatrix}$$

$$[B3021] = \frac{1}{36} \begin{bmatrix} 1 & -4 & -2 & 2 \\ 1 & -2 & -1 & 1 \\ 1 & -1 & -2 & 1 \\ 1 & 1 & -6 & 4 \\ 1 & 1 & -1 & 1 \\ 1 & 1 & -2 & 1 \\ 1 & 1 & -2 & 4 \\ 1 & 1 & -2 & 1 \\ 1 & 1 & -2 & 1 \\ 1 & 1 & -2 & 1 \\ 1 & 1 & -2 & 1 \\ 1 & 1 & -2 & 1 \\ 1 & 1 & -2 & 1 \\ 1 & 1 & -2 & 1 \end{bmatrix}$$

$$[B40000] = \frac{1}{900}$$

144	36	9	36	36	24	6	9	9	6	4	6	36	9	6	24
36	24	6	9	24	36	9	6	6	9	6	4	9	6	4	6
9	6	4	6	6	9	6	4	4	6	9	6	6	4	6	9
36	9	6	24	9	6	4	6	6	4	6	9	24	6	9	36
36	24	6	9	24	36	9	6	6	9	6	4	9	6	4	6
24	36	9	6	36	144	36	9	9	36	24	6	6	9	6	4
6	9	6	4	9	36	24	6	6	24	36	9	4	6	9	6
9	6	4	6	6	9	6	4	4	6	9	6	6	4	6	9
9	6	4	6	6	9	6	4	4	6	9	6	6	4	6	9
6	9	6	4	9	36	24	6	6	24	36	9	4	6	9	6
4	6	9	6	6	24	36	9	9	36	144	36	6	9	36	24
6	4	6	9	4	6	9	6	6	9	36	24	9	6	24	36
36	9	6	24	9	6	4	6	6	4	6	9	24	6	9	36
9	6	4	6	6	9	6	4	4	6	9	6	6	4	6	9
6	4	6	9	4	6	9	6	6	9	36	24	9	6	24	36
24	6	9	36	6	4	6	9	9	6	24	36	36	9	36	144

$$[B40010] = \frac{1}{900}$$

-36	-12	-3	-9	36	12	3	9	9	3	2	6	-9	-3	-2	-6
-12	-12	-3	-3	12	12	3	3	3	3	2	2	-3	-3	-2	-2
-3	-3	-2	-2	3	3	2	2	2	2	3	3	-2	-2	-3	-3
-9	-3	-2	-6	9	3	2	6	6	2	3	9	-6	-2	-3	-9
-12	-12	-3	-3	12	12	3	3	3	3	2	2	-3	-3	-2	-2
-12	-36	-9	-3	12	36	9	3	3	9	6	2	-3	-9	-6	-2
-3	-9	-6	-2	3	9	6	2	2	6	9	3	-2	-6	-9	-3
-3	-3	-2	-2	3	3	2	2	2	2	3	3	-2	-2	-3	-3
-3	-3	-2	-2	3	3	2	2	2	2	3	3	-2	-2	-3	-3
-3	-9	-6	-2	3	9	6	2	2	6	9	3	-2	-6	-9	-3
-2	-6	-9	-3	2	6	9	3	3	9	36	12	-3	-9	-36	-12
-2	-2	-3	-3	2	2	3	3	3	3	12	12	-3	-3	-12	-12
-9	-3	-2	-6	9	3	2	6	6	2	3	9	-6	-2	-3	-9
-3	-3	-2	-2	3	3	2	2	2	2	3	3	-2	-2	-3	-3
-2	-2	-3	-3	2	2	3	3	3	3	12	12	-3	-3	-12	-12
-6	-2	-3	-9	6	2	3	9	9	3	12	36	-9	-3	-12	-36

$$[B40020] = \frac{1}{360}$$

-36	-9	-3	-12	-9	-6	-2	-3	9	6	2	3	36	9	3	12
-9	-6	-2	-3	-6	-9	-3	-2	6	9	3	2	9	6	2	3
-3	-2	-2	-3	-2	-3	-3	-2	2	3	3	2	3	2	2	3
-12	-3	-3	-12	-3	-2	-2	-3	3	2	2	3	12	3	3	12
-9	-6	-2	-3	-6	-9	-3	-2	6	9	3	2	9	6	2	3
-6	-9	-3	-2	-9	-36	-12	-3	9	36	12	3	6	9	3	2
-2	-3	-3	-2	-3	-12	-12	-3	3	12	12	3	2	3	3	2
-3	-2	-2	-3	-2	-3	-3	-2	2	3	3	2	3	2	2	3
-3	-2	-2	-3	-2	-3	-3	-2	2	3	3	2	3	2	2	3
-2	-3	-3	-2	-3	-12	-12	-3	3	12	12	3	2	3	3	2
-2	-3	-9	-6	-3	-12	-36	-9	3	12	36	9	2	3	9	6
-3	-2	-6	-9	-2	-3	-9	-6	2	3	9	6	3	2	6	9
-12	-3	-3	-12	-3	-2	-2	-3	3	2	2	3	12	3	3	12
-3	-2	-2	-3	-2	-3	-3	-2	2	3	3	2	3	2	2	3
-3	-2	-6	-9	-2	-3	-9	-6	2	3	9	6	3	2	6	9
-12	-3	-9	-36	-3	-2	-6	-9	3	2	6	9	12	3	9	36

$$[B40100] = \frac{1}{360}$$

-36	-12	-3	-9	-12	-12	-3	-3	-3	-3	-2	-2	-9	-3	-2	-6
-12	-12	-3	-3	-12	-36	-9	-3	-3	-9	-6	-2	-3	-3	-2	-2
-3	-3	-2	-2	-3	-9	-6	-2	-2	-6	-9	-3	-2	-2	-3	-3
-9	-3	-2	-6	-3	-3	-2	-2	-2	-2	-3	-3	-6	-2	-3	-9
36	12	3	9	12	12	3	3	3	3	2	2	9	3	2	6
12	12	3	3	12	36	9	3	3	9	6	2	3	3	2	2
3	3	2	2	3	9	6	2	2	6	9	3	2	2	3	3
9	3	2	6	3	3	2	2	2	2	3	3	6	2	3	9
9	3	2	6	3	3	2	2	2	2	3	3	6	2	3	9
3	3	2	2	3	9	6	2	2	6	9	3	2	2	3	3
2	2	3	3	2	6	9	3	3	9	36	12	3	3	12	12
6	2	3	9	2	2	3	3	3	3	12	12	9	3	12	36
-9	-3	-2	-6	-3	-3	-2	-2	-2	-2	-3	-3	-6	-2	-3	-9
-3	-3	-2	-2	-3	-9	-6	-2	-2	-6	-9	-3	-2	-2	-3	-3
-2	-2	-3	-3	-2	-6	-9	-3	-3	-9	-36	-12	-3	-3	-12	-12
-6	-2	-3	-9	-2	-2	-3	-3	-3	-3	-12	-12	-9	-3	-12	-16

$$[B40200] = \frac{1}{360}$$

-36	-9	-3	-12	-9	-6	-2	-3	-3	-2	-2	-3	-12	-3	-3	-12
-9	-6	-2	-3	-6	-9	-3	-2	-2	-3	-3	-2	-3	-2	-2	-3
-3	-2	-2	-3	-2	-3	-3	-2	-2	-3	-9	-6	-3	-2	-6	-9
-12	-3	-3	-12	-3	-2	-2	-3	-3	-2	-6	-9	-12	-3	-9	-36
-9	-6	-2	-3	-6	-9	-3	-2	-2	-3	-3	-2	-3	-2	-2	-3
-6	-9	-3	-2	-9	-36	-12	-3	-3	-12	-12	-3	-2	-3	-3	-2
-2	-3	-3	-2	-3	-12	-12	-3	-3	-12	-36	-9	-2	-3	-9	-6
-3	-2	-2	-3	-2	-3	-3	-2	-2	-3	-9	-6	-3	-2	-6	-9
9	6	2	3	6	9	3	2	2	3	3	2	3	2	2	3
6	9	3	2	9	36	12	3	3	12	12	3	2	3	3	2
2	3	3	2	3	12	12	3	3	12	36	9	2	3	9	6
3	2	2	3	2	3	3	2	2	3	9	6	3	2	6	9
36	9	3	12	9	6	2	3	3	2	2	3	12	3	3	12
9	6	2	3	6	9	3	2	2	3	3	2	3	2	2	3
3	2	2	3	2	3	3	2	2	3	9	6	3	2	6	9
12	3	3	12	3	2	2	3	3	2	6	9	12	3	9	36

$$[B40110] = \frac{1}{360}$$

24	12	3	6	-24	-12	-3	-6	-6	-3	-2	-4	6	3	2	4
12	24	6	3	-12	-24	-6	-3	-3	-6	-4	-2	3	6	4	2
3	6	4	2	-3	-6	-4	-2	-2	-4	-6	-3	2	4	6	3
6	3	2	4	-6	-3	-2	-4	-4	-2	-3	-6	4	2	3	6
-24	-12	-3	-6	24	12	3	6	6	3	2	4	-6	-3	-2	-4
-12	-24	-6	-3	12	24	6	3	3	6	4	2	-3	-6	-4	-2
-3	-6	-4	-2	3	6	4	2	2	4	6	3	-2	-4	-6	-3
-6	-3	-2	-4	6	3	2	4	4	2	3	6	-4	-2	-3	-6
-6	-3	-2	-4	6	3	2	4	4	2	3	6	-4	-2	-3	-6
-3	-6	-4	-2	3	6	4	2	2	4	6	3	-2	-4	-6	-3
-2	-4	-6	-3	2	4	6	3	3	6	24	12	-3	-6	-24	-12
-4	-2	-3	-6	4	2	3	6	6	3	12	24	-6	-3	-12	-24
6	3	2	4	-6	-3	-2	-4	-4	-2	-3	-6	4	2	3	6
3	6	4	2	-3	-6	-4	-2	-2	-4	-6	-3	2	4	6	3
2	4	6	3	-2	-4	-6	-3	-3	-6	-24	-12	3	6	24	12
4	2	3	6	-4	-2	-3	-6	-6	-3	-12	-24	6	3	12	24

$$[B40220] = \frac{1}{360}$$

24	6	3	12	6	4	2	3	-6	-4	-2	-3	-24	-6	-3	-12
6	4	2	3	4	6	3	2	-4	-6	-3	-2	-6	-4	-2	-3
3	2	4	6	2	3	6	4	-2	-3	-6	-4	-3	-2	-4	-6
12	3	6	24	3	2	4	6	-3	-2	-4	-6	-12	-3	-6	-24
6	4	2	3	4	6	3	2	-4	-6	-3	-2	-6	-4	-2	-3
4	6	3	2	6	24	12	3	-6	-24	-12	-3	-4	-6	-3	-2
2	3	6	4	3	12	24	6	-3	-12	-24	-6	-2	-3	-6	-4
3	2	4	6	2	3	6	4	-2	-3	-6	-4	-3	-2	-4	-6
-6	-4	-2	-3	-4	-6	-3	-2	4	6	3	2	6	4	2	3
-4	-6	-3	-2	-6	-24	-12	-3	6	24	12	3	4	6	3	2
-2	-3	-6	-4	-3	-12	-24	-6	3	12	24	6	2	3	6	4
-3	-2	-4	-6	-2	-3	-6	-4	2	3	6	4	3	2	4	6
-24	-6	-3	-12	-6	-4	-2	-3	6	4	2	3	24	6	3	12
-6	-4	-2	-3	-4	-6	-3	-2	4	6	3	2	6	4	2	3
-3	-2	-4	-6	-2	-3	-6	-4	2	3	6	4	3	2	4	6
-12	-3	-6	-24	-3	-2	-4	-6	3	2	4	6	12	3	6	24

$$[B40120] = \frac{1}{144}$$

9	3	1	3	3	3	1	1	-3	-3	-1	-1	-9	-3	-1	-3
3	3	1	1	3	9	3	1	-3	-9	-3	-1	-3	-3	-1	-1
1	1	1	1	1	3	3	1	-1	-3	-3	-1	-1	-1	-1	-1
3	1	1	3	1	1	1	1	-1	-1	-1	-1	-3	-1	-1	-3
-9	-3	-1	-3	-3	-3	-1	-1	3	3	1	1	9	3	1	3
-3	-3	-1	-1	-3	-9	-3	-1	3	9	3	1	3	3	1	1
-1	-1	-1	-1	-1	-3	-3	-1	1	3	3	1	1	1	1	1
-3	-1	-1	-3	-1	-1	-1	-1	1	1	1	1	3	1	1	3
-3	-1	-1	-3	-1	-1	-1	-1	1	1	1	1	3	1	1	3
-1	-1	-1	-1	-1	-3	-3	-1	1	3	3	1	1	1	1	1
-1	-1	-3	-3	-1	-3	-9	-3	1	3	9	3	1	1	3	3
-3	-1	-3	-9	-1	-1	-3	-3	1	1	3	3	3	1	3	9
3	1	1	3	1	1	1	1	-1	-1	-1	-1	-3	-1	-1	-3
1	1	1	1	1	3	3	1	-1	-3	-3	-1	-1	-1	-1	-1
1	1	3	3	1	3	9	3	-1	-3	-9	-3	-1	-1	-3	-3
3	1	3	9	1	1	3	3	-1	-1	-3	-3	-3	-1	-3	-9



$$[B40210] = \frac{1}{144}$$

9	3	1	3	-9	-3	-1	-3	-3	-1	-1	-3	3	1	1	3
3	3	1	1	-3	-3	-1	-1	-1	-1	-1	-1	1	1	1	1
1	1	1	1	-1	-1	-1	-1	-1	-1	-3	-3	1	1	3	3
3	1	1	3	-3	-1	-1	-3	-3	-1	-3	-9	3	1	3	9
3	3	1	1	-3	-3	-1	-1	-1	-1	-1	-1	1	1	1	1
3	9	3	1	-3	-9	-3	-1	-1	-3	-3	-1	1	3	3	1
1	3	3	1	-1	-3	-3	-1	-1	-3	-9	-3	1	3	9	3
1	1	1	1	-1	-1	-1	-1	-1	-1	-3	-3	1	1	3	3
-3	-3	-1	-1	3	3	1	1	1	1	1	1	-1	-1	-1	1
-3	-9	-3	-1	3	9	3	1	1	3	3	1	-1	-3	-3	-1
-1	-3	-3	-1	1	3	3	1	1	3	9	3	-1	-3	-9	-3
-1	-1	-1	-1	1	1	1	1	1	1	3	3	-1	-1	-3	-3
-9	-3	-1	-3	9	3	1	3	3	1	1	3	-3	-1	-1	-3
-3	-3	-1	-1	3	3	1	1	1	1	1	1	-1	-1	-1	-1
-1	-1	-1	-1	1	1	1	1	1	1	3	3	-1	-1	-3	-3
-3	-1	-1	-3	3	1	1	3	3	1	3	9	-3	-1	-3	-9

**DA  
FILM**